

University of Southampton Research Repository

Copyright © and Moral Rights for this thesis and, where applicable, any accompanying data are retained by the author and/or other copyright owners. A copy can be downloaded for personal non-commercial research or study, without prior permission or charge. This thesis and the accompanying data cannot be reproduced or quoted extensively from without first obtaining permission in writing from the copyright holder/s. The content of the thesis and accompanying research data (where applicable) must not be changed in any way or sold commercially in any format or medium without the formal permission of the copyright holder/s.

When referring to this thesis and any accompanying data, full bibliographic details must be given, e.g.

Thesis: Author (Year of Submission) "Full thesis title", University of Southampton, name of the University Faculty or School or Department, PhD Thesis, pagination.

Data: Author (Year) Title. URI [dataset]

University of Southampton

Faculty of Environmental and Life Sciences

School of Ocean and Earth Science

Drivers of Warm Water Variability In Atlantic Hurricane Regions

by

Elizabeth Anne Harris

MRes

ORCID ID https://orcid.org/0000-0002-0274-560X

Thesis for the degree of Doctor of Philosophy

August 2024

University of Southampton Abstract

Faculty of Environmental and Life Sciences
School of Ocean and Earth Science

<u>Doctor of Philosophy</u>

Drivers of Warm Water Variability In Atlantic Hurricane Regions

by

Elizabeth Anne Harris

Tropical North Atlantic Ocean Heat Content has increased materially over the past 40-50 years, and has been linked to an uptick in major hurricane landfalls. This increasing damage potential has led to fears for the future from extreme events. In this thesis, the volume of water warmer than 26.5 °C is used to diagnose observed historical and modelled future changes in the underlaying fuel source available for the development of intense hurricanes. The processes driving changes in this fuel source are examined using complimentary Eulerian and Lagrangian techniques.

From the Eulerian perspective, observed month-to-month volume changes in water warmer than 26.5 °C in the North Atlantic can be explained by changes in the anomalous volume of warm water transformed across the 26.5 °C isotherm by atmospheric heat flux; this is primarily attributed to surface heat gain in some years. An inference is that ocean heat transport is more important for warm water volume anomaly development in other years. Transformed volume changes are calculated using the Water Mass Transformation Framework in temperature space. Anomalies are notably driven by latent heat flux, which is highly correlated with wind speed and cloud fraction over most of the warm water surface.

The residual warm water volume accumulated by ocean heat transport also plays a key role in heat content accumulation in the tropical North Atlantic. Lagrangian analysis is used to analyse heat flux along ocean currents into the Main Development Region (MDR) for Atlantic hurricanes. ARIANE particle tracking output highlights that a large number of particles are resident in the MDR (20-40%), and relatively fewer particles are transported into the MDR via the North Brazil Current (5-15%) or Ekman drift across 10 °N six months before the start of hurricane season, in years with high hurricane activity. The results are consistent with the view that a reduced meridional circulation is likely to lead to accumulation of warm water in the tropical North Atlantic and more active hurricane seasons.

Both Eulerian and Lagrangian analyses are applied to a high-resolution climate model, HadGEM3-GC31-HH, to examine evolving mechanisms impacting the growth of the Atlantic Warm Pool under future high anthropogenic greenhouse gas emissions. Warm water convergence due to reduced ocean transport is confirmed to be the driver of additional future heat available to fuel major hurricane development in this model. The total heat accumulation along modelled particle tracks crossing 10 °N and ending at 20 °N after 6 months, which are warmer than 26.5 °C, is 14% higher (4.2 GW) in 2041-2050 than 2001-2010. The results imply an increasing importance for ocean transport over atmospheric heat flux as the Atlantic continues warming.

Table of Contents

Table of Contents	3
Table of Tables	6
Table of Figures	7
Research Thesis: Declaration of Authorship	12
Acknowledgements	13
Abbreviations	14
Chapter 1 Introduction	16
1.1 Atlantic Hurricane Climatology	16
1.1.1 Hurricane Formation	16
1.1.2 Seasonality	17
1.1.3 Tracks and Landfall	18
1.2 Variability in Hurricane Activity	19
1.2.1 Multidecadal Variability of the Atlantic Ocean	21
1.2.2 Interannual Variability	24
1.2.3 Intraseasonal Variability	25
1.3 Climate Change and Hurricanes	26
1.3.1 Observed Trends in Hurricanes	26
1.3.2 Climate Model Projections	28
1.4 Summary	29
Chapter 2 The Water Mass Transformation Framework and Varia	-
Hurricane Activity	31
Abstract	31
2.1 Introduction	31
2.2 Methods	33
2.3 Data	36
2.4 Results	37
2.4.1 Warm Water Volume and Hurricane Activity	37

Table of Contents

	2.4.2	Characteristics of Water Mass Transformation	40
	2.4.3	Inferred Warm Water Volume Changes	42
	2.4.4	Drivers of warm water volume Changes	46
2.5	Cor	nclusions	47
Acl	knowl	edgements	48
Cha	pter 3	3 Tracing Oceanic Sources of Heat Content Available for Atlantic	
	•	Hurricanes	49
Key	y Poin	ts:	49
Pla	in Lan	guage Summary	49
3.1	Intr	oduction	50
3.2	Dat	a and Methods	52
	3.2.1	IBTrACS	53
	3.2.2	GODAS	53
	3.2.3	NEMO hindcast	53
	3.2.4	Lagrangian analysis	53
3.3	Res	ults	55
	3.3.1	Climatology of oceanic sources of warm water into the summertime MDR	56
	3.3.2	Climatology of dynamical influences on MDR heat content and Atlantic	
		hurricanes	59
	3.3.3	Interseasonal variability of oceanic pathways into the MDR in relation to	
		hurricane activity	60
	3.3.4	MDR heat content linked to modes of climate variability	65
3.4	Cor	nclusions	67
Acl	knowl	edgements	68
Cha	pter 4	Meridional Heat Convergence will Increase Tropical North	
		Atlantic Heat Content Available for Hurricane Intensification	69
Key	y Poin	ts:	69

Abstra	ct6	9
4.1 In	ntroduction6	9
4.2 D	ata and Methods7	2
4.2.	.1 CMIP6 HighResMIP (High-Resolution Model Intercomparison Project) 7	2
4.2.	.2 Ocean Data7	3
4.2.	.3 Atmospheric and Surface Flux Data7	3
4.2.	.4 Hurricane Data7	3
4.2.	.5 Water Mass Transformation	4
4.2.	.6 Back-tracking warm water (TRACMASS)	4
4.3 R	esults7	5
4.3.	.1 Future Trends in Available Heat Content7	5
4.3.	.2 Changes in Atmospheric Heat Flux7	7
4.3.	.3 Climate change and Tropical Atlantic Advective Heat Flux 8	0
4.4 C	conclusions8	4
Acknow	wledgements8	5
Chapte	r 5 Summary 8	5
5.1 C	Context and Overview8	6
5.2 W	Varm water transformation – the Eulerian perspective8	7
5.3 Tr	racing sources of warm water – the Lagrangian perspective8	8
5.4 D	rivers of future changes in Warm Water Volume of likely consequence for	
h	urricane seasons8	9
5.5 C	Concluding Remarks and Outlook9	0
liet of B	Qafarancas Q	2

Table of Tables

Table of Tables

Table 4	.1 HighResMIF	P Model configurations	7
Table 4	1 HighResMIF	^o Model configurations	

Figure 1.1 Ocea	anic and atmospheric conditions conducive to hurricane genesis and development17
	4676(6pm6m:
Figure 1.2 Num	ber of Atlantic named storms and hurricanes per 100 years between May 1 and
	December 31 based on HURDAT track data 1944-2020, normalized to 100
	years, 5-day running average smoothing (NHC, 2023)18
Figure 1.3 The r	number of hurricanes whose centres pass within 150 nautical miles of a point on
	the map, using HURDAT track data 1944 to 2020, but normalized to 100 years
	(NHC, 2023)19
Figure 1.4 Hurri	cane counts for the Atlantic Basin 1970-2022 (top) and the US coastline 1900-
	2023 (bottom), and 10-year centred average20
Figure 1.5 AMO	C heat transfer dynamics in strong (left) transport regime and weak (right)
	showing surface northwards (red) and mid-ocean (blue) southwards transport,
	and the consequences for SST (Duchez et al., 2016)21
Figure 1.6 NCEI	P/NCAR September average MDR SST (°C) 1900-2021, 10-year smoothing (Kalnay
	et al., 1996), emphasising the emergence of anomalous warmth after around
	1995
Figure 1.7 GOD	AS (blue) at 26 °N to 1000 m and RAPID array (red) transport (Sv)23
Figure 1.8 AMO	Index 1851-2019 and significant tropical volcanic eruptions (Sousounis, 2021)
	23
Figure 1.9 Majo	r US Landfalling hurricanes and AMO index by decade (Sousounis, 2021) 24
Figure 1.10 Ann	nual number of Category 4 and 5 hurricanes 1950-202227
Figure 1.11 Trop	oical Atlantic anomalous heat content investigation identifying the main open
	question identified in this thesis, components which are investigated, the
	methods used, and how these feed into the final results chapter30
Figure 2.1 Heat	transfer mechanisms leading to water warmer than 26.5 °C, critical to hurricane
	development, in the region southwards and upwards of thick red lines34
Figure 2.2 NCE	P 1980-2019 Mean Q _{net} (Wm ⁻² , positive into the ocean), MDR outlined in red: (a)
	Jan-Dec, (b) Apr-Sept35

Figure 2.3 HURI	DAT Annual North Atlantic Hurricane count (blue bars) and GODAS volume
	anomalies of water warmer than 26.5 °C in the Atlantic north of 10 °N 1980-
	2019, applying 12-month centred moving average (orange line). For GODAS
	volume anomalies, the zero-line is aligned with the mean hurricane count.
	38
Figure 2.4 Pears	son correlation coefficient between Atlantic basin seasonal hurricane count
	1980-2019 and depth of the 26.5 °C isotherm in different months: (a) r(Z26.5,
	hurricane count), April; (b) r(SST, hurricane count), April; (c) r(Z26.5, hurricane
	count), May; (d) r(SST, hurricane count), May. Stippling indicates 95%
	significance level
Figure 2.5 Annu	al-mean transformation rate (Sv) for the Atlantic north of 10 °N as a function of
	SST 1980-2019, given diathermal temperature fluxes at 0.25 °C intervals;
	positive values imply transformation of water towards higher temperatures has
	occurred over the period40
Figure 2.6 1980	-2019 mean monthly volume transformed across 26.5 °C isotherm (purple, right
	axis) and actual volume warmer than 26.5 °C (red, left axis) (million km³).41
Figure 2.7 (a) M	ean 1980-2019 April-September Q _{net} (Wm ⁻²) into the ocean where SST exceeds
	26.5 °C, (b) 1980-2019 September mean depth of 26.5 °C isotherm (m) with
	HURDAT 1980-2019 hurricane formation points overlaid)42
Figure 2.8 Anon	nalous observed month-to-month (red) volume change of water warmer than
	26.5 °C and the anomalous transformation rate (i.e. million km³ per month)
	across the 26.5 °C isotherm (purple), applying 12-month centred moving
	average42
Figure 2.9 1998	(blue) volume transformed across 26.5 °C isotherm (million km³) versus 1980-
	2019 climatology (purple)
Figure 2.10 Ano	maly of June-September Q_{net} (Wm ⁻²) in 1998 where SST > 26.5 $^{\circ}$ C44
Figure 2.11 Diffe	erence in 4-month warm water volume anomalies (Blue) between observed
	(EN4) July to October volume anomalies $>$ 26.5 $^{\circ}$ C and that inferred by the
	anomalous integrated May to August transformation across the 26.5 °C
	isotherm, with negative RAPID heat transport anomalies across 26 °N (red),
	applying 12-month centred moving average45

Figure 2.12 Trai	nsformation rate anomalies (units: million of km³ per month) across the 26.5 °C
	isotherm calculated from Q_{net} (purple) and Q_{lh} (blue), applying 12-month
	centred moving average46
Figure 2.13 (a) F	Pearson correlation coefficient heat map for Q _{lh} and wind speed (b) correlation
	coefficient heat map for $Q_{\text{\scriptsize lh}}$ and cloud fraction using NCEP-NCAR data
	spanning 1980-2019. Values are only plotted where 1980-2019 September
	mean depth of 26.5 °C isotherm is greater than 10 m. Stippling indicates 95%
	significance level47
Figure 3.1 IBTrA	ACS Annual North Atlantic Hurricane count (blue bars) and GODAS June volume
	anomalies of water warmer than 26.5 °C in the Atlantic north of 10 °N 1980-
	2021 (orange line). For GODAS volume anomalies, the black zero-line is aligned
	with the mean hurricane count51
Figure 3.2 Num	ber of particles initially warmer than 26.5 °C in MDR on 30 June (purple) and on
	30 September (red)54
Figure 3.3 Sam	ple of back-trajectories from September 2010, colour-coded by particle id; MDR -
	black box, North Brazil Current measured across red line at 10 $^{\rm o}$ N55
Figure 3.4 Num	ber of particles per 0.5 $^{\circ}$ grid cell at 1-month intervals from start date. Tracing
	particles that were in the MDR and warmer than 26.5 $^{\rm o}{\rm C}$ on June 30 (top, tracing
	backwards), September 30 (middle, tracing backwards) and June 30 (bottom,
	tracing forwards). The MDR is outlined57
Figure 3.5 1988	-2010 ORCA12 mean heat flux (top row) and particle age (middle row) for ARIANE
	experiments BAC06 (backwards form June, left column), BAC09 (backwards
	from September, middle column), and FOR06 (forwards from June, right
	column); with mean Eulerian heat flux for the same 6-month periods as ARIANE
	experiments (bottom row; January to June left, March to September, middle,
	July to December, right)58
Figure 3.6 ORC	A12 1988-2010 averages of 6-month means for wind stress (Nm ⁻²) and surface
	current (ms ⁻¹). January-June corresponds to the time of BAC06, April-
	September to BAC09 and Jul-December to FOR0659
Figure 3.7 Phys	ical mechanisms influencing ocean heat transport divergence in the MDR shown
	as arrows (see main text above for details)60

Figure 3.8 Perc	rentage of particles in the MDR at each timestep that were in the MDR and warmer
	than 26.5 $^{\rm o}\text{C}$ at the start of the experiments, for each of the three experiments:
	BAC06, BAC09, and FOR06 by year (top panels). Time series of the percentage
	of these warm particles in the MDR at the end of the 6-month experiments
	(bottom panel)61
Figure 3.9 Perc	entage of particles in the North Brazil Current at each timestep that were in the
	MDR and warmer than 26.5 $^{\rm o}{\rm C}$ at the start of the experiments, for BAC06 and
	BAC09, by year (top panels). Time series of the percentage of these warm
	particles in the North Brazil Current at the end of the 6-month experiments
	(bottom panel)62
Figure 3.10 Nu	mber of particles per 0.5 $^{\circ}$ grid cell in January which are in the MDR and warmer
	than 26.5 °C in June of the same year64
Figure 3.11 Me	an January-June 2005 wind stress anomalies (Nm ⁻²) (a) and ocean current
	anomalies (ms ⁻¹) (b) vs 2009 (c, d) and 2010 (e, f)64
Figure 3.12 Anr	nual mean AMM-index (purple), ANI °C (red), and annual Hurricane count 1988-
	2010. (Chiang and Vimont (2004)
Figure 4.1 Sept	ember HADGEM3-GC3.1-HH 1950-2050 forced run mean monthly volume
	(million km³) in the North Atlantic north of 10 °N of water warmer than 26.5 °C
	(green, solid), 27.5 °C (blue), and 28.5 °C (purple); warmer than 26.5 °C in the
	control run (green, dashed), and EN4 1950-2022 (green, dotted)75
Figure 4.2 Sept	ember mean monthly area of water (million km²) warmer than 26.5 °C in the
	North Atlantic north of 10 °: HADGEM3-GC3.1-HH 1950-2050 forced run (green)
	and depth of the 26.5 °C isotherm (black)76
Figure 4.3 Dept	th of the September 26.5 °C isotherm (m) in the North Atlantic north of 10 °N by
	decade 1950-2049 HADGEM3-GC3.1-HH forced run (rows 1 and 3) and 1980-
	2019 GODAS (rows 2 and 4)
Figure 4.4 1980	0-2022 Mean depth of GODAS September 26.5 °C isotherm (m) and IBTrACS
	points 1980-2022 where hurricanes intensified into major hurricanes 78
Figure 4.5 Mea	n monthly Q _{net} into the Atlantic Ocean (Wm ⁻²) 10 °N to 30 °N with 12-month
	centred moving average: HADGEM3-GC3.1-HH 1950-2050 forced run (green)
	and control (blue), compared with observed ERA5 (black)78

Figure 4.6 Mean	monthly volume (million km³) of water transformed across the 26.5 °C (green),
	27.5 °C (blue) and 28.5 °C (purple) isotherm, with 12-month centred moving
	average79
Eiguro 4 7 Mont	hly meridional convergence of warm water volume (million km³) convergence
rigule 4.7 Mont	
	between 10 °N and 30 °N with 12-month centred moving average for water
	warmer than 26.5 °C (green), 27.5 °C (blue), and 28.5 °C (purple) in HADGEM3-
	GC3.1-HH, HADGEM3-GC3.1-HM, ECE and CESM81
Figure 4.8 GOD	AS July 1 volume (million km3) of water warmer than 26.5 °C between 10 °N and
	30 °N (red) and annual major hurricane count (black) 1980-202282
Figure 4.9 Left: Smoothed mean zonally integrated January-June heat flux into particles back-	
	tracked from 20 °N, which cross 10 °N (GWm ⁻¹ positive for heat gain) by
	latitude, averaged over 1951-1960 (blue), 2001-2010 (green), and 2041-2050
	(red). Right: January-June mean particle temperature (°C) within 0.5 degree grid
	boxes averaged over a decade; 1951-1960 (top), 2001-2010 (middle), and 2041-
	2050 (bottom)
Figure 5.1 Sche	matics highlighting the relative importance of local and remote forcing of the
	warm water volume: (a) strong recirculation and heat gain in the MDR leading to
	enhanced warm water volume (WWV), coincident with weakening imports from
	the south via the North Brazil Current and Ekman drift; (b) reversed scenario,
	leading to reduced warm water volume (WWV). Note that the North Brazil
	Current and Ekman drift are not necessarily strengthened in (b) relative to (a),
	but are found to contribute proportionately more to the warm water volume in
	(b), when this volume is back-tracked over 6 months91

Research Thesis: Declaration of Authorship

Research Thesis: Declaration of Authorship

Print name: Elizabeth Harris

Title of thesis: Drivers of Warm Water Variability In Atlantic Hurricane Regions

I declare that this thesis and the work presented in it are my own and has been generated by me

as the result of my own original research.

I confirm that:

1. This work was done wholly or mainly while in candidature for a research degree at this

University;

2. Where any part of this thesis has previously been submitted for a degree or any other

qualification at this University or any other institution, this has been clearly stated;

3. Where I have consulted the published work of others, this is always clearly attributed;

4. Where I have quoted from the work of others, the source is always given. With the exception

of such quotations, this thesis is entirely my own work;

5. I have acknowledged all main sources of help;

6. Where the thesis is based on work done by myself jointly with others, I have made clear

exactly what was done by others and what I have contributed myself;

7. Parts of this work have been published as:-

Harris, E., Marsh, R., Grist, J.P., and G.D. McCarthy (2022). The water mass transformation

framework and variability in hurricane activity. Climate Dynamics, 59 (3-4), 961-972.

Harris, E. A., Marsh, R., & Grist, J. P. (2023). Tracing oceanic sources of heat content available

for Atlantic hurricanes. Journal of Geophysical Research: Oceans, e2022JC019407.

Harris, E., Dey, D., Marsh, R., & Grist, J. (2024). Meridional Heat Convergence Will Increase

Tropical North Atlantic Heat Content Available for Hurricane Intensification. In Advances in

Hurricane Risk in a Changing Climate (pp. 77-95). Cham: Springer Nature Switzerland.

Signature: Date: August 5, 2024

12

Acknowledgements

I am deeply grateful to my Advisors, Robert Marsh and Jeremy Grist for their guidance throughout the development of this thesis. They dedicated a significant amount of time and expertise into shaping a though-provoking journey from which I've emerged with a sharpened knowledge of hurricane climate dynamics, tools, and enhanced skillset for climate data analysis. Bob helped me to very clearly define the analysis questions from early on in the investigation. Jeremy was able to be available at short notice for questions on both datasets and climate dynamics, spotting potential errors immediately. Additional support was gained from Gerard McCarthy, who offered robust advice on observational datasets used in the first results chapter, and Dipanjan Dey, an expert in Lagrangian analysis in atmospheric and oceanic data. Jeffrey Blundell makes himself available to student IT requests at short notice and many projects would not cross the finish line without his assistance. I would also like to thank fellow PhD students Samantha Hallam, Emma Worthington, and Jess Cartwright for helping me see the light at the end of the tunnel and pushing me to keep going during weekly calls, especially critical for morale in the days of the pandemic. I appreciate the time and funding facilitated at Ariel Re by Federico Waisman, without whose support I would have struggled to begin this lengthy endeavour. Of course, the patience of my kind and generous partner, Stanley Harris and our son Nayland was absolutely necessary to allow time and effort to be devoted to completion of this thesis.

Abbreviations

Abbreviations

ACE Accumulated Cyclone Energy
AMM Atlantic Meridional Mode
AMOC Atlantic Meridional Overturning Circulation
AMVAtlantic Multidecadal Variability
ANI Atlantic Niño Index
BAC06 Backwards from June
BAC09 Backwards from September
C Celsius
C3S Copernicus Climate Change Service
CMIP6Coupled Model Intercomparison Project 6
CPI Consumer Price Index
DFS DRAKKAR Forcing Set
E East
ECMWF European Centre for Medium-Range Weather Forecasts
ENSO El Niño Southern Oscillation
FOR06 Forwards from June
GODAS Global Ocean Data Assimilation System
HighResMIP High-Resolution Model Intercomparison Project
IBTrACS International Best Track Archive for Climate Stewardship
IPCCIntergovernmental Panel on Climate Change
ITCZIntertropical Convergence Zone
QBOQuasi-Biennial Oscillation
Q _{in}
Q _{lh} Latent heat flux
Q _{Lagrangian} Lagrangian heat flux
Q _{lw} Long wave radiation
Q _{net} Net heat flux

Abbreviations

Q _{sh} Sensible heat flux
Q _{sw} Short wave radiation
MDR Main Development Region
MJO Madden-Julian Oscillation
N North
NAO North Atlantic Oscillation
NCAR National Center for Atmospheric Research
NCEI Nation Centre for Environmental Information
NCEP National Centers for Environmental Prediction
NEMO Nucleus for European Modelling of the Ocean
NHC National Hurricane Center
NOC National Oceanography Centre
OHC Ocean Heat Content
S South
SAL Saharan Air Layer
SSP585 Shared Socioeconomic Pathway 585
SST Sea Surface Temperature
T Temperature
TCTropical Cyclone
W West
WMT Water Mass Transformation Framework

Chapter 1 Introduction

I moved from weather forecasting for Bermuda public, marine, and aviation into natural catastrophe modelling for reinsurance in 2007, at a time when several major hurricanes had recently made landfall in successive years after a long relatively quiet period. After the very active years of 2004 and 2005, the science community began trying to gain deeper understanding of the observed upwards trend in Atlantic basin hurricane activity since 1980. 17 years later, science and industry are still trying to quantify the contributions of anthropogenic climate change and natural variability (Vecchi et al., 2021), drivers of internal variability in the tropical Atlantic, the extent to which climate change and other human activity have already impacted hurricane development (Knutson et al., 2019), and what to expect from the future (Knutson et al., 2020). As the ocean effectively drives the climate on longer timescales (Yeager and Robson, 2017), I have looked to the ocean for answers to this problem, using historical and future ocean model data.

In the first section of this chapter, Atlantic hurricane climatology will be outlined. Following this, hurricane variability on a variety of timescales and concepts surrounding drivers of activity will be discussed. Finally, recent investigations into the impact of a warming atmosphere and ocean due to greenhouse gas forcing on these drivers of variability will be considered, which reference both observational data and climate model output.

1.1 Atlantic Hurricane Climatology

A description of hurricane climatology is presented to identify the atmospheric and oceanic conditions conducive to hurricane genesis and development. Hurricane seasonality, tracks, and landfall regions will be described as these details are pertinent to the time of year and region selected for analysis in the experiments in subsequent chapters.

1.1.1 Hurricane Formation

Tropical cyclones (TCs) are a global weather phenomenon which play an important part in the redistribution of heat polewards (Emanuel, 2001). They generally form over the ocean where sea surface temperature (SST) is greater than 26.5 °C (Dare & McBride, 2011; McTaggert-Cowan et al., 2015). Deep convection is facilitated by low vertical wind shear (DeMaria, 2001). Spin-up is more likely with sufficient Coriolis force at latitudes 5 ° or more from the equator (Gray, 1975). An existing atmospheric disturbance, usually a tropical wave or other thunderstorm complex, provides the seed for development (Gray, 1982). Ideal atmospheric conditions for tropical storm

genesis include a moist, unstable atmosphere with low atmospheric pressure at the surface and high pressure aloft (DeMaria, 2001). While atmospheric conditions are important for storm genesis and development, a warm Atlantic provides the energy necessary to fuel the system (Shapiro and Goldenberg, 1998); hence the importance of understanding drivers of anomalous oceanic heat. Figure 1.1 depicts several of these processes, including an underlying warm ocean, low vertical wind shear, atmospheric instability, and some initial rotation from an existing disturbance.

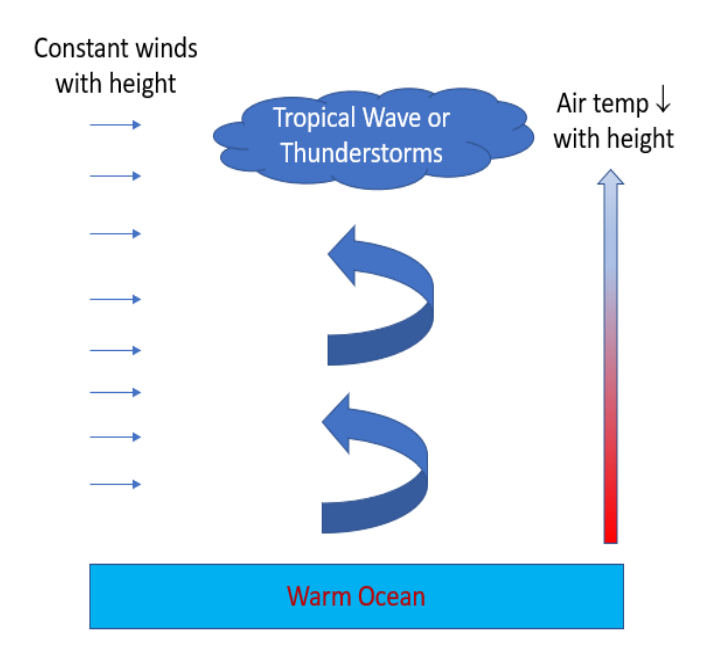


Figure 1.1 Oceanic and atmospheric conditions conducive to hurricane genesis and development

The studies referenced above describe how tropical oceans allow development of deep, intense tropical cyclones with high winds, damaging waves, high storm surge and heavy precipitation which pose a great danger to human life and property. In the North Atlantic, large population centres along coastlines throughout the Caribbean, Central America, and North America are at risk from these impacts, so much study has been undertaken in order to understand the physics of these events in the present and future climate.

1.1.2 Seasonality

The National Hurricane Center (NHC) defines the Atlantic hurricane season as June 1 to November 30. However, a small percentage of tropical storms and even hurricanes have formed on either side of these dates, and it has been suggested that the length of the hurricane season may increase in future (Truchelut et al., 2022; Patricola et al., 2024). The 1944-2020 average peak of the hurricane season is September 15, when the tropical Atlantic SST is at its warmest

point of the year (Figure 1.2), allowing for greater intensification of storms (Fraza and Elsner, 2015). This is therefore the time of year where anomalous tropical Atlantic heat has the greatest impact on hurricane intensification. (NHC, 2023)

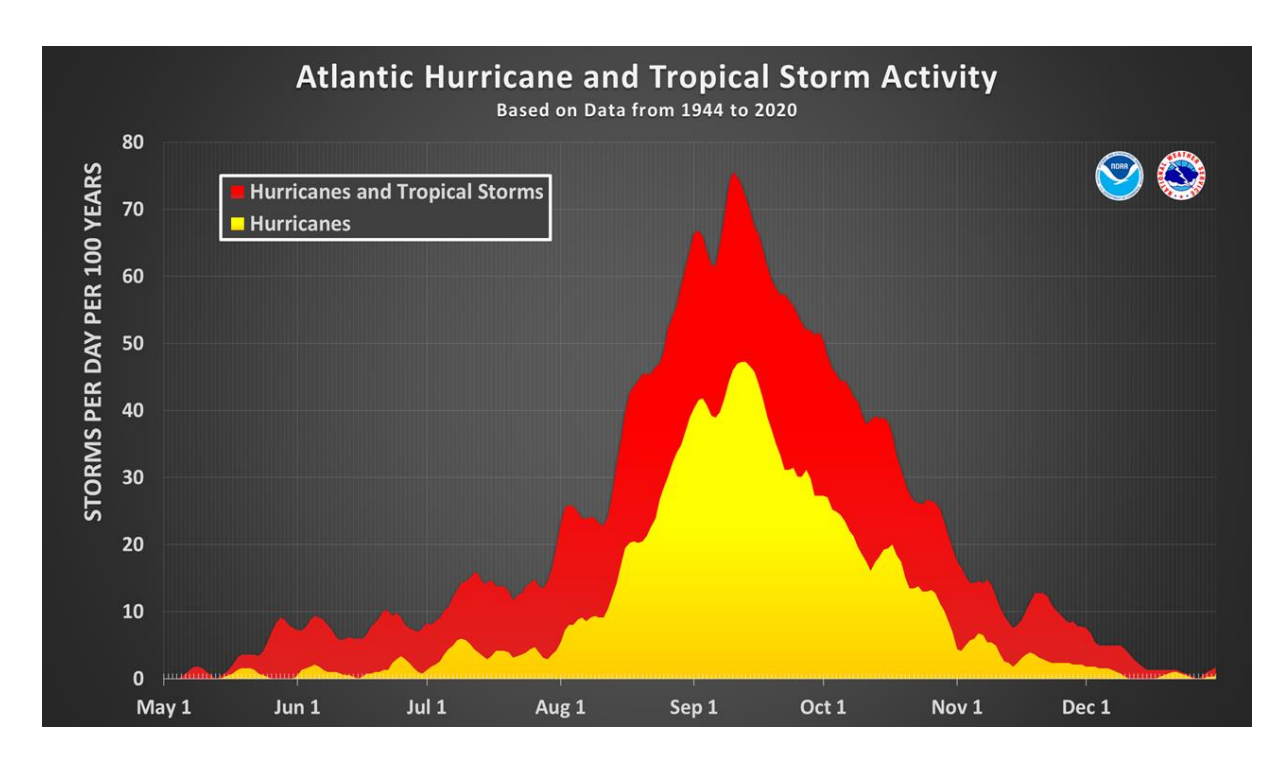


Figure 1.2 Number of Atlantic named storms and hurricanes per 100 years between May 1 and

December 31 based on HURDAT track data 1944-2020, normalized to 100 years, 5
day running average smoothing (NHC, 2023)

1.1.3 Tracks and Landfall

Most Atlantic TCs have formed in a region defined as the Main Development Region (MDR) for Atlantic hurricanes, 10 to 20 0 N, 20 to 80 0 W (Goldenberg et al., 2001). A typical track moves northwest and then recurves in a northeasterly direction (Kossin et al., 2010). TCs are driven by 500 mb steering winds, generally tracking around the edge of the Bermuda-Azores High (George and Gray, 1976). Storms are more likely to form in the Gulf of Mexico earlier in the season, with genesis points moving eastwards and northwards in the open Atlantic, due to the Atlantic Warm Pool of water warmer than 26.5 0 C expanding in these directions as the season progresses (NHC, 2023). Hurricane landfalls in July are more likely to be along the Gulf coast, with hurricane landfalls becoming more likely along other coastlines of the western North Atlantic by August and through October (Figure 1.3). Hurricane landfalls are possible as far north as Canada in August and particularly September. Ocean temperature in the eastern MDR and north of the MDR can be influential in landfall intensity along the US northeast coastline and eastern Canada (Kossin, 2010).

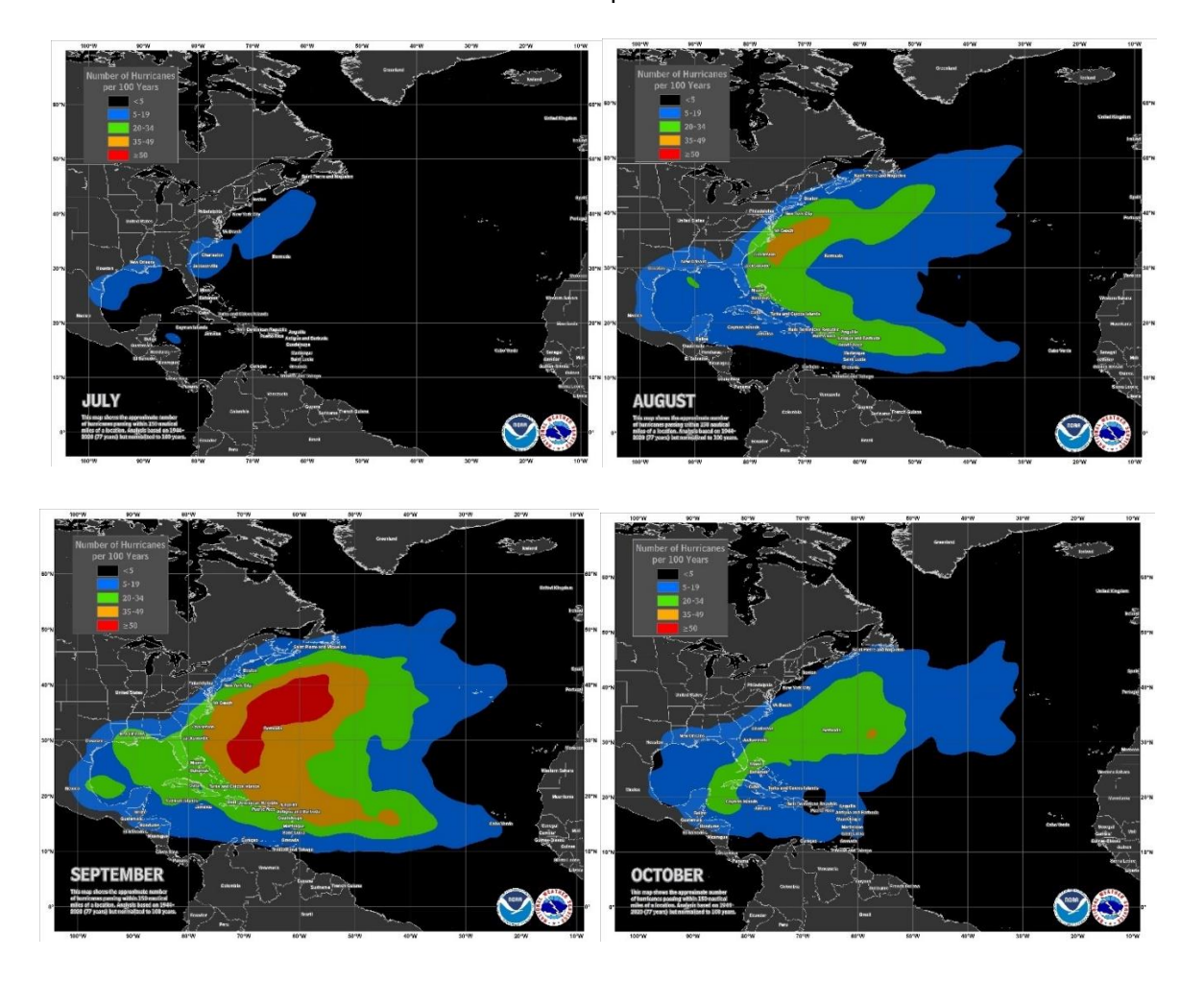
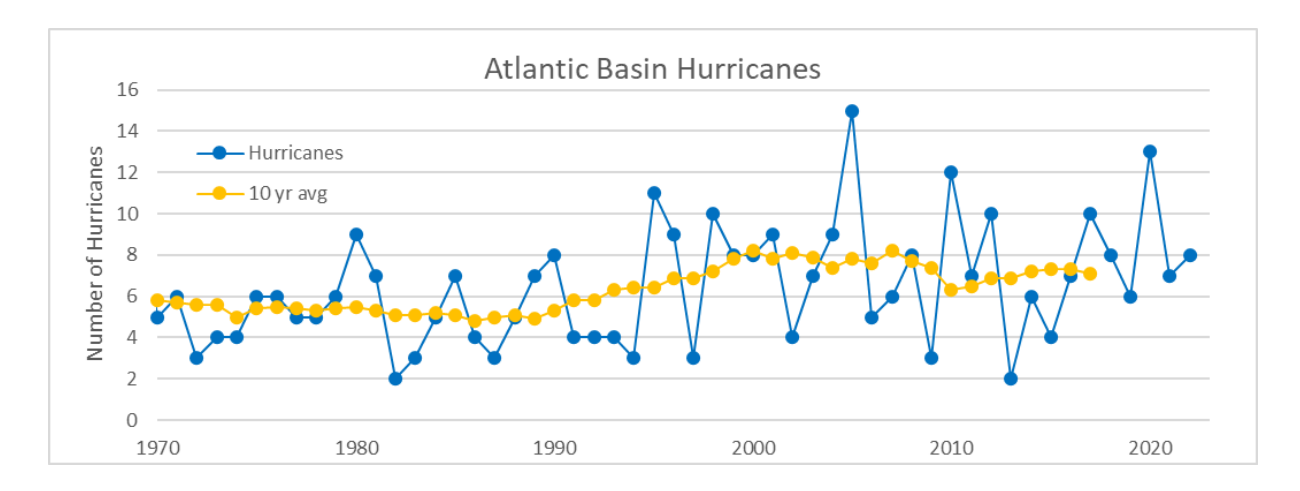


Figure 1.3 The number of hurricanes whose centres pass within 150 nautical miles of a point on the map, using HURDAT track data 1944 to 2020, but normalized to 100 years (NHC, 2023)

1.2 Variability in Hurricane Activity

The NHC database of storm tracks, HURDAT2 (Landsea et al., 2013), covers 1851 to the present. Observational networks have varied significantly during that time. Land-based meteorological station cover has increased over time. Over the ocean, ship traffic has also increased. Measuring equipment of wind speeds, and air and ocean temperature, have become more accurate (Landsea, 1993). Critically for basin activity metrics, satellite-based imagery has allowed collection of much more complete, continuous data over the ocean since the launch of the first geostationary weather satellites in 1966. Landfalling hurricane variability is usually analysed from 1900 (Klotzbach et al., 2018), during which time the US coastline has been fairly continuously populated, and basin activity from 1970, after the dawn of the satellite era. Prior to these dates, some storms are missing in the dataset due to incomplete coverage (Vecchi et al., 2021), particularly by ship traffic which would naturally try to avoid hurricanes where possible. It is important to understand the how the fidelity of the historical hurricane record has evolved through time when analysing trends occurring with changes in ocean heat.

Hurricane basin activity exhibits variability on multidecadal, interannual, and intraseasonal timescales (Figure 1.4). This also varies by landfall region. An anomalously quiet period occurred in the 1970s and 80s (Nyberg et al, 2007). 2004 and 2005 are notable for higher-than-average activity. Landfalling US hurricanes were less common between 2006 and 2017, (Hall & Hereid, 2015), and have been more common since then. There is a slight downwards linear trend in US landfalling hurricane frequency 1900-2022. A downwards but not significant trend with a p value of 0.33 has been calculated by Klotzbach et al. (2018).



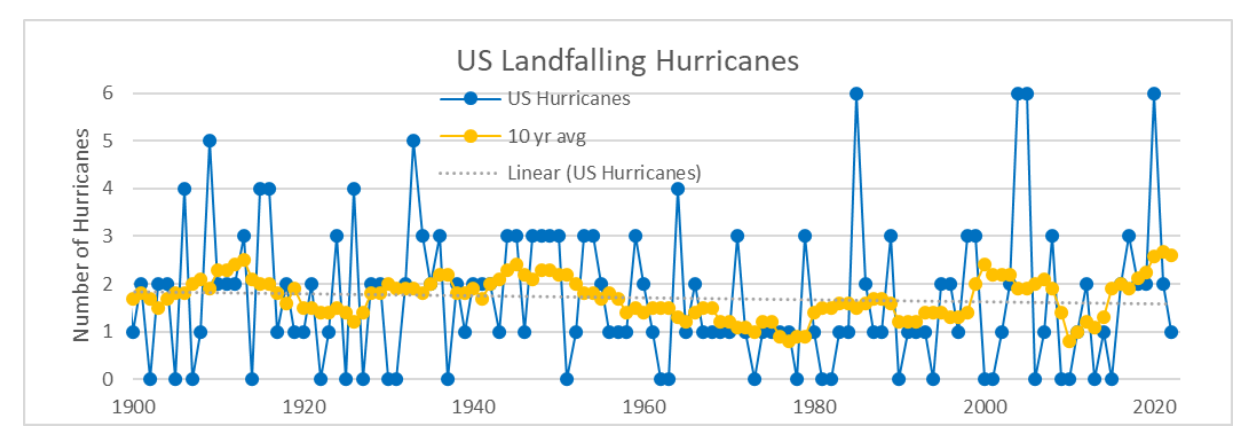


Figure 1.4 Hurricane counts for the Atlantic Basin 1970-2022 (top) and the US coastline 1900-2023 (bottom), and 10-year centred average

Hurricane variability has been linked to large-scale oceanic and atmospheric processes on multidecadal scales, including the Atlantic Meridional Overturning Circulation (AMOC, Xan et al., 2017), and Atlantic Multidecadal Variability (AMV, Zhang et al., 2019), the drivers of which remain under scrutiny. In additional to anomalous heat in the North Atlantic, interannual variability in hurricane frequency is related to the El Niño Southern Oscillation (ENSO), which influences tropical Atlantic wind shear (Lin et al., 2020), and the North Atlantic Oscillation (NAO), which, in a negative phase, is associated with warm MDR SST anomalies and lower vertical wind shear

(Mazza and Chen, 2023). Hurricane tracks also vary with the strength and position of the Bermuda-Azores high (Bell & Chelliah, 2006).

1.2.1 Multidecadal Variability of the Atlantic Ocean

The AMOC is responsible for Ocean Heat Content (OHC) accumulation in the tropical Atlantic (Johns et al., 2023). Dense water at high latitudes of the North Atlantic forms over the Greenland and Iceland seas during cold winters, displacing large volumes of water as it sinks and spreads southwards at depth, creating the overturning circulation (Dickson and Brown, 1994). In the tropics, divergent trade winds cause upwelling of cooler water via Ekman dynamics (Roberts et al., 2013). The western boundary currents of the North Atlantic, the Gulf Stream and the North Brazil Current transport most of the Atlantic Ocean surface heat northwards (Buckley & Marshall, 2016).

The heat content of the MDR is impacted by the strength of the AMOC at these latitudes (Duchez et al., 2016). The slower the AMOC transport is in the months leading up to the peak of the Atlantic hurricane season, the more heat accumulates in this region through heat transfer with the atmosphere (Figure 1.5), rather than being transported to higher latitudes. This dynamic is examined in depth in the following chapters, in which historical and future climate model simulations are analysed on interannual timescales. Changes in the volume of warm water which accumulates in the tropical Atlantic are used to explain hurricane variability from an oceanic heat perspective.

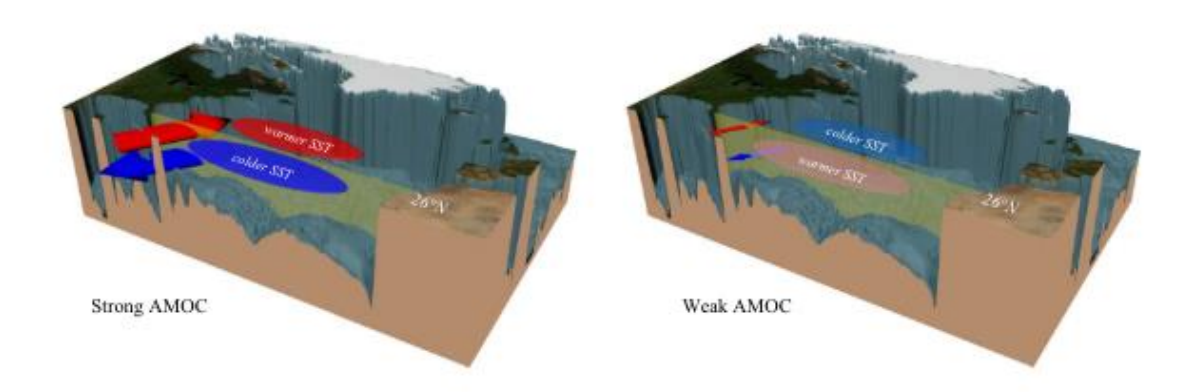


Figure 1.5 AMOC heat transfer dynamics in strong (left) transport regime and weak (right) showing surface northwards (red) and mid-ocean (blue) southwards transport, and the consequences for SST (Duchez et al., 2016)

Atlantic MDR SST has increased 0.8 °C since 1980 (Figure 1.6), which many studies have attributed to multidecadal variability, rather than climate change (Goldenberg et al., 2001).

Enfield et al. (2001) first described the Atlantic Multidecadal Oscillation (AMO), a naturally occurring cycle of SST anomaly patterns to explain variability in US rainfall extremes, which are largely driven by TC precipitation. Later studies (Booth et al, 2012; Dunstone et al, 2013) found that this signal could be replicated in climate models using atmospheric aerosols. They suggest that increasing sulphates and other pollutants caused an anomalously cool period in Atlantic SST by reducing incoming shortwave radiation. The United States Clean Air Act of 1970 reduced atmospheric aerosol content, allowing increasingly warm MDR SST anomalies to develop, after which the impact of anthropogenic climate change could be the driver of unprecedented warm SST since 2000 (Figure 1.6). Recent analyses of Saharan dust (Rousseau-Rizzi et al., 2022) find that associated optical depth variability explains nearly half of the anomalously cool period in the Atlantic.

September MDR SST 10-year smoothing

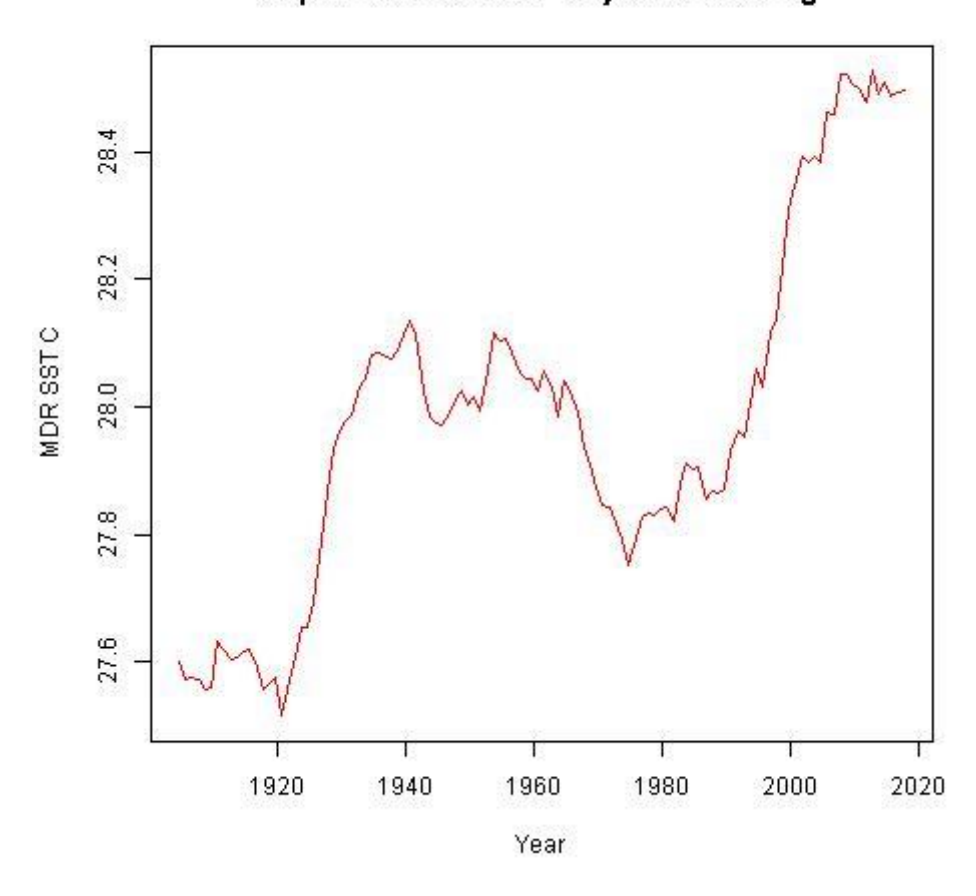


Figure 1.6 NCEP/NCAR September average MDR SST (°C) 1900-2021, 10-year smoothing (Kalnay et al., 1996), emphasising the emergence of anomalous warmth after around 1995.

Other investigations using coupled models suggest that while atmospheric aerosols did contribute to the observed decrease in Atlantic SST in the 1970s and 1980s, changes in ocean circulation do play a role in the development of Atlantic SST anomalies on decadal timescales (Zhang et al., 2019). Smeed et al. (2018) analyse RAPID array measurements of AMOC heat

transport northwards at 26 $^{\circ}$ N, presenting an example on interannual timescales of an AMOC slowdown resulting in anomalously warm Atlantic SST in 2009/10. This decrease in meridional transport across 26 $^{\circ}$ N can be seen in NCEP Global Ocean Data Assimilation System (GODAS, Behringer and Xue, 2004) and RAPID (Cunningham et al., 2007; Kanzow et al., 2009) observational timeseries (Figure 1.7). Resulting warm SSTs contributed to an active hurricane season in 2010, with 12 storms reaching maximum wind speeds of 64 knots, the third most active season during 1970-2022 (Hallam et al., 2019).

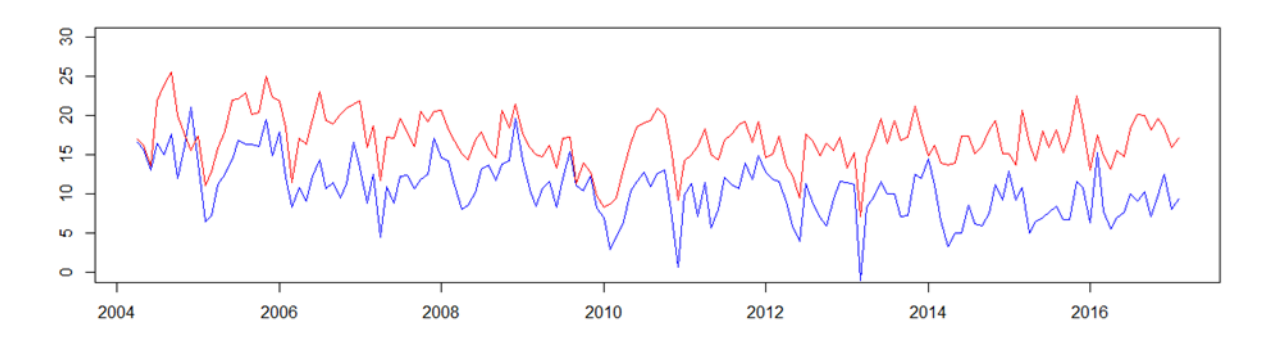


Figure 1.7 GODAS (blue) at 26 °N to 1000 m and RAPID array (red) transport (Sv)

More recent studies have linked the AMO signal with volcanic eruptions (Mann et al., 2021), suggesting volcanic aerosols as the source of reduced heat flux from the atmosphere into the ocean following significant tropical eruptions (Figure 1.8).

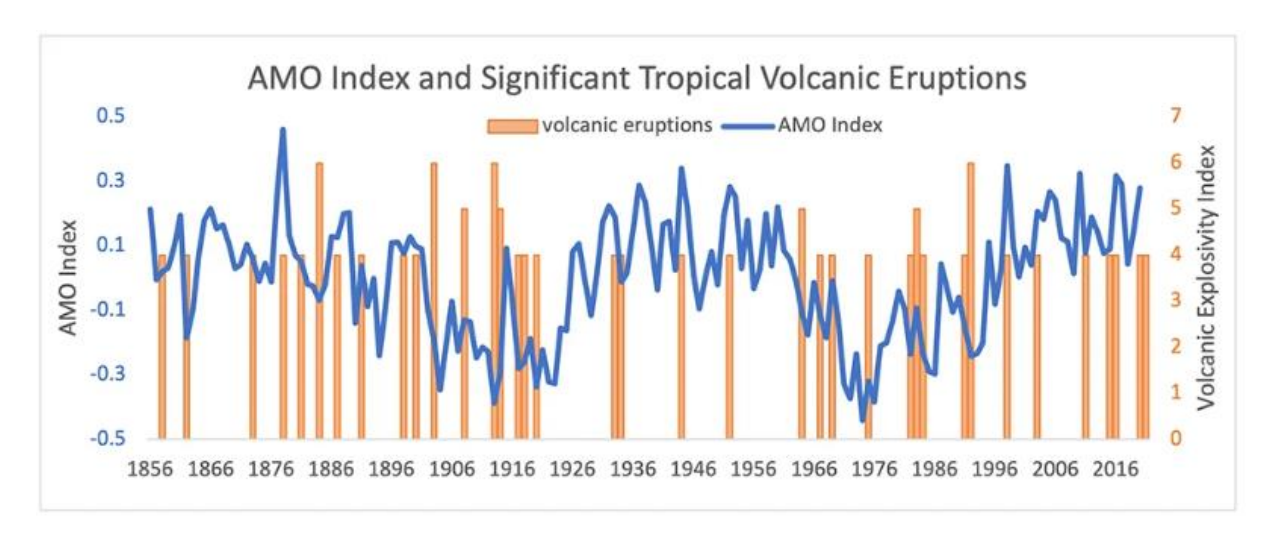


Figure 1.8 AMO Index 1851-2019 and significant tropical volcanic eruptions (Sousounis, 2021)

Regardless whether anomalous atmospheric and oceanic conditions in the Atlantic region are a result of human activity or internal variability, AMV has been noted in connection with many features of the climate system. The AMV signal includes a pattern of warm MDR SST, reduced tropical wind speed, increased specific humidity and lower cloudiness (Yan et al., 2019).

Hurricane activity is closely related to changes in these conditions of the tropical ocean (Figure 1.9).

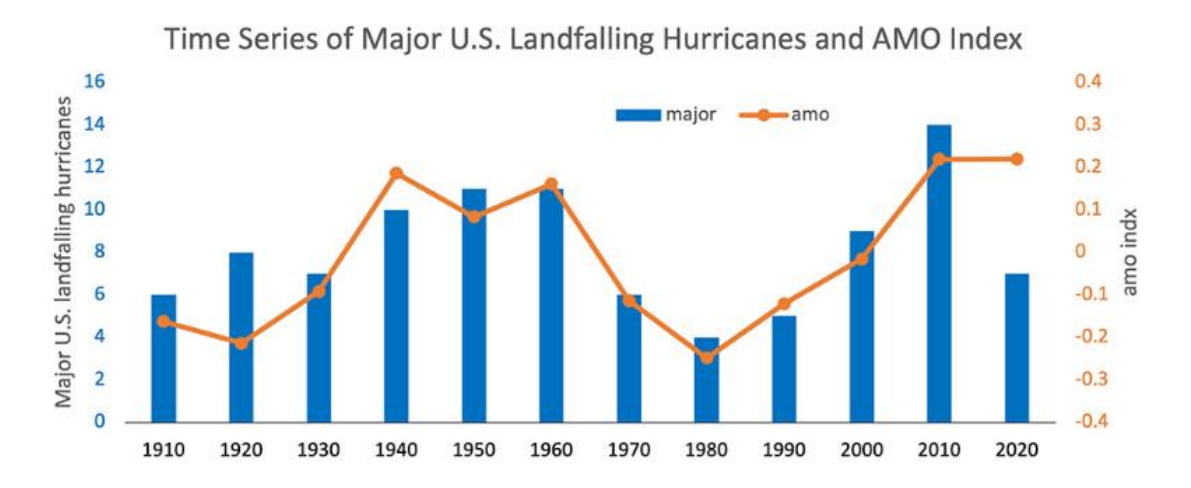


Figure 1.9 Major US Landfalling hurricanes and AMO index by decade (Sousounis, 2021)

1.2.2 Interannual Variability

Atlantic hurricane count per year has ranged from 2 to 15 storms during 1970-2022. ENSO is the climate index most highly correlated with annual hurricane frequency (Lin et al., 2020). As eastern Pacific trade winds slacken, less upwelling occurs off the west coast of South America, and warm SST pools across the central tropical Pacific, with a period of 1-2 years, generally (Wan & Picaut, 2004). This large area of anomalously warm (or cool) water drives climate changes globally. The Walker circulation increases with enhanced convection over the warmer waters of the tropical Pacific. This causes increased vertical wind shear over the tropical Atlantic due stronger upper-level westerly winds, in particular over the Gulf of Mexico, hence limiting conditions conducive to TC development in this region (Klotzbach et al., 2011). Since 1950, there has been an average of 1 US landfalling hurricane when the average August to October ENSO index is in an El Niño state, and an average of 1.9 US landfalling hurricanes when La Niña conditions are present during this time.

NAO conditions of the previous winter have also been observed to be related to Atlantic basin hurricane activity. Trade wind strength is lower with a negative NAO, when the pressure gradient taken between Iceland and the Azores is weaker (McCloskey et al., 2013). Not only is vertical wind shear reduced with lower surface tropical easterly winds, but less divergence in the surface Ekman transport leads to less upwelling of cooler water.

Similarly, the pressure differential between Bermuda and the Azores defines the Bermuda-Azores High. The strength and position of this large high-pressure area in the summer months determines hurricane track and landfall patterns (Knowles & Leitner, 2007). A stronger highpressure area pushes storms along the southern edge into the Caribbean and Gulf of Mexico. Weaker conditions allow for more recurving to the north and east around the western edge; hence, more landfalls are possible along the east coast of the US and Canada. It has been proposed that a warmer Atlantic SST regime results in a weaker Bermuda High and more recurvature of strong storms into the open ocean (Wang, 2011).

An increased understanding of interannual variability in hurricane activity helps society to prepare for potential landfalling events. However, many of these climate conditions have proven difficult to predict very far into the future, and annual hurricane forecasts ahead of the start of hurricane season have shown little skill compared to 10-year climatology (Lea, 2024). However, it is possible that including additional variables could improve seasonal prediction. For example, Atlantic SST anomalies vary somewhat predictably from year to year, as cloudiness inhibits incoming solar radiation, and increased surface divergence drives cooling due to Ekman dynamics. From an ocean heat perspective, quantification of heat convergence due to these processes will provide insight into potentially more predictable seasonal hurricane variability, which is explored in chapters 2 and 3.

1.2.3 Intraseasonal Variability

Within any one hurricane season, there are shorter timescale climate factors which can impact hurricane development. If these impact deep convection during the time when MDR SST is warmest, seasonal activity is affected. If intraseasonal factors enhance convection at the seasonal SST peak, large, intense storms can develop quickly, in quick succession. If factors inhibit convection, systems will not develop into potentially dangerous storms.

The Madden-Julian Oscillation (MJO) is an eastward moving wave of enhanced precipitation with a 30- to 60-day period (Jiang et al., 2020). In MJO phases 1 and 2, convection is enhanced over the tropical Atlantic, during which time several TCs may be spawned in the peak months of hurricane season (Klotzbach, 2010). If the timing of the MJO phases conducive to hurricane development are in phase with the peak of the warmest waters, most of the Accumulated Cyclone Energy (ACE) for the season will occur during this time.

Several past hurricane years which were forecast to have had above average activity proved to be quieter years than expected due to an outbreak of the Saharan Air Layer (SAL) over the tropical Atlantic during the peak of hurricane season. The SAL is dry, dusty, and accompanied by a mid-level jet. Hence, tropical convection is less likely due to cooling of MDR SST by aerosols, higher vertical wind shear, and lower moisture content of the atmosphere (Dunion & Velden, 2004).

In other years, like 2013, while tropical Atlantic SST was anomalously warm, high frequency weather events (e.g. cold fronts) impacted hurricane activity (Klotzbach et al., 2013). While wind shear from approaching cold fronts generally inhibits TC development, in some circumstances, like sub-tropical storms, they can aid intensification (Guishard et al., 2007). Hence, on shorter timescales, the chaotic nature of weather systems can affect tropical Atlantic climate conditions, reducing total seasonal hurricane activity from the level which was expected.

In summary, while hurricane variability is impacted by natural climate variability on a variety of timescales, longer timescale variability tends to be driven by oceanic processes.

1.3 Climate Change and Hurricanes

Anthropogenic carbon dioxide emissions from burning fossil fuels in energy production, industry and transport have exceeded the potential to be absorbed by global forests and oceans for decades (IPCC, 2023), creating a layer of insulation in the upper atmosphere which has trapped outgoing longwave radiation within Earth's atmosphere. The global oceans have absorbed much of this heat (Johnson et al., 2020). Global mean annual SST has increased 0.06 °C per decade since 1900 (Garcia-Soto at al., 2021), with record heat content increase recorded in 2023 (Cheng et al., 2023). The Atlantic has warmed at a faster rate than the global mean; the September mean SST has increased 1 °C since 1900 (Figure 1.6). Drivers of variability including atmospheric sulphate emissions (Booth et al, 2012; Dunstone et al, 2013), ocean-atmosphere heat flux (Mann et al., 2021), and the AMOC (Xan et al., 2017) have been discussed. The impact which the upward trend in Atlantic SST is likely to have had on Atlantic hurricane frequency and severity to date, as well as investigations into the effect of a projected continuing increase in Atlantic SST by the end of the century, will be reviewed in this section.

1.3.1 Observed Trends in Hurricanes

Several studies have analysed trends in tropical storm parameters using global TC track data. These studies have revealed that tropical storm peak intensity has moved polewards (Kossin et al., 2014), forward speed has decreased (Kossin, 2018), the intensity of the strongest storms in the International Best Track Archive for Climate Stewardship (IBTrACS) (Knapp et al., 2010; Knapp et al., 2018) dataset has increased (Holland and Bruyere, 2014, Figure 1.10), and TC precipitation has increased (Hallam et al., 2023). These factors could all potentially contribute to increased risk to human activity if these trends translate to landfalling severe storms. Large, high population density areas are further polewards of the tropics in the North Pacific and North Atlantic.

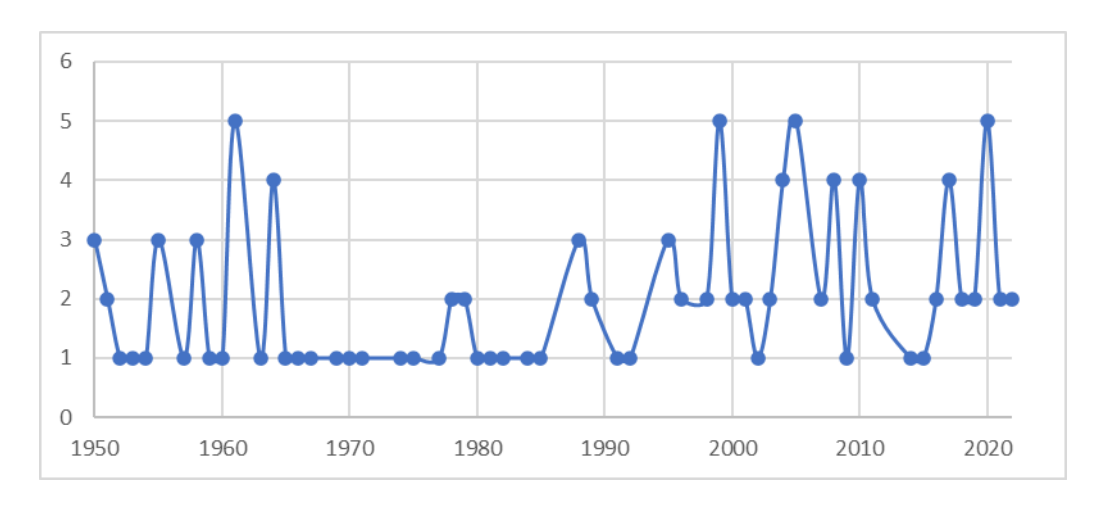


Figure 1.10 Annual number of Category 4 and 5 hurricanes 1950-2022

TC precipitation over land increases with large storms (Lavender & McBride, 2021) which have reached a higher lifetime maximum intensity (Touma et al., 2019), have a slower translation speed at landfall (Titley et al., 2021), and are impacted by orographic uplift in the vicinity of mountains (Houze, 2012), which also tend to be closer to more northern areas of the North American coastline. It has been argued that TC translation speed has decreased due to a slowdown in global atmospheric circulation (Kossin, 2018), which would have increased TC flood footprints over land. A larger pool of warm water available for TC development increases the region able to sustain TCs further north and east (Wang et al., 2011), as warmer SSTs provide fuel and vertical instability for stronger storms. A warmer atmosphere is capable of holding more moisture; the Clausius-Clapyron equation shows that the atmosphere can absorb 7% more water with a 1 °C increase in surface air temperature. However, Hallam et al. (2023) show that the recent increase in TC rain rate has been much greater than this, due to other changes in TC behaviour, like increase in size and intensity. The dynamics underlying some of these concepts are clearer than others, and historical data is complicated by internal variability. Furthermore, there is only a fairly short record of accurate historical data points, complicated by the chaotic nature of atmospheric events, Nevertheless, past trends are one representation of actual climate behaviour, and are an important test to validate climate models. However, increasing global temperatures (IPCC, 2023) and potential tipping points in atmospheric and oceanic feedback mechanisms (van Westen at al., 2024) may materially alter dynamics going forward.

Extending trends in global basin activity to landfalling severe storms is complicated by changes in both climate variability and in the observational record in both the Atlantic and the Pacific. Additionally, there may have been changes in storm track with a warming atmosphere and ocean, affecting the percentage of storms which make landfall. It has been suggested that storms are more likely to recurve into the open ocean when the AMO is positive (Wang et al., 2011). Uncertainty in trends in he number of landfalling hurricanes in some regions is very high

due to reduced sample size (Dailey et al., 2009). Annual US landfalling hurricane count over 1900-2022 has no significant upwards or downwards trend (Figure 1.4). However, the 4 years with the highest number of landfalls, 6 in one season, have all occurred during the last 40 years.

While analysis of global TC data by basin has yielded some interesting trends in storm metrics, it remains unclear how much can be attributed to climate change, internal variability, atmospheric sulphate emissions, or observational network changes, particularly as many global trends are driven by multidecadal variability of Atlantic SST. Hence, further analysis of the drivers of anomalous Atlantic SST can help answer some important questions about likely hurricane activity in today's climate and potential for the future by extrapolation of recent trends. This is addressed in chapter 4.

1.3.2 Climate Model Projections

Numerical weather prediction for weather forecasting, including hurricane track (Landsea & Cangialosi, 2018) and intensity (Cangialosi et al., 2020), has yielded increasingly reliable forecasts extending several days. On longer timescales, increasing horizontal, vertical, and temporal resolution for climate modelling has been shown to represent internal climate variability more accurately in hindcast simulations (Roberts et al., 2019) than lower resolution configurations. Climate conditions conducive to TC development can be identified in climate models, specifically tropical Atlantic and Pacific SST and atmospheric moisture content. As in the current climate (Patricola et al., 2022), future states of AMV and ENSO will likely determine the frequency and severity of hurricanes with climate change.

Tropical cyclones generated by high resolution climate models decrease in frequency as global temperature increases in climate change projections (Roberts et al., 2020). Major hurricanes, however, are still not resolved at the grid resolution of even high-resolution climate models, though the intensity of these tropical cyclones is a marked improvement on previous lower-resolution climate models (Davis, 2018; Roberts et al., 2020). Downscaling techniques have been used to spin up hurricanes from projected climate conditions (Emmanuel, 2021), which suggest increasing frequency and severity. Tropical cyclone frequency is not that well understood (Sobel et al., 2021), but the driver of Atlantic tropical cyclone frequency is more likely the temperature differential between the tropical Atlantic and tropical Pacific, than the absolute temperature of the tropical Atlantic, as tropical instability in the Atlantic increases with warmer surface layers in addition to lower vertical wind shear as a result of a cooler tropical Pacific (Murakami et al., 2018).

Atlantic SST and the Atlantic Warm Pool increase in surface extent and depth in global coupled climate models forced with greenhouse gas emissions (Cheng et al., 2022), despite generally

cold or warm biases, which suggests increasing severity of hurricanes with further warming of the planet. The tropical North Atlantic could begin to warm much more quickly than has been observed to date, with slower northwards heat transport via the AMOC (Madan et al., 2024).

Tropical Pacific SST will also be impacted by a warmer climate. Model based studies mainly agree that interannual variability of ENSO amplitude will continue to increase in the future (Cai et al., 2021; Cai et al., 2023), which would impact interannual hurricane variability. Furthermore, studies have shown that spatial variations in El Niño events impact Atlantic hurricane frequency differently; a central Pacific El Niño does not generate as much wind shear over the western Atlantic as an eastern Pacific El Niño (Mueller et al., 2024).

Considering expected changes in all variables impacting hurricane development, the IPCC (2023) has concluded in the most recent report that hurricane frequency will decrease, and intensity of the strongest storms will increase. Further analysis of existing model output to identify oceanic and atmospheric drivers, and development of increasingly high-resolution models which will overcome existing model biases and can spatially resolve intense hurricanes, would likely increase confidence in projections of future activity.

1.4 Summary

Given the importance of tropical Atlantic SSTs in the development of TCs, the following chapters analyse historical and future climate model data to determine the drivers of tropical Atlantic OHC, using novel techniques. The drivers are associated with changes in either air-sea interaction, the ocean circulation or both (Figure 1.11). In Chapter 2, the Water Mass Transformation framework is used as a tool to diagnose the volume of water transformed across the critical temperature threshold for hurricane development. This is related to month-to-month changes in the total volume of water above the temperature threshold and attributed to air-sea heat fluxes. This mechanism explains warm water development for some hurricane seasons but not every year, indicating that oceanic processes (advection and mixing) also contribute to the development of warm water to fuel hurricanes.

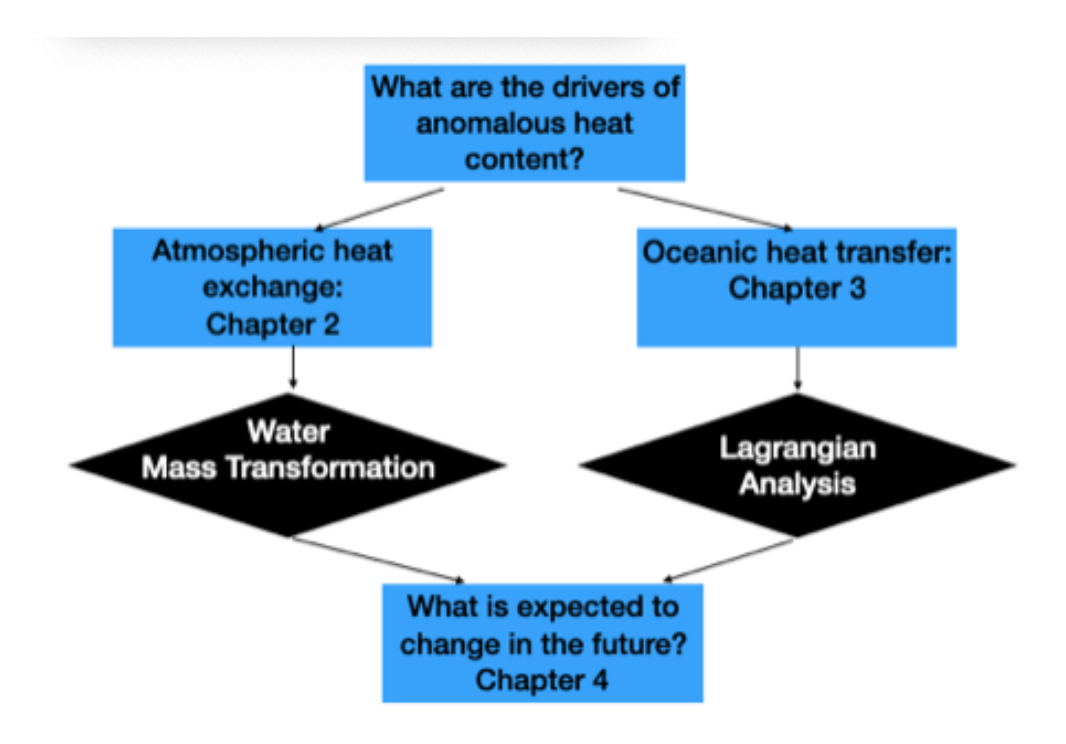


Figure 1.11 Tropical Atlantic anomalous heat content investigation identifying the main open question identified in this thesis, components which are investigated, the methods used, and how these feed into the final results chapter

Chapter 3 traces warm water in the MDR backwards over a 6-month period, to examine potential heat sources in the region. The study suggests that the major heat source for active hurricane seasons is the MDR itself, as in situ water from slower-moving Ekman drift across 10 °N absorbs more heat from the atmosphere.

To consider how these processes might evolve in a warming climate, Chapter 4 applies the techniques in the previous two chapters to an eddy-resolving, high resolution coupled ocean model.

Chapter 5 synthesises the results of the previous chapters. Contributions of this work to the state of the science surrounding the atmospheric and oceanic dynamics behind the development of warm water available for hurricane development will be summarised. Potential future work will be suggested which could increase understanding of this problem and societal preparedness for these disasters.

Chapter 2 The Water Mass Transformation Framework and Variability in Hurricane Activity

Abstract

Hurricane activity has been higher since 1995 than in the 1970s and 1980s. This rise in activity has been linked to a warming Atlantic. In this study, we consider variability of the volume of water warmer than 26.5 °C, considered widely to be the temperature threshold crucial to hurricane development. We find the depth of the 26.5 °C isotherm better correlated with seasonal hurricane counts than SST in the early part of the Atlantic hurricane season in some regions. The volume of water transformed by surface heat fluxes to temperatures above 26.5 °C is directly calculated using the Water Mass Transformation framework. This volume is compared with the year-to-year changes in the volume of water of this temperature to see how much of the volume can be explained using this calculation. In some years, there is notable correspondence between transformed and observed volume anomalies, but anomalies in other years must be largely associated with other processes, such as the divergence of horizontal heat transport associated with the AMOC. This technique provides evidence that, in a given year, coordinated physical mechanisms are responsible for the build-up of anomalous ocean heat; not only net surface heat exchange but also the convergence of horizontal heat transport from ocean currents, to provide fuel for larger numbers of intense hurricanes.

2.1 Introduction

Recent North Atlantic hurricane seasons have produced several high impact hurricanes, including Harvey, Irma, and Maria in 2017, Florence and Michael in 2018, and Dorian in 2019, which resulted in 335 billion USD damage and over 3,000 deaths (NCEI, 2020). Questions remain open on drivers of high activity seasons. Variability in hurricane activity on a range of timescales has been linked to large scale climate oscillations, including the AMO (Goldenberg et al. 2001), or AMV (Zhang and Delworth, 2006), ENSO (Bove et. al, 1998), the NAO (Elsner and Jagger, 2004), the Quasi-Biennial Oscillation (QBO) (Gray, 1992), as well as variations in atmospheric aerosols (Evan et al., 2009), including dust (Wang, 2012), volcanic emissions (Birkel et at., 2018), and pollution (Watanabe and Tatebe, 2019).

On interannual timescales, the Atlantic hurricane season is subject to variable atmospheric processes. For example, Atlantic hurricane variability is negatively correlated with El Niño indices, as anomalously warm tropical Pacific SSTs result in higher-than-average vertical wind

shear in the tropical Atlantic, which inhibits vertical motion necessary for Atlantic hurricane formation (DeMaria, 1996). On timescales longer than interannual, slower modes of ocean variability are important. Associated with warmer ocean temperatures in the tropical North Atlantic is an increase in available energy in the upper ocean to fuel hurricane development (Shapiro and Goldenberg, 1998).

Much attention has focused on the role of oceanic warmth as a driver of Atlantic hurricane seasons, on a range of timescales. SST has been found to be more highly correlated with hurricane intensification than thermocline depth over most of the North Atlantic (Balaguru et al., 2013). However, it is likely that in some regions, the volume of potentially hurricane-producing water may be a more physically meaningful metric than area-averaged SST. For example, intensity estimates of tropical cyclones around Bermuda were improved by use of subsurface temperatures rather than SST alone (Hallam et al, 2021).

Other investigations have found a meaningful role for aerosol concentration in multidecadal warming of the North Atlantic. This result has been simulated in climate modelling studies (Booth et al., 2012) due to variation in anthropogenic aerosols, and point to an influence on tropical cyclone activity (Dunstone et al., 2013). A modelled increase in anthropogenic sulphate aerosols can explain much of the observed cool period in the 1970s and 80s in the North Atlantic (Watanabe and Tatebe, 2019). Mann (2021) now suggests that multidecadal variability in Atlantic SST is mainly driven by volcanic activity, and finds no evidence for internal variability.

Rather than suggesting large-scale physical mechanisms for heat transfer into the ocean, this study directly quantifies the contribution of surface heat flux (Q_{net}) processes to the variability of warm water volume available for hurricane development through the holistic Water Mass Transformation (WMT) framework (Groeskamp et al. 2019). The volume of water transformed across isotherms through Q_{net} is calculated using WMT. Accumulated transformation fluxes over a time interval are compared with observed changes in volume of water above a temperature threshold over the same interval.

This approach has the advantage of referencing the total volume of water above a temperature threshold intimately connected with hurricane development, 26.5 °C (of enduring practical use as the temperature threshold for tropical cyclogenesis – see McTaggert-Cowan et al. 2015 and references therein), geographically confined to the Atlantic. This removes limits of fixed latitude and longitude, as for the conventional MDR (Goldenberg et al., 2001), generally defined as 10-20 °N, 20-80 °W.

Oceanic conditions which sustain hurricane winds are not constrained to the MDR. In particular, warm water availability outside this region is one factor which could result in major

hurricane landfall further north. Wang et al. (2011) investigated the areal extent of the Atlantic Warm Pool and correlation with hurricane activity, emphasizing the importance of the Atlantic Warm Pool to the west of the MDR, extending across the Caribbean and the Gulf of Mexico. In summary, we quantify Atlantic Warm Pool volume anomalies attributed to anomalous air-sea interaction, with residual Atlantic Warm Pool volume anomalies attributed to a combination of mixing and advection.

The rest of the paper is organized as follows. In Sections 2 and 3, we outline the WMT framework used in temperature space, and the datasets used here. In Section 4, we present our results, starting with an overview of changes in the volume of warm water and hurricane activity over the last 40 years. We then outline the WMT at temperatures relevant to hurricane formation. Using this approach, we attribute changes in the volume of warm tropical waters directly to anomalous surface fluxes, and further consider the extent to which anomalous surface fluxes drive enhanced warm water volume in specific years, when hurricane activity was particularly intense. In Section 5, we conclude with a discussion of the extent to which our findings inform the wider efforts to associate active hurricane seasons with a warming tropical Atlantic.

2.2 Methods

In this section, the calculations used to quantify the volume of water warmer than 26.5 °C, generated from net surface heat flux using the WMT framework, are described. Returning to the original formulation of Walin (1982), the WMT framework (Groeskamp et al. 2019) can be applied in temperature space, quantifying volume fluxes across isotherms which are associated with variations of heat fluxes in that property space.

The net surface heat flux, Q_{net} , combines radiative processes with turbulent fluxes. Shortwave (Q_{sw}) radiation is absorbed from the sun and net longwave (Q_{tw}) radiation is obtained by balancing upwelling and downwelling heat fluxes. Sensible heat (Q_{sh}) is transferred directly between the ocean surface and the atmosphere, and latent heat (Q_{th}) flux transfer results from evaporation, which cools the ocean, and condensation, which transfers heat into the ocean. These processes are depicted schematically in Figure 2.1, for a region warmer than 26.5 °C in the North Atlantic, along with heat transfer by vertical mixing and ocean currents, such as those associated with the Atlantic Meridional Overturning Circulation (AMOC). Throughout this study, our convention is that heat flux components are positive into the ocean, hence the net surface heat flux follows as:

$$Q_{net} = Q_{sw} + Q_{lw} + Q_{sh} + Q_{lh} \tag{1}$$

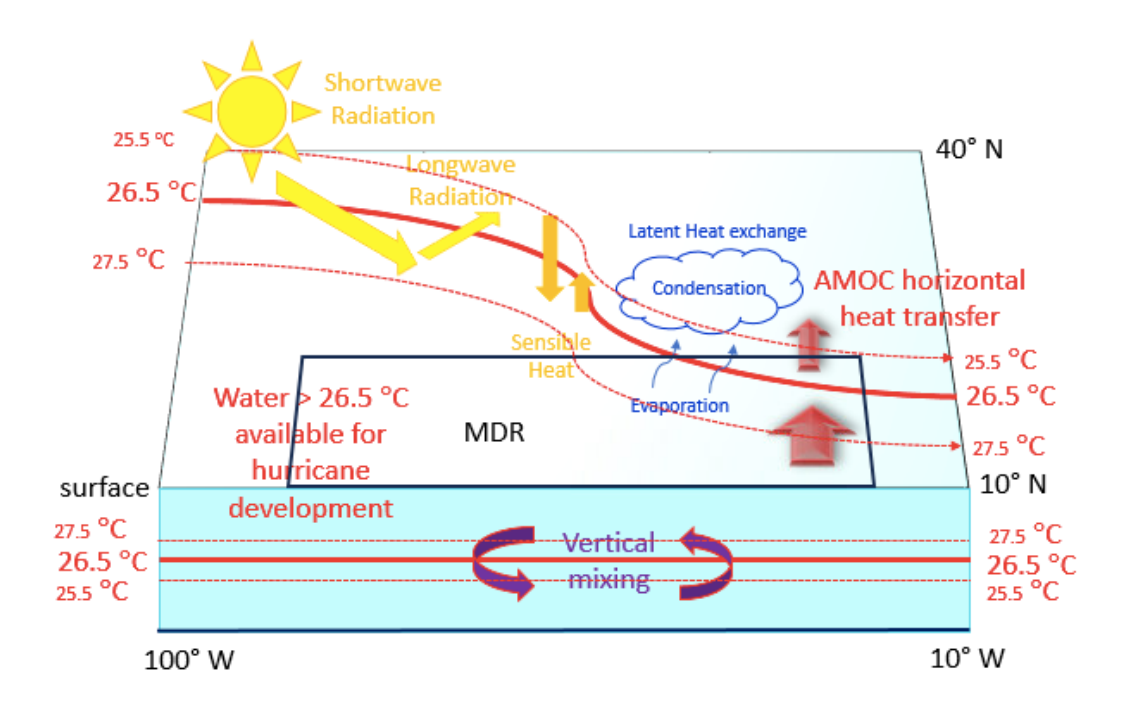


Figure 2.1 Heat transfer mechanisms leading to water warmer than 26.5 °C, critical to hurricane development, in the region southwards and upwards of thick red lines.

In Figure 2.2, we show the long-term annual and April-September mean Q_{net} , across the tropical and subtropical North Atlantic. In most months, heat is lost to the atmosphere from the warm tropical surface waters of the MDR, particularly through the winter. The annual-mean heat flux is consequently negative across most of the MDR (Figure 2.2a), although there is some net warming during April-September, most notably in the eastern MDR (Figure 2.2b). It follows that years with less heat loss from the ocean, through these processes, will result in more water being transformed to warmer temperatures which can support potential hurricane development.

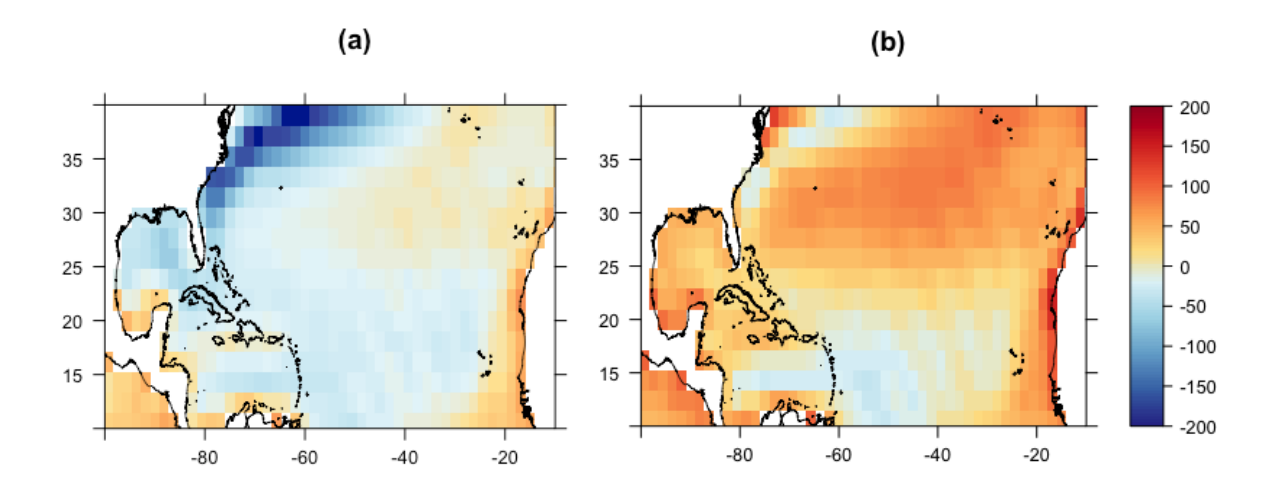


Figure 2.2 NCEP 1980-2019 Mean Q_{net} (Wm⁻², positive into the ocean), MDR outlined in red: (a) Jan-Dec, (b) Apr-Sept.

Groeskamp and ludicone (2018) discuss the influence of Q_{sw} depth penetration for WMT due to the redistribution of heat with depth. In relation to local optical properties (notably related to the local concentration profile of chlorophyll-a) and thermal stratification, a small percentage of shortwave radiation will be absorbed at slightly lower temperatures. However, accounting for typical chlorophyll-a levels and globally averaging, they estimate that only around 3.3% of shortwave radiation is absorbed below the mixed layer. Even given relatively shallow mixed layer depths in our region of interest – from a summer minima of typically 20 m to a maxima of around 40 m in the eastern tropics and around 100 m in the western tropics (Holte et al., 2017) – this percentage is apparently also small across the tropical Atlantic, where 2-6% of shortwave radiation is absorbed below the mixed layer (Groeskamp and Iudicone, 2018). We therefore adopt the conventional approach (Grist et al., 2014) of assuming all net Q_{sw} is absorbed at the surface, with negligible shortwave transmission and absorption beneath the surface. The calculated change in water mass volume is thus associated with the net heating of the surface in the region of interest.

The volume of water transformed across isotherms by Q_{net} is calculated over the North Atlantic, north of 10 °N, where there is sufficient Coriolis force for tropical storm spin up. Firstly, the diathermal temperature flux, Q_{in} (T) (°C m³ s⁻¹) (2), is found by area-integrating Q_{net} , where SST is at or above a given value of temperature, T, then dividing by reference density, ρ_o , and specific heat capacity, c_p , where that isotherm is outcropped.

$$Q_{in}(T) = \frac{1}{\rho_o c_p} \int_{x_w}^{x_e} \int_{y_s}^{y_n} Q_{net}(x, y) \Gamma(SST(x, y), T) dx dy \quad (2)$$

where x, y are distance in west (w) to east (e) and south (s) to north (n) directions, integrating from a west limit (x_w) to an east limit (x_e) , and from a south limit (y_s) to a north limit (y_n) , and Γ is a sampling function; $\Gamma = 1$ where SST > T, otherwise $\Gamma = 0$; Q_{net} values at the selected temperatures are found using bilinear interpolation between both latitude and longitude points of the gridded data at each depth level. The diathermal temperature flux is proportional to the heat flux across a selected isotherm but constructed as a temperature flux to obtain a diathermal volume flux, as outlined below.

The diathermal volume flux, or thermal water mass transformation rate, F_T (T) (m³ s⁻¹), can then be arrived at by taking differences between Q_{in} (T) across two temperature surfaces.

$$F_T(T) = \frac{Q_{in}(T - \Delta T/2) - Q_{in}(T + \Delta T/2)}{\Delta T}$$
 (3)

where Q_{in} is calculated at temperature intervals of ΔT . This transformation rate is equivalent to rate of change of the volume of water with temperature exceeding T.

In this way, the volume of water transformed via surface heat fluxes across a particular temperature threshold can be calculated for each month. Other processes playing a role in WMT are considered as the residual of observed volume anomalies after water transformed by surface heat fluxes is accounted for. An additional advantage of the WMT framework is that changes in water mass properties can be analysed without the limitations of an arbitrary reference temperature otherwise used in the calculation of OHC (Holmes et al., 2019).

2.3 **Data**

The National Center for Environmental Prediction/National Center for Atmospheric Research (NCEP/NCAR) reanalysis (Kalnay et al., 1996) is used for monthly mean values of heat transfer from the atmosphere into the ocean from 1980 through 2019 in order to calculate Q_{net} anomalies. Wind speed and cloud cover values used in further analysis are also from this source. Incorporating all available observational data, the reanalysis product consists of data at 2.5 ° horizontal resolution from 1950 onwards. Previous similar uses of this reanalysis data in the WMT framework include studies of the subtropical and subpolar North Atlantic (Grist et al. 2014).

The NCEP Global Ocean Data Assimilation System (GODAS) ocean reanalysis product (Behringer and Xue, 2004) contains gridded global potential temperature at 40 discrete depths, at 1/3 ° latitude and 1 ° longitude spacing, from 1980 to present. It is important to note that observations assimilated into these products are increasingly scarce with depth and further back in time, so the degree of constraint afforded by the observations will vary in a corresponding manner. GODAS potential temperatures are used to calculate observed volume anomalies of water warmer than 26.5 °C.

The US NHC tropical cyclone data, HURDAT, was used to obtain annual hurricane counts and location of the onset of hurricane force winds. This dataset includes storm centre coordinates and maximum winds at 6 hourly intervals over the ocean. These wind speeds are rounded to the nearest 5 knots. This data has been incorporated in a global tropical cyclone dataset in a standard format, maintained by the International Best Track Archive for Climate Stewardship (IBTrACS) (Knapp et al., 2010, Knapp et al., 2018).

Ocean heat transport across 26.5 °N from the RAPID-MOCHA array 2004-2018 (Cunningham et al., 2007; Kanzow et al., 2009) is comprised of 4 components. Gulf Stream transport is measured by the amount of electrical current generated by flow across an underwater cable

which runs between Florida and the Bahamas. Ekman transport is derived from satellite scatterometer surface wind observations. The southward mid ocean transport is calculated using current meters at shallower depths. Further down the water column, current is calculated from temperature and salinity measurements at various depths by zonally integrating the geostrophic profile. Instruments are attached to a variety of deep-water moorings spanning 26.5 °N.

2.4 Results

We first summarise the extent to which warm water volume and hurricane activity have covaried since 1980. We then introduce the WMT framework in temperature space, applied to the warm water pool. Over our study period, we present evidence of a leading role for surface fluxes as the dominant driver of anomalous upper ocean warmth in several years of the last four decades.

2.4.1 Warm Water Volume and Hurricane Activity

North Atlantic hurricane activity has generally been above the 1970-2019 average of 6.2 hurricanes per year since 1995, with an average of 7.5 hurricanes per year 1995-2019. This is 50% higher than the mean of 5 hurricanes per year during 1970-1995 (Figure 2.3). In only 6 of the 25 years during 1995-2019 was annual hurricane activity below the 1970-2019 mean, aligned with the GODAS volume anomalies zero-line in Figure 2.3. Recent years with the highest annual hurricane counts include 2005 and 2010. Anomalous volume of water warmer than 26.5 °C in the North Atlantic shows similar multidecadal variability, with warm episodes becoming more frequent after 1995. While the most active years don't always occur when the volume of water warmer than 26.5 °C is highest, due to, for example, the important role of vertical wind shear (DeMaria, 1996), active years have become more frequent during this recent regime of a larger volume of warm water. The annual average anomalous volume water warmer than 26.5 °C is positively correlated with annual Atlantic hurricane count, with a Pearson correlation coefficient of 0.42, statistically significant at the 99% level.

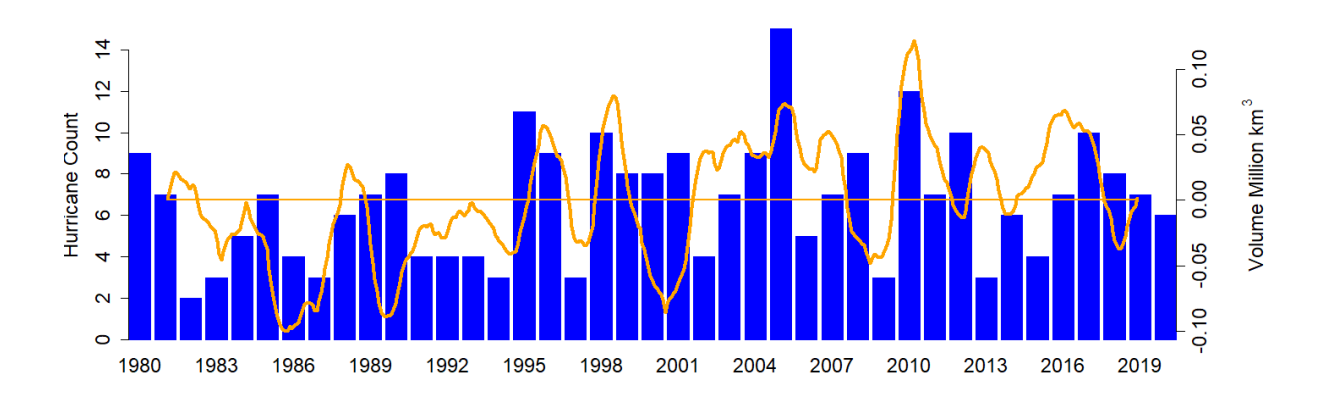


Figure 2.3 HURDAT Annual North Atlantic Hurricane count (blue bars) and GODAS volume anomalies of water warmer than 26.5 °C in the Atlantic north of 10 °N 1980-2019, applying 12-month centred moving average (orange line). For GODAS volume anomalies, the zero-line is aligned with the mean hurricane count.

The relationship between Atlantic SST and seasonal hurricane counts is well established (Goldenberg et al., 2001; Gray et al., 1992; Wang et al., 2012). Rather than SST, we however find better correlation between the depth of the 26.5 °C isotherm (Z26.5) at each grid point with North Atlantic basin seasonal hurricane count, in some regions of the North Atlantic in the spring. This is most clearly seen in April (Figure 2.4a), focussed in the tropics at 60 °W. These correlations are significant at the 95% level, as indicated by stippling on the plots. This finding is in line with studies which highlight the importance of OHC as a hurricane intensity forecasting tool (Mainelli et al., 2008).

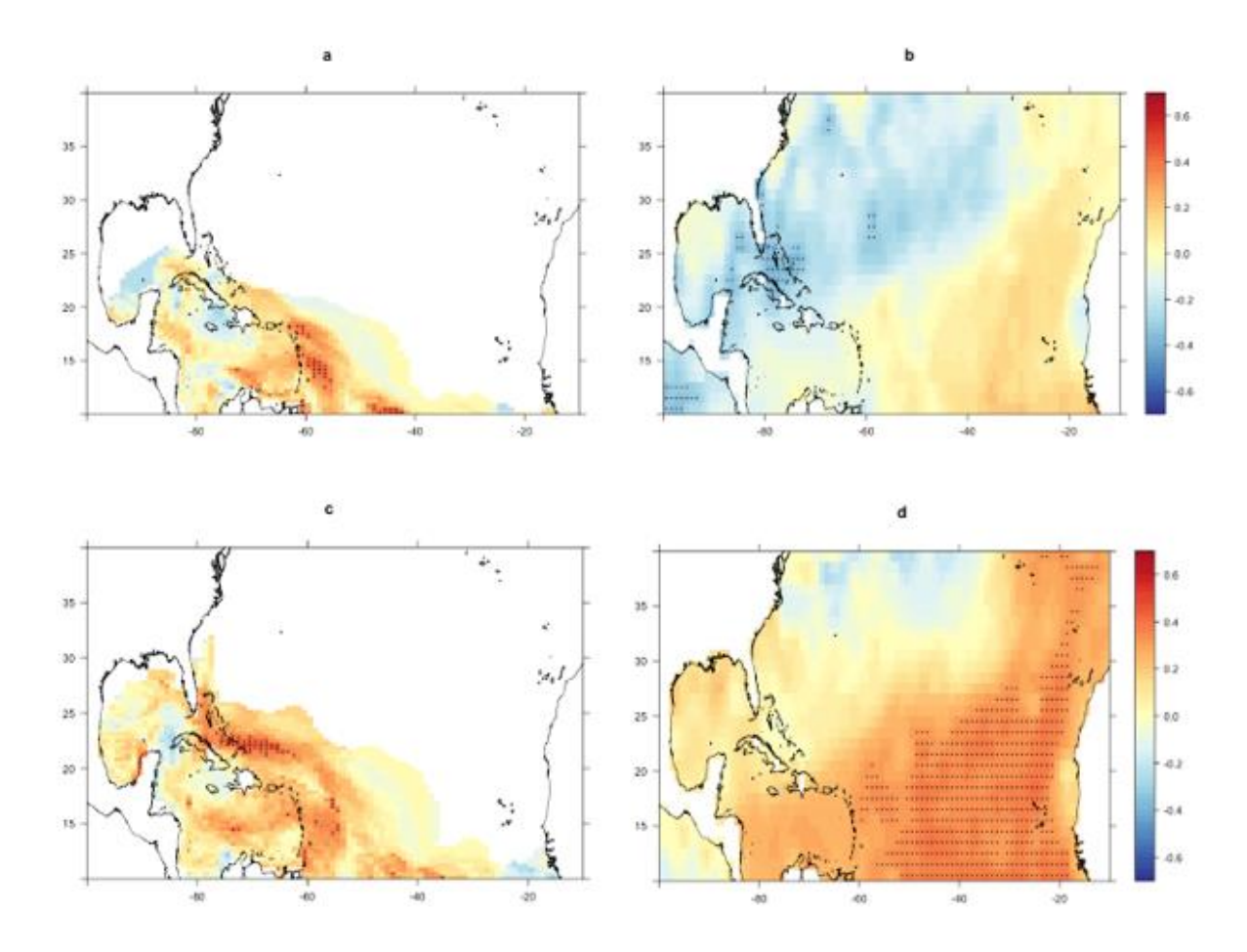


Figure 2.4 Pearson correlation coefficient between Atlantic basin seasonal hurricane count 1980-2019 and depth of the 26.5 °C isotherm in different months: (a) r(Z26.5, hurricane count), April; (b) r(SST, hurricane count), April; (c) r(Z26.5, hurricane count), May; (d) r(SST, hurricane count), May. Stippling indicates 95% significance level.

Local SST correlation patterns with seasonal basin hurricane count show the pattern typical of AMV, particularly by May (Figure 2.4d), where value are higher in the tropics and eastern Atlantic, and lower in the subtropical gyre. Areas of deep warm water in the spring indicate water warm enough to sustain tropical development early in the Atlantic hurricane season, which is likely to increase total hurricane count for the year by adding early season storms and suggests a deeper pool of warm water will be available later in the season.

These correlations were examined in detail to see if better correlation existed between early season hurricane count (hurricanes forming before July 1) and 26.5 °C isotherm depth in a particular month (April or May for example), than hurricane counts for the whole season, but that did not seem to be the case. This observation implies that early season hurricanes are not driving the correlation. As the sample size of these hurricanes since 1980 is quite small (8 hurricanes), it is unlikely that a high correlation would be observed. Indeed, some of these early

season storms are generated from unusual atmospheric conditions rather than underlying oceanic heat. One example is Hurricane Alex, which formed in January 2016 from an extratropical low (Jesús González-Alemán, 2018).

2.4.2 Characteristics of Water Mass Transformation

Surface WMT calculates the rate that water masses are transformed across isotherms by heat transfer between the ocean and the atmosphere. A North Atlantic WMT climatology shows the transformation rate across all isotherms found in the North Atlantic, from 0 °C to 31 °C (Figure 2.5). The climatology is consistent with annual net cooling and warming in different temperature ranges. Surface water is transformed by Q_{net} across isotherms: towards cooler temperatures in the range 0 to 27 °C, where Q_{net} < 0; towards higher temperatures between 27 °C and 30 °C, where Q_{net} > 0. The latter temperatures are of particular relevance to hurricane and major hurricane development. This indicates that in general, local surface fluxes act to increase the volume of water warmer than 27 °C.

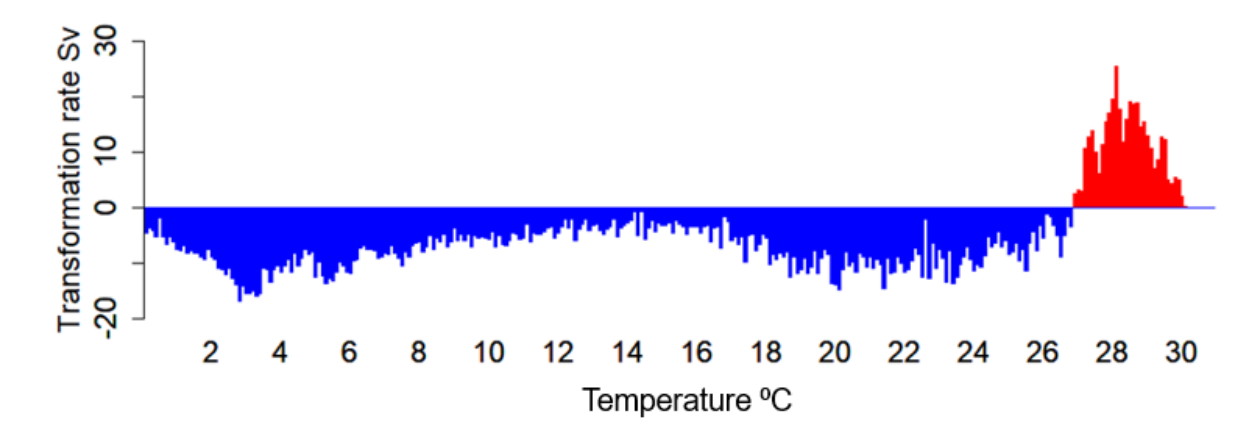


Figure 2.5 Annual-mean transformation rate (Sv) for the Atlantic north of 10 °N as a function of SST 1980-2019, given diathermal temperature fluxes at 0.25 °C intervals; positive values imply transformation of water towards higher temperatures has occurred over the period.

In general, WMT produces distinct water masses via either warming or cooling while other processes act in the opposite sense to mix or homogenize the distribution in Figure 2.5. Transports across lateral boundaries (in particular 10 °N) import and export water masses in different temperature ranges. Vertical mixing by sub-mesoscale eddies distributes heat down the water column (Hieronymus et al., 2014; Holmes et al., 2019), to depths inaccessible for hurricane development. Heat is also advected poleward with the large-scale ocean circulation, into cooler regions of the North Atlantic. A portion of the air-sea heat flux into the tropical ocean

is thus redistributed by mixing and advected poleward, reducing the volume of warm water generated by WMT.

Considering water temperatures affecting hurricane development, annual average cumulative transformed water volume of temperatures warmer than 26.5 °C peaks in August. This leads actual warm water volume, which peaks in September (Figure 2.6), over the 1980-2019 time period. This is consistent with atmosphere-ocean heat exchange being a critical process in forming these warm waters. We note that in a case where the surface fluxes are solely responsible for the volume variability, then actual volume anomaly would equal the time-integral of the transformation rate.

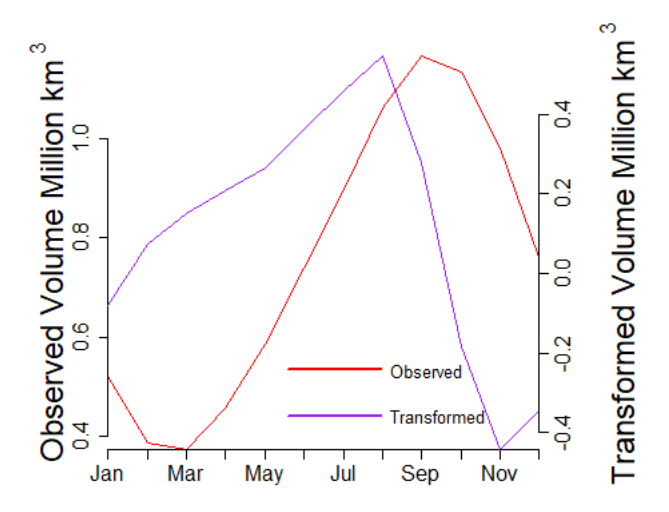


Figure 2.6 1980-2019 mean monthly volume transformed across 26.5 °C isotherm (purple, right axis) and actual volume warmer than 26.5 °C (red, left axis) (million km³).

The net surface heat flux, Q_{net} transforms water from cooler SST to water warmer than 26.5 °C under the hurricane genesis and track regions through the spring and summer months. Figure 2.7a plots climatological Q_{net} during 1980-2019 transferred into the ocean, time-integrated from April to September, where SST exceeds 26.5 °C – the integrand of Equation 2, where T = 26.5 °C. While other processes also contribute to the observed September climatological depth of the 26.5 °C isotherm in the North Atlantic (Figure 2.7b), spatial coherence between the area which can be transformed to temperatures warmer than 26.5 °C through the spring and early summer, and the observed climatological area of 26.5 °C waters in September is suggested by comparison between these two plots. Relating this more closely to hurricane development metrics, the point at which 1980-2019 tropical cyclones strengthened into hurricanes with maximum sustained 1-minute mean winds of 64 knots or greater is overlaid onto the climatological depth of the 26.5 °C isotherm. These points are found south of 40 °N, west of 40 °W and south of 20 °N, east of 40 °W, and are bounded to the south around 10 °N. Few points are found north of this region of the North Atlantic, providing additional observational evidence

to connect this water mass with hurricane development. The patterns of strong net warming and $26.5\,^{\circ}$ C isotherm depth, which span the breadth of the Atlantic basin and extend to $\sim 40\,^{\circ}$ N, reinforce our emphasis that ocean warming of consequence for hurricane genesis is not confined to the MDR.

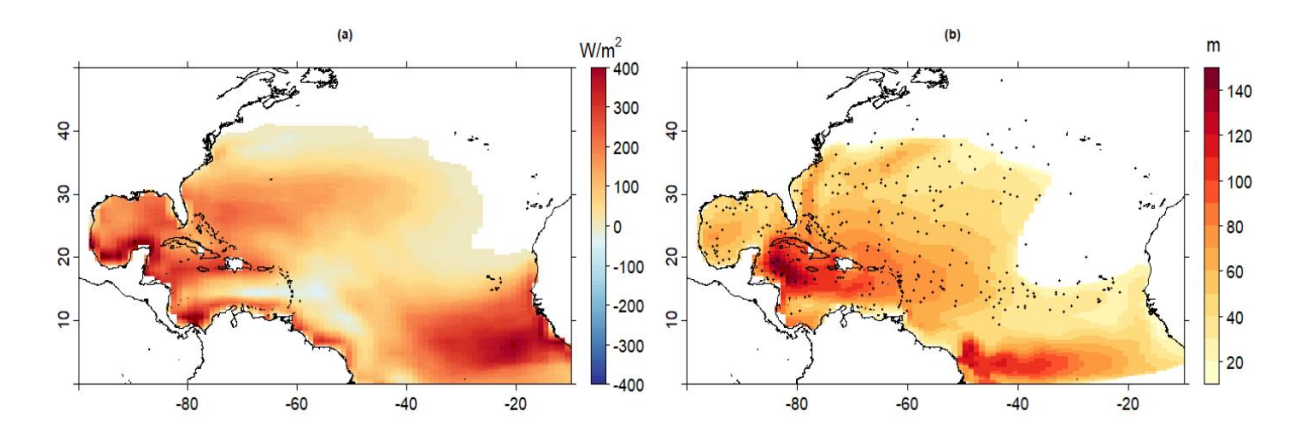


Figure 2.7 (a) Mean 1980-2019 April-September Q_{net} (Wm⁻²) into the ocean where SST exceeds 26.5 °C, (b) 1980-2019 September mean depth of 26.5 °C isotherm (m) with HURDAT 1980-2019 hurricane formation points overlaid).

2.4.3 Inferred Warm Water Volume Changes

In Figure 2.8, time series of GODAS 1980-2019 differences from one month to the next of observed volume anomalies of water warmer than 26.5 °C are plotted with NCEP-NCAR anomalous monthly transformation rate across 26.5 °C, both expressed as million km 3 per month. The aim is to see how closely these may be linked, and how Q_{net} processes may therefore drive development of this warm water to fuel hurricanes, and, by inference, the extent to which other processes must contribute to form this water mass. Monthly anomalies of water transformed by Q_{net} are positively correlated with month-to-month actual volume change anomalies of water warmer than 26.5 °C (Figure 2.8). The Pearson correlation coefficient is 0.32, which is statistically significant at the 99% confidence level.

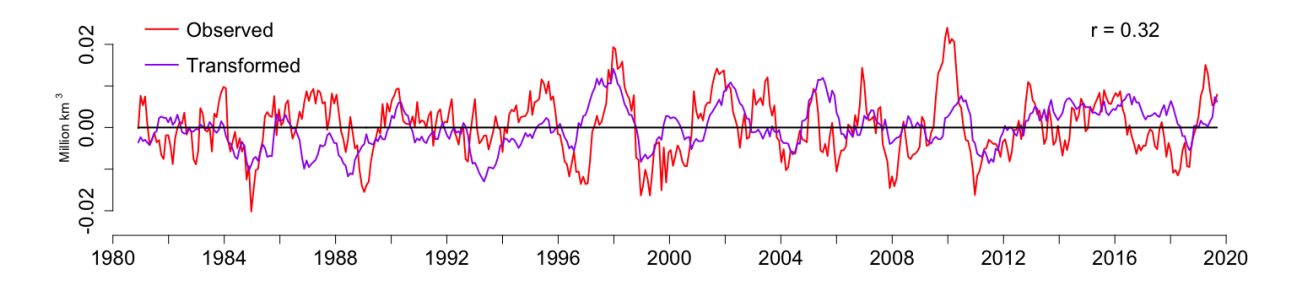


Figure 2.8 Anomalous observed month-to-month (red) volume change of water warmer than 26.5 °C and the anomalous transformation rate (i.e. million km³ per month) across the 26.5 °C isotherm (purple), applying 12-month centred moving average.

However, while the correlation is significant, it is also clear that the level of agreement between WMT and the observed warm water volume exhibits marked temporal variability. In particular, there is particularly close correspondence between the two time series during several periods. One such period was 1998, when there was a notable peak in both time series, and the transformation rate led the observed volume change of water warmer than 26.5 °C by a few months. This also coincided with the beginning of the multi-decadal (post-1998) period of above-average warm water volume available for hurricane development. Examining 1998 in more detail, in most months there was anomalously positive transformation, but this was particularly marked during June through September (Figure 2.9). This is important as it highlights that surface fluxes during as well as before the hurricane season can be important in driving anomalies in warm water volume.

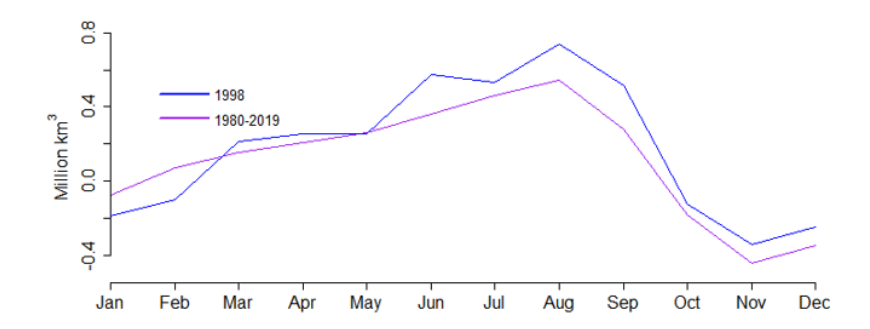


Figure 2.9 1998 (blue) volume transformed across 26.5 °C isotherm (million km³) versus 1980-2019 climatology (purple).

In Figure 2.10, we show anomalies of monthly Q_{net} over waters warmer than 26.5 °C for June to September of 1998, relative to 1980-2020 climatological values. These positive anomalies led to anomalous warm water transformation during these peak months of the 1998 hurricane season.

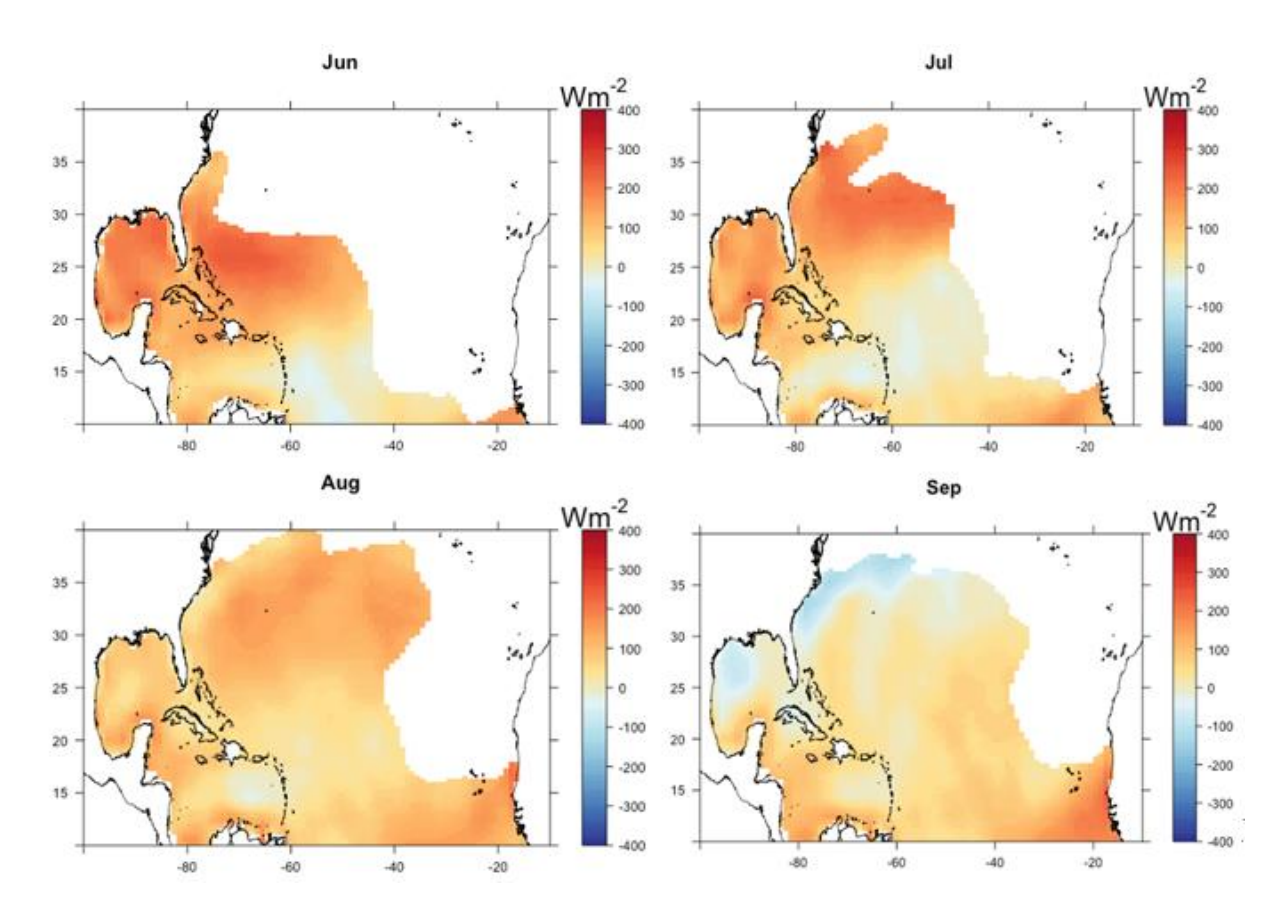


Figure 2.10 Anomaly of June-September Q_{net} (Wm⁻²) in 1998 where SST > 26.5 $^{\circ}$ C.

In 1998, hurricane activity was well above average (Pasch et al. 2001), with an Accumulated Cyclone Energy (ACE) of 182, 67% higher than that of the 1980-2019 average ACE, and the 5th highest since 1970, when satellite data coverage extended basin-wide and this metric could be diagnosed appropriately (Kossin, 2007). Major Hurricanes Bonnie, Georges, and Mitch all made landfall in 1998. Anomalous net surface heating heavily contributed to this, the deadliest Atlantic Hurricane season in the last 200 years. The period 1995-1998 of enhanced transformation appears to have also been important in sustaining a shift from below average to above average warm water volume that occurred near this time (Figure 2.3).

By contrast, in other years, it is clear from the difference between the two signals in Figure 2.8 that additional processes must have contributed to accumulation of warm waters. The warm water volume will further vary as a consequence of anomalies in heat transport divergence associated with both large-scale geostrophic currents and Ekman dynamics. In 2009-2010, Q_{net} fails to explain up to 0.015 million km³ of anomalous volume of water warmer than 26.5 °C in a month. Bryden et al. (2014) calculate a 0.4 PW reduction in ocean heat transport across 26 °N during this period. A decrease in the AMOC then allowed a greater accumulation of heat in the tropical Atlantic in this period, leading to a much greater volume of water warmer than 26.5 °C during the very active 2010 hurricane season.

The relative contributions of these heat sources will also vary on longer timescales over the study period. A downward trend has been observed in AMOC transport since 2008 in the RAPID array measurements at 26.5 °N (Smeed et al., 2018) which would help develop anomalously larger volume of warm North Atlantic water on a decadal timescale. Bryden et al. (2020) note a decrease of 0.17 PW across this latitude since 2009. Hallam et al. (2019) discuss the importance of this slowdown to the 2010 hurricane season in comparison with the 2017 hurricane season, where they show that weaker net heat loss to the atmosphere in the northeastern MDR was a driver of anomalously warm SST.

These differences between observed and transformed volume of warm water are plotted in Figure 2.11 along with negative RAPID heat transport anomalies, suggesting the amount of heat retained in the tropical Atlantic. There is a correspondence between the anomalous residual warm water volume not explained by surface fluxes and the anomalous export of ocean heat from the tropics associated with AMOC variability, notably in 2009 and 2012. The Pearson correlation coefficient for the residual volume of water warmer than 26.5 °C after accounting for the volume transformed by Q_{net}, and annual mean RAPID heat flux anomalies, is -0.60.

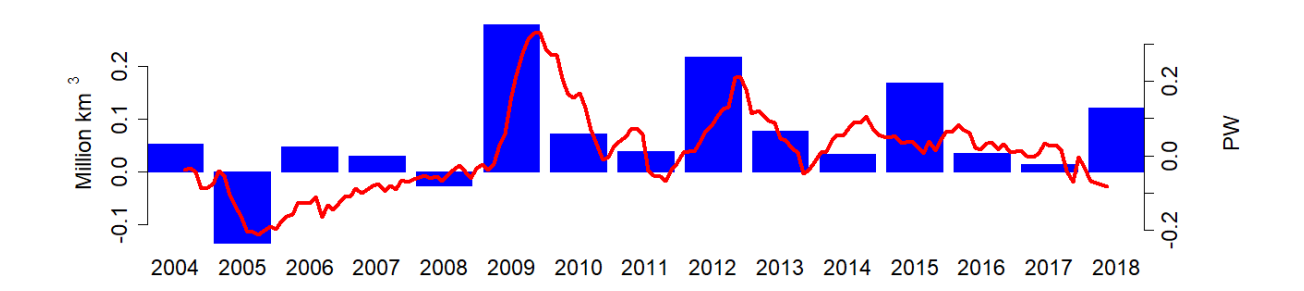


Figure 2.11 Difference in 4-month warm water volume anomalies (Blue) between observed (EN4) July to October volume anomalies > 26.5 °C and that inferred by the anomalous integrated May to August transformation across the 26.5 °C isotherm, with negative RAPID heat transport anomalies across 26 °N (red), applying 12-month centred moving average.

To be more specific about the physical processes behind Q_{net} , we examine anomalies in the four terms of the net heat flux (Equation 1). To isolate the dominant component in heat flux variability for warm water in this region of the ocean, the transformation rate across the 26.5 °C isotherm was separately calculated for each component of Q_{net} . The transformation rate calculated with latent heat flux, Q_{lh} (Figure 2.12) explains 35% (r = 0.59) of the transformation rate calculated using Q_{net} for this particular temperature threshold. In comparison, calculating the transformation rate with other components of Q_{net} , including Q_{lw} and Q_{sw} explains 3% (3% and less than 1% respectively) of the total variance. The transformation rate calculated with Q_{sh} is

highly correlated (r = 0.72) with the total, but is an order of magnitude smaller, and so on its own contributes little to the WMT variability.

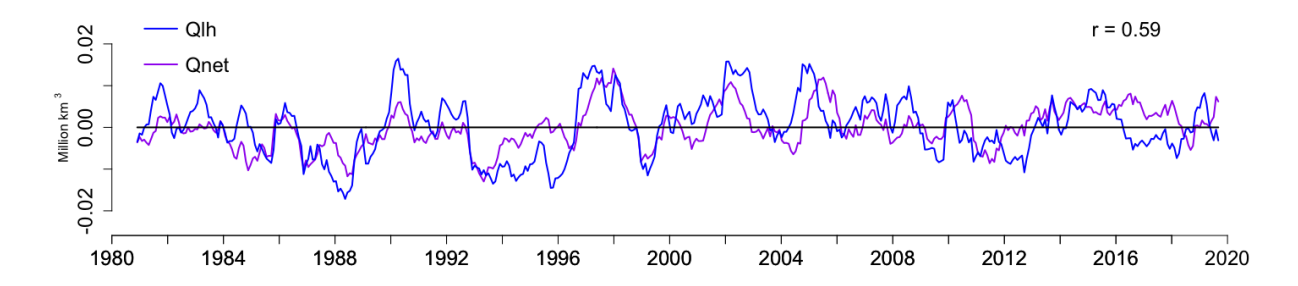


Figure 2.12 Transformation rate anomalies (units: million of km³ per month) across the 26.5 °C isotherm calculated from Q_{net} (purple) and Q_{th} (blue), applying 12-month centred moving average.

2.4.4 Drivers of warm water volume Changes

Having identified Q_{th} as the main driver of anomalous transformation of water towards temperatures above 26.5 °C, the impact of the atmospheric conditions on latent heat exchange into the ocean are now considered. Heat is gained by the ocean when there is a lower rate of evaporation or less latent heat flux to the atmosphere. In Figure 2.13, we plot the local correlation coefficient between Q_{th} and wind speed (Figure 2.13a) and cloud cover (Figure 2.13b). Conditions conducive to a low evaporation rate and reduced latent heat loss include high surface humidity and light winds. Q_{th} is negatively correlated to a larger degree (r < -0.5) with wind speed across the majority of the hurricane MDR, and cloud cover in the eastern MDR (Figure 2.13), implying weaker winds lead to reduced latent heat loss and an increase of net heat flux into the ocean. Figure 2.13b however, implies that enhanced latent heat loss is associated with increased cloudiness. This relationship suggests that whereas latent heat flux variability is likely to be influence by wind speed variations, cloud cover variability is more likely to respond to it. These conditions have been found to strengthen under a positive phase of tropical AMV (Bellomo et al., 2016).

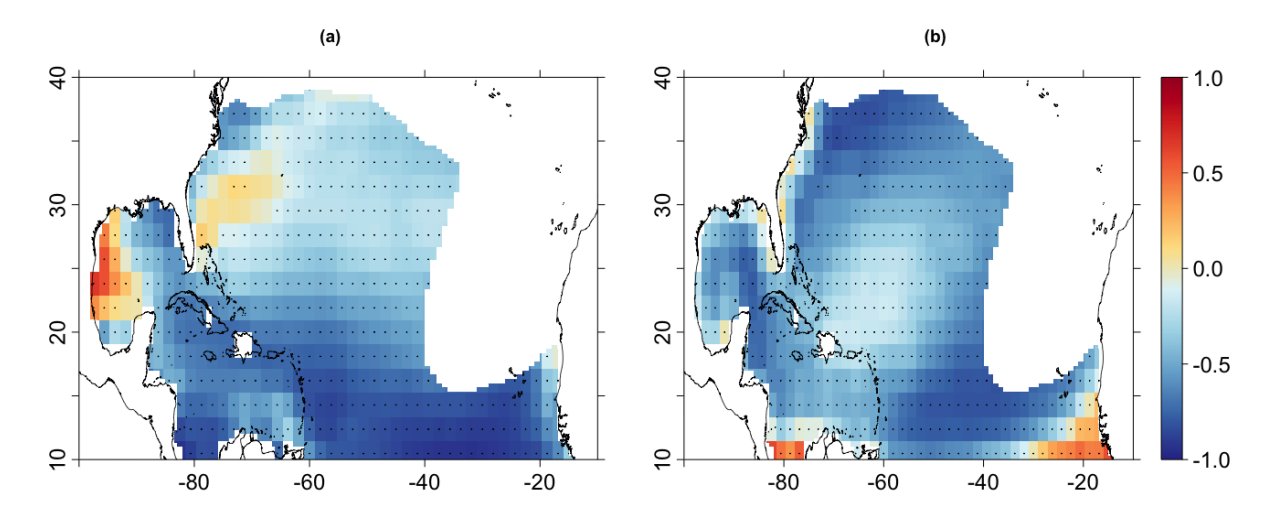


Figure 2.13 (a) Pearson correlation coefficient heat map for Q_{th} and wind speed (b) correlation coefficient heat map for Q_{th} and cloud fraction using NCEP-NCAR data spanning 1980-2019. Values are only plotted where 1980-2019 September mean depth of 26.5 °C isotherm is greater than 10 m. Stippling indicates 95% significance level.

2.5 Conclusions

Multidecadal hurricane activity is largely associated with anomalously warm water in the tropical and subtropical North Atlantic. We have applied the WMT framework (Groeskamp et al. 2019) in temperature space to quantify the volume of water transformed at the surface through air-sea interaction, attributed to the net surface heat flux, Q_{net}. It is shown that the amount of water warmer than 27 °C has increased in the last 40 years, with the transformed volume of water warmer than 26.5 °C leading observed volume anomalies through the spring and early summer. The transformed volume of water warmer than 26.5 °C shows signs of spatial coherence with the observed volume, which is closely tied to the area identified earlier, where storms are able to intensify into hurricanes.

Anomalous positive WMT increases the volume of warm water to the north and east of this hurricane development area. Wang et al. (2010) note that years where the Atlantic Warm Pool is larger than average have increased genesis further east and more re-curving tracks. While some of these tracks may remain over the open ocean, the chance of landfall in the US Northeast states is also likely to increase (Dailey et al., 2009). Similarly, Kossin et al. (2010) group Atlantic storms into clusters, finding that increasing trends in recent hurricane activity are driven by the storm clusters originating in the deep tropics. These storms make up the largest proportion of major hurricanes and also account for the majority of storms making landfall further north along the US coastline.

Transformation rate anomalies across 26.5 °C in the North Atlantic are highly variable on timescales from intra-seasonal to multidecadal. A time dependent fraction of this variability is attributed to Q_{net}, using the WMT framework to calculate monthly volume anomalies that can be compared with observed anomalies of warm water volume. We identify the active and deadly hurricane season of 1998 (Pasch et al. 2001) as a year with particularly close correspondence between transformed and observed volume anomalies of substantial magnitude.

The other major influences on intraseasonal variability of the warm water volume are likely anomalous ocean heat transport divergence, associated with changes in both the AMOC (Zhang et al. 2019, and references therein) and Ekman dynamics, both of which are related in turn to the same anomalous winds that modulate the turbulent surface fluxes. Heat transport changes associated with the 30% AMOC downturn of 2010 account for the observed increase of warm water volume in that exceptional year.

This analysis, using the WMT framework, quantifies the amount of warm water available for hurricane development which is transformed, accounting for air-sea heat flux variability that is primarily related to surface winds. This mechanism only appears effective in some years, due to contribution in other years of variable heat transfer from ocean currents. This reinforces ideas that, at interannual and decadal timescales, coordinated physical mechanisms must come together to explain recent warming of the tropical North Atlantic which has been conducive to more intense hurricane seasons and more frequent landfalls of destructive storms.

Acknowledgements

This analysis was possible due to the public availability of the NCEP/NCAR Reanalysis Monthly Means and Other Derived Variables data

(https://psl.noaa.gov/data/gridded/data.ncep.reanalysis.derived.surfaceflux.html), the NCEP Global Ocean Data Assimilation System (GODAS) data

(https://psl.noaa.gov/data/gridded/data.godas.html) and International Best Track Archive for Climate Stewardship (IBTrACS) data (https://www.ncdc.noaa.gov/ibtracs/index.php?name=ib-v4-access).

We thank two anonymous reviewers for perceptive comments, helping us to substantially improve the manuscript.

Chapter 3 Tracing Oceanic Sources of Heat Content Available for Atlantic Hurricanes

Key Points:

- 20-40% of the warm water available in the MDR for Atlantic hurricanes in June is resident there 6 months previously.
- Of the remaining warm water, which arrives from outside the MDR, 5-15% arrives via the North Brazil Current.
- Years of anomalous warmth in the MDR are associated with reduced arrival from outside the MDR and more local air-sea heat exchange.

Abstract

In the MDR, the volume of water warmer than 26.5 °C quantifies the potential source of energy for major storms. Taking a Lagrangian perspective, this warm water is backtracked on seasonal timescales in an eddy-resolving ocean model hindcast spanning 1988-2010. Being confined near the surface and assuming a mixed layer depth of 50 m, net heat fluxes into or out of water parcels advected towards the MDR are inferred from along-trajectory temperature tendencies. To first order, these heat fluxes match surface net heat fluxes during the months over which water advects into the region. Contributions to this warm water in the preceding 6 months include water resident in the MDR (20-40%), arriving via the North Brazil Current (5-15%), or via Ekman drift across 10 °N. In relative terms, decreased contributions from the North Brazil Current and Ekman drift and more in situ warming within the MDR lead to warmer, more active hurricane seasons.

Plain Language Summary

More and stronger hurricanes can be maintained by a larger quantity of warm ocean water in the North Atlantic. This water can be tracked backwards through time in high resolution model data to see where it originated. While some of the warm water is already in the tropical Atlantic six months before the hurricane season, some moves into the area via ocean currents or is pushed northwards by local winds. More and stronger hurricanes are more likely to occur in years where there is less movement of water into the tropical North Atlantic, along with more local heating of the region in the months leading into the hurricane season.

3.1 Introduction

North Atlantic hurricanes continue to be a major cause of natural catastrophe damage and loss of life. The 2017 to 2021 seasons consistently produced damaging landfalling storms, driving the 5-year average annual economic loss in the US alone to 102.5 B USD (CPI-adjusted, NCEI, 2022), an unprecedented level. These years include the particularly damaging hurricanes Harvey, Irma, and Maria in 2017. Category 5 Michael in 2018 had the strongest recorded maximum windspeed for US landfall. Dorian decimated islands in the Bahamas in 2019. Six hurricanes made landfall in the US in 2020. Category 4 Ida hit New Orleans in 2021. 2022 brought Category 4 Ian to the west coast of Florida, the most damaging US hurricane since 2005. These active recent seasons have mainly occurred in years with anomalous warm water in the tropical North Atlantic (Figure 3.1).

Hurricane development requires an underlying heat source of water warmer than 26.5 °C, combined with a low vertical wind shear atmospheric profile. This is in addition to an existing disturbance, atmospheric instability, and mid-level moisture to aid genesis of individual events (Demaria et al., 2001). McTaggert-Cowan et al. (2015) summarise work identifying the aforementioned temperature threshold as key to generating and sustaining hurricanes. Hence, a deep understanding of the oceanic heat sources necessary to support these storms is required to increase societal preparedness for possible disasters on seasonal and longer timescales.

The June monthly-mean anomalous volume of water warmer than 26.5 °C in the North Atlantic north of 10 °N is shown in Figure 3.1 along with annual hurricane count in the Atlantic basin. These metrics have a Pearson correlation coefficient of 0.43, statistically significant at the 99% level. This anomalous volume of warm water varies on multidecadal and interannual timescales, and is mainly negative prior to 1995, then generally higher after that. Peaks in the volume occur in 1998, 2005, 2010-11 and 2016-17, years with some of the highest hurricane counts.

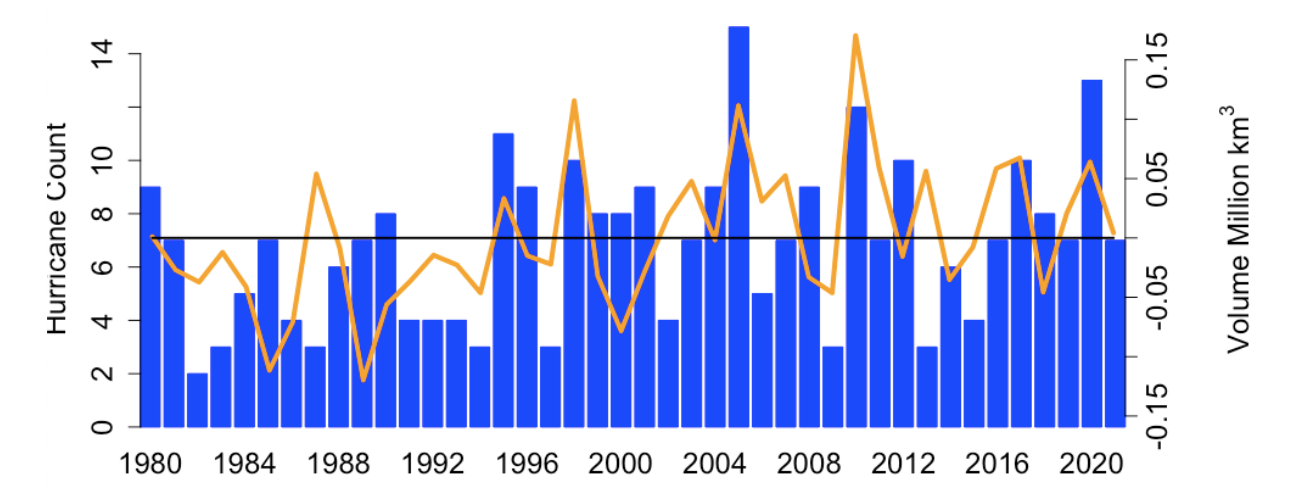


Figure 3.1 IBTrACS Annual North Atlantic Hurricane count (blue bars) and GODAS June volume anomalies of water warmer than 26.5 °C in the Atlantic north of 10 °N 1980-2021 (orange line). For GODAS volume anomalies, the black zero-line is aligned with the mean hurricane count.

Efforts continue to unravel the oceanic and atmospheric systems contributing to anomalous heat in the tropical North Atlantic. It has become clear that atmospheric heat flux plays a major role in heat transfer into the ocean on interannual timescales. Booth et al. (2012) found that variation in anthropogenic aerosols, modulating the incoming shortwave radiation, impacted North Atlantic SST in a climate model. Dunstone et al. (2013) then linked this to tropical cyclone activity. Later studies (Watanabe and Tatebe, 2019) found that much of the anomalously cool North Atlantic SSTs observed in the 1970s and 80s can be explained by increasing anthropogenic sulphate aerosols in climate model studies. Another source of aerosols into the atmosphere is volcanic activity, which Mann et al. (2021) suggest as the driver of multidecadal variability in Atlantic SST. Recent studies have confirmed the role of anomalous surface heating, and specifically a reduction of the oceanic latent heat loss in producing anomalous warm water in the tropical North Atlantic (Hallam et al., 2019; Harris et al., 2022).

While the role of air-sea heat flux in establishing Atlantic SST anomalies has been established in previous studies, heat transfer by ocean transport also plays a role in the development of Atlantic SST anomalies. Yan et al. (2017) argue that major hurricane frequency has increased since 2005, during which time aerosol concentration has been stable, while the AMOC has weakened. A slowdown in the AMOC has been suggested to have driven anomalously positive OHC in 2010, in contrast with 2017 when warming was attributed to changes in regional air-sea interaction (Hallam et al., 2019). Zhang et al. (2019) compile evidence for anomalous ocean heat transport divergence in the Atlantic, associated with changes in both the AMOC and Ekman dynamics which contribute to the changing circulation, notably in 2009-10.

Different ocean currents feed into the MDR (Goldenberg et al., 2001). To the north of the MDR, the basin-integrated AMOC is monitored at 26 °N, and comprises contributions from the Gulf Stream, mid and deep ocean, as well as Ekman transport (Cunningham et al., 2007). Seasonal variability is driven by basin-wide wind stress (Yang, 2015). The Ekman component was anomalously low in 2009-10 (Smeed et al., 2018), allowing accumulation of heat in the MDR. The westward-flowing North Equatorial Current traverses the southern MDR, while the eastward-flowing North Equatorial Counter Current lies immediately to the south (Philander, 2001), and hence both potentially impact MDR temperature development. Amazon river outflow via the North Brazil Current has been proposed as a mechanism for hurricane intensification via a stratifying influence (Ffield, 2007). Despite the ground covered by these studies, the oceanic sources of warm MDR water in the lead up to the Atlantic hurricane season have not been examined collectively. This study aims to quantify transport into the MDR from these different regions in the lead up to the hurricane season, using a realistic high-resolution eddy-resolving ocean model hindcast.

Closing a heat budget for the MDR using Eulerian methods to quantify heat transport into this region via ocean transport is difficult due to disparate observational networks. Adopting a novel approach to investigating heat transfer into the MDR, we use the ARIANE particle tracking algorithm (Blanke and Raynaud, 1997), with data from the ocean model, to back-trace MDR warm water for 6 months. In a related study, ARIANE was used with this model hindcast in the same region to forecast the drift of sargassum on seasonal timescales (Marsh et al., 2021). ARIANE is specifically used here to examine flows into the MDR that are associated with anomalously warm or cool hurricane seasons.

Data and methods will be described in more detail in the following section. Following this will be an investigation into the climatology of these oceanic pathways using model hindcast data to further understand the ocean dynamics in the study region. This will be compared with oceanic and atmospheric influences. Interseasonal variability will then be analysed, to explain individual hurricane seasons. Finally, connections with Atlantic modes and mechanisms will be discussed, to link intraseasonal and interannual variability.

3.2 Data and Methods

We outline the various datasets used here to provide information on interannual variations in hurricane seasons and the associated warm water volume, and to obtain Lagrangian diagnostics. We further outline how the Lagrangian analysis is developed to partition waters inside and outside the MDR (here defined at 10 to 20 °N, 30 to 60 °W), to associate timescales to

MDR arrival, and to infer (Lagrangian) heat fluxes along flow pathways for evaluation with (Eulerian) net surface heat fluxes.

3.2.1 IBTrACS

Atlantic basin hurricane count by year was compiled using the International Best Track Archive for Climate Stewardship (IBTrACS) (Knapp et al., 2010, Knapp et al., 2018). Unique storms reaching greater than 64 knots of maximum wind speed were identified from this storm-centred point data which includes maximum winds at 6-hourly intervals over the ocean, more frequent near land, rounded to the nearest 5 knots.

3.2.2 **GODAS**

The observed volume of Atlantic water warmer than 26.5 °C north of 10 °N was calculated using the GODAS ocean reanalysis product (Behringer and Xue, 2004). This dataset contains gridded global potential temperature at 40 discrete depths, at 1/3° latitude and 1° longitude spacing, from 1980. While observations used to create this data are increasingly scarce with depth and further back in time, the data used in this study is near the surface and relatively recent.

3.2.3 NEMO hindcast

A 1988-2010 hindcast model run was used to track particles. This dataset is output from the Nucleus for European Modelling of the Ocean (NEMO) ocean model (Madec, 2008), run in a high-resolution 1/12° eddy-resolving global configuration (ORCA12). Data used to compute trajectories comprise 5-day averages 3D ocean currents, temperature, and salinity; surface winds and net heat fluxes were used in further analysis.

NEMO-ORCA12 is forced with surface datasets produced by the DRAKKAR project (Brodeau et al., 2010), comprising 6-hourly mean 10-m winds, 2-m air temperature, 2-m humidity, daily mean radiative fluxes, and monthly-mean precipitation fields, adjusted from ERA40 reanalysis (Uppala et al., 2005). The hindcast used here is obtained with NEMO v3.2 and the following DRAKKAR Forcing Sets (DFS): DFS4.1 forcing up to the end of 2007, switching to NEMO v3.3.1 and DFS5.1.1 forcing in an extension to the end of 2010. Details of model parameterisation and initialisation are outlined in Blaker et al. (2015).

3.2.4 Lagrangian analysis

The ARIANE package is used for tracing water parcels using the NEMO-ORAC12 model output data described above. Starting points are selected, and positions are saved at 5-day intervals up

to 170 days forwards or backwards from the start date. Start points on June 30 and September 30 are defined at grid points within the MDR where the temperature in the water column is greater than 26.5 °C, in each year of the dataset. Constraining the start points to the MDR allows for identification of movement of particles and heat transfer into this highly studied region intimately connected with hurricane development, at a temperature threshold identified as a minimum for sustaining hurricanes.

The number of particles warmer than 26.5 °C can be used as a proxy for heat content in the MDR. In Figure 3.2, this number is plotted for June and September of each year in the ORCA12 dataset. The variability in June is much greater than September. By September, most of the MDR SST particles are already warmer than 26.5 °C. As a consequence, the amount of warm water in the MDR is less variable than in June. As the number of 'warm water particles' in the MDR in June is indicative of MDR OHC, it is naturally linked to hurricane activity in the Atlantic Basin, with notable peaks in the active hurricane seasons 1995, 1998, 2005, and 2010 in Figure 3.1.

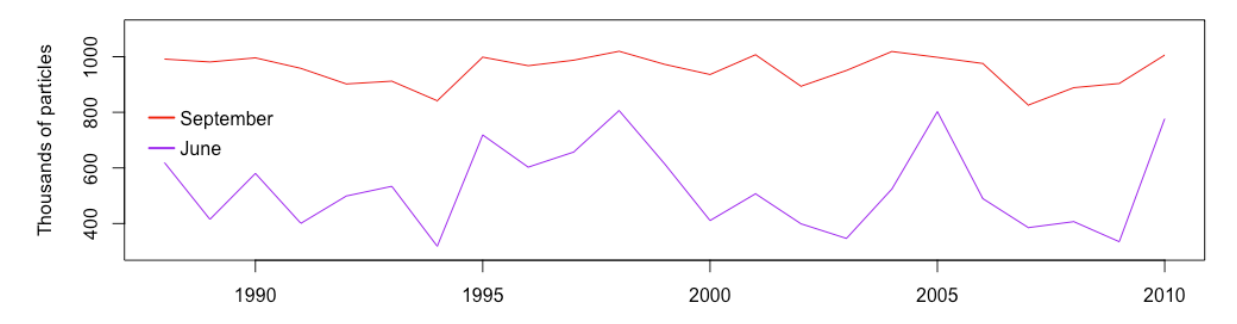


Figure 3.2 Number of particles initially warmer than 26.5 $^{\circ}$ C in MDR on 30 June (purple) and on 30 September (red).

From the start points, ARIANE runs backwards (or forwards) to trace the path of the water parcels into (out of) the MDR, recording the tendencies of temperature and other properties along flow pathways. A forwards run from June 30 was run to quantify potential heat loss out of the region. Net heat fluxes, $Q_{Lagrangian}$, are inferred from temperature (T) tendencies between the 5-day output intervals (t, t + Dt, etc.,), so $T(t+\Delta t)-T(t)$, for a representative mixed layer depth h = 50 m, as:

$$Q_{Lagrangian} = \rho C_p h \frac{T(t + \Delta t) - T(t)}{\Delta t}, \quad (1)$$

where ρ and C_p are respectively a representative density and the specific heat of seawater. The value of h is informed by a recent mixed layer climatology for the tropical Atlantic (Holte et al., 2017). Located midway between particle locations at arbitrary latitudes and longitudes, these heat fluxes are then averaged on a 0.5 $^{\circ}$ grid along with mean age and other particle properties.

Figure 3.3 shows the tracks of a sample of particles at 1 ° spacing within the MDR and warmer than 26.5 °C in September 2010, tracking particles backwards for 6 months. While the lengths of some particle tracks are contained within the MDR, longer tracks of faster moving particles are evident, clustered along the northeast coast of Brazil (North Brazil Current). The remainder of the particles move more slowly into the MDR across the southern boundary.

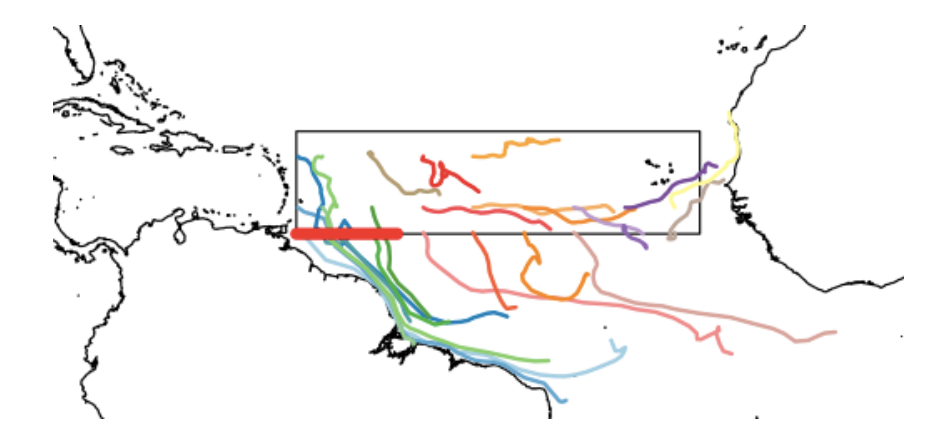


Figure 3.3 Sample of back-trajectories from September 2010, colour-coded by particle id; MDR – black box, North Brazil Current measured across red line at 10 $^{\circ}$ N

This Lagrangian approach to examining different routes of ocean heat transfer into the MDR is a novel methodology for investigating the variability of warm water available for hurricane development. The analysis reveals new insights into quantification of the sources of warm water flowing into this region and inter-seasonal variability leading to anomalously warm (cool) years in which the MDR heat content can support more (fewer) potentially damaging hurricanes.

3.3 Results

Output from the three experiments: the particle back-trajectories from June 30 (BAC06) and September 30 (BAC09), as well as forward trajectories from June 30 (FOR06), are analysed in the following sections. To understand the climatology of warm water transport into and out of the MDR, averages over the hindcast period of 1988-2010 are examined. This is demonstrated using monthly snapshots of the number of particles and average properties through the 6 months per 0.5 ° grid cell, including particle age and Lagrangian heat fluxes, which are compared with corresponding Eulerian surface heat fluxes from the hindcast. Mean ocean currents and wind stress are referenced as drivers of particle movement. Dynamics of heat transfer via ocean currents are then summarised schematically.

Individual years are compared to consider interannual variability, by identifying various source regions for water warmer than 26.5 °C and quantifying the number of particles originating via individual pathways. The differences between particularly warm, active years in the dataset and

cooler, inactive years are then examined, along with ocean currents and wind stress for those years, to highlight atmospheric and oceanic dynamics driving anomalously warm or cool conditions in the MDR that are of consequence for hurricane seasons.

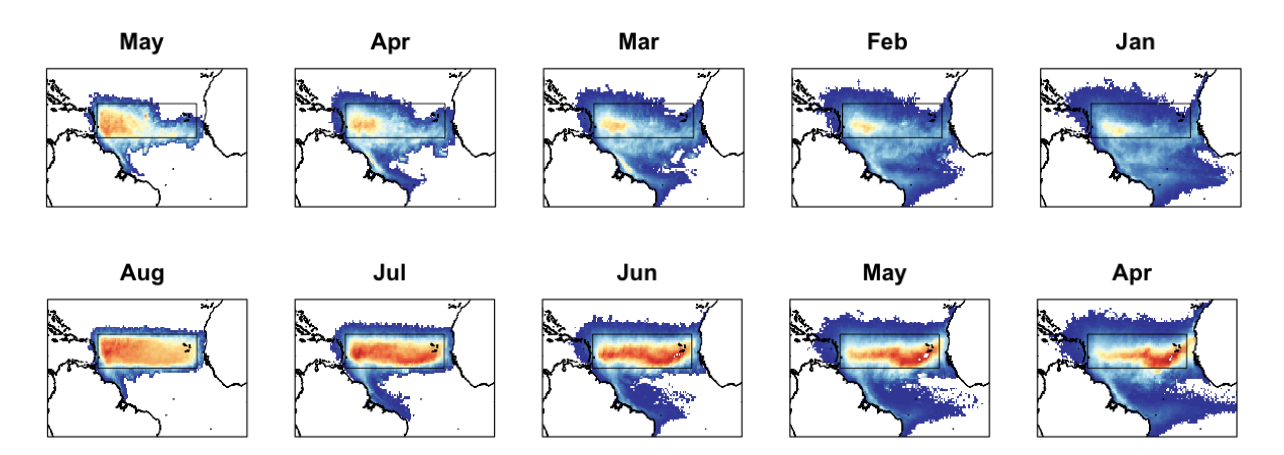
Finally, we examine climate modes and mechanisms over the hindcast period, relating the variable development of MDR heat content via oceanic pathways to established analyses of tropical Atlantic variability.

3.3.1 Climatology of oceanic sources of warm water into the summertime MDR

In this section, the climatology of oceanic sources of water warmer than 26.5 °C are discussed, by examining the backwards (forwards) trajectories of particles from June 30 and September 30, for 170 days (approximately 6 months), to January or April (November) respectively. Particles in Figure 3.4 converge (diverge) gradually into (out of) the MDR with time along the backwards (forwards) trajectories.

In the top row, starting in June, and back-tracking one month earlier to May, particles are largely within the MDR, with some particles arriving via the North Brazil Current. In March, the North Brazil Current pathway is very clear along the north coast of Brazil. There is also a high density of particles visible south of 10 °N in March, clearly to the north of the North Brazil Current. We can infer that these particles will move northwards more slowly than the North Brazil Current. In January, while the highest particle concentration is the MDR itself, particle origins are also well dispersed, from 10 °S to 10 °N, and largely west of 20 °W.

The North Brazil Current also contributes to warm water particles residing in the MDR in September (middle row), though the local maximum in particle numbers in the eastern MDR in April is very pronounced, indicating far less movement into the MDR from other water sources over the spring and summer months. This suggests some westwards movement of particles within the MDR through this period.



Chapter 3

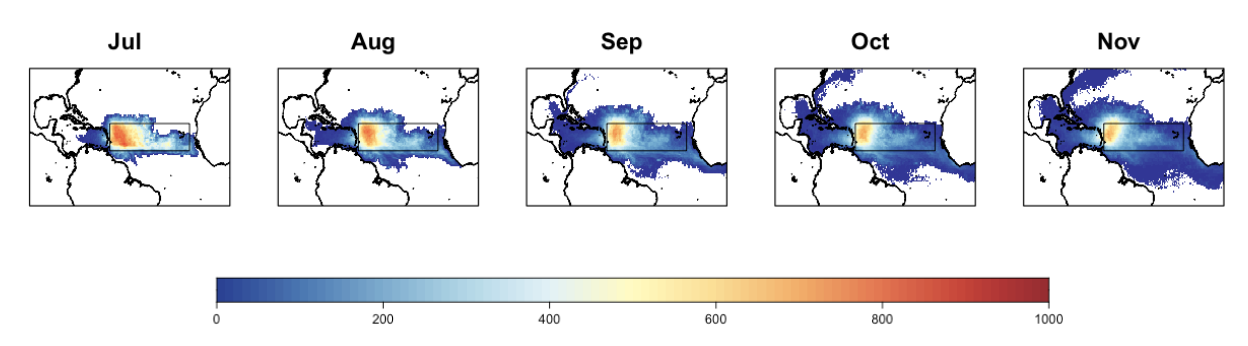


Figure 3.4 Number of particles per 0.5 ° grid cell at 1-month intervals from start date. Tracing particles that were in the MDR and warmer than 26.5 °C on June 30 (top, tracing backwards), September 30 (middle, tracing backwards) and June 30 (bottom, tracing forwards). The MDR is outlined.

To identify the extent to which warm water is being lost from the MDR via ocean currents, a forward run from June 30 is also undertaken (bottom row). Warm water particles move into the Gulf of Mexico in 2 to 3 months, some reaching the Gulf Stream by 4-5 months, along with general dispersal up to 10 ^o to the north and south of the MDR.

While the Lagrangian analysis identifies the basic source regions of warm water, the particles also gain and lose heat along their track towards or away from the MDR, so the impact of ocean currents as heat sources or sinks cannot be isolated from air-sea heat flux, or Ekman dynamics, with this methodology. To elucidate this, the along-track heat flux via Equation (1), per 0.5 ° grid cell over the 6 months of each experiment, is plotted in the top row of Figure 3.5. The average particle age per experiment, in the middle row of Figure 3.5, is helpful for understanding the Lagrangian heat fluxes, as heat transfer processes are highly variable on intraseasonal timescales, with the ocean losing heat to the atmosphere in the northern hemisphere winter, and starting to gain heat from the atmosphere by early summer. As particle tracks begin in the MDR, and move quickly backwards along the North Brazil Current, away from the MDR, this brings down the average particle age in these areas, but regions furthest from the MDR have an average age closer to the end of the experiment. Over the 6 months of BAC06, on the left, heat is gained in the MDR in May and June, off the west coast of Africa where cool water upwells due to offshore easterly trade winds, and south of the equator in January.

The Eulerian 6-month averaged heat flux (Q_{net}) in the left panel of the bottom row (averaged January to June) also shows general heat loss in the Atlantic north of 5 $^{\circ}$ N, as this winter heat loss to the atmosphere in the northern hemisphere outweighs the heat gain in early summer, and heat gain south of this latitude, in the deep tropics, and for the upwelling area along the west coast of Africa.

In contrast, heat is gained over most of the particle tracks ending in September, in the middle column of Figure 3.5, which corresponds to April to September averaged Q_{net} on the bottom row (middle panel), as the ocean gains considerable heat from the atmosphere in the late spring and through the summer.

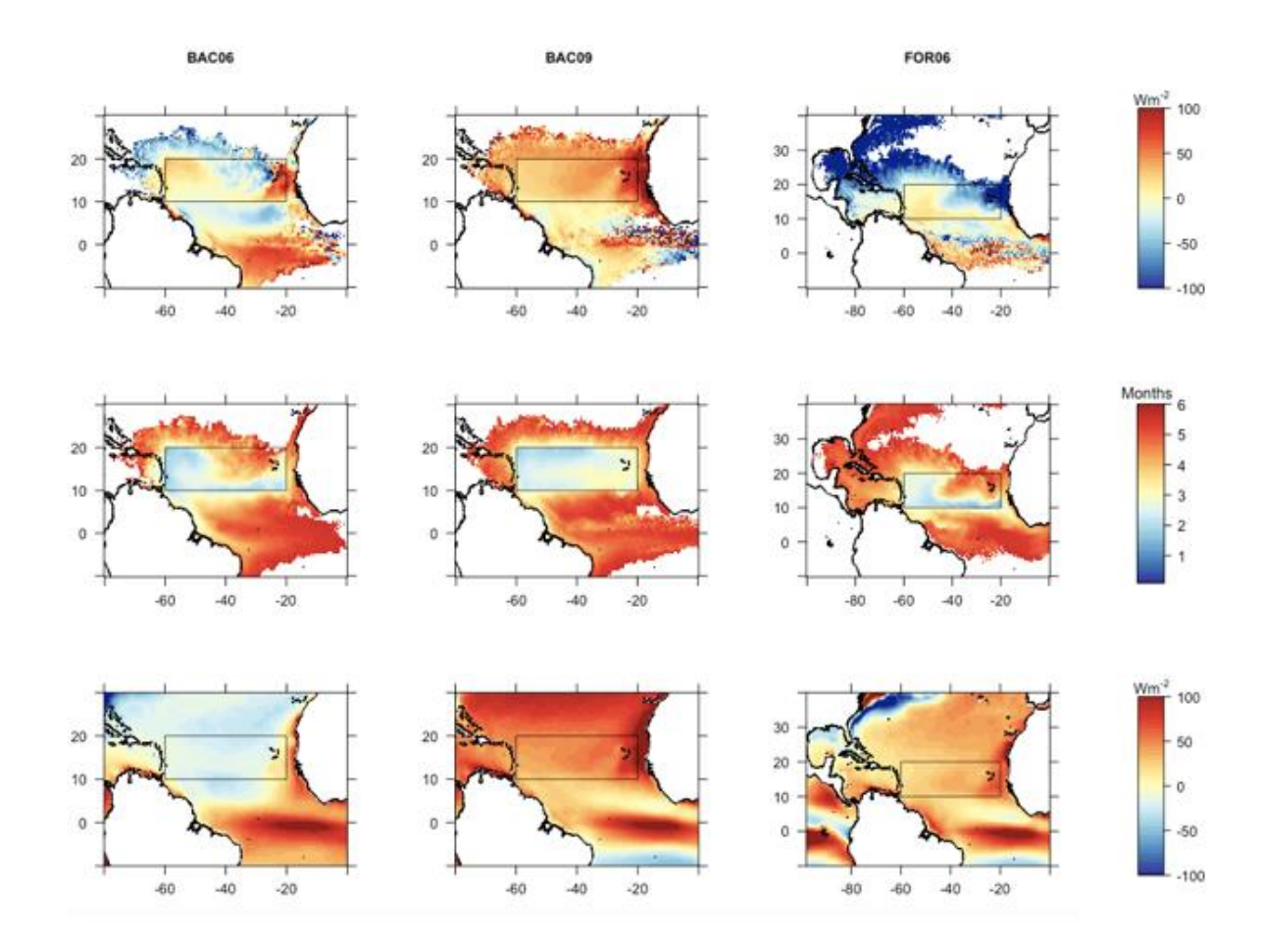


Figure 3.5 1988-2010 ORCA12 mean heat flux (top row) and particle age (middle row) for ARIANE experiments BAC06 (backwards form June, left column), BAC09 (backwards from September, middle column), and FOR06 (forwards from June, right column); with mean Eulerian heat flux for the same 6-month periods as ARIANE experiments (bottom row; January to June left, March to September, middle, July to December, right)

FOR06, on the other hand (right panels), shows heat loss where warm water particles move north, as they mix with cooler water and lose heat to the atmosphere, particularly via the Gulf Stream. Some heat is gained in June and July in the MDR and equatorial regions in November and December. Mean monthly Q_{net} for July to December (bottom right), shows mainly heat transfer into the ocean during the peak of summer and through the fall, with heat loss along the Gulf Stream as warm water moves quickly northwards.

The Lagrangian heat flux thus provides a complementary, time-varying perspective of oceanatmosphere dynamics along flow pathways, contributing to the warm water pool available for hurricane development. This novel analysis reveals the role of oceanic pathways in the development of hurricane seasons, by highlighting heat transfer into the region in the months preceding the start of the Atlantic season, sourced within, or remote from, the MDR.

3.3.2 Climatology of dynamical influences on MDR heat content and Atlantic hurricanes

In addition to seasonal change in Q_{net} , winds and ocean currents also vary seasonally, and contribute to varying mechanisms of heat transfer into the MDR through the year. Figure 3.6 highlights that winter/spring MDR wind stresses (top row) are stronger, leading to more mixing with cooler sub-surface waters and stronger advection. Weakening of wind stress through spring/summer subsequently favours heat accumulation in the MDR by September. The impact of the North Brazil Current (bottom row) will be examined in more detail on interannual timescales.

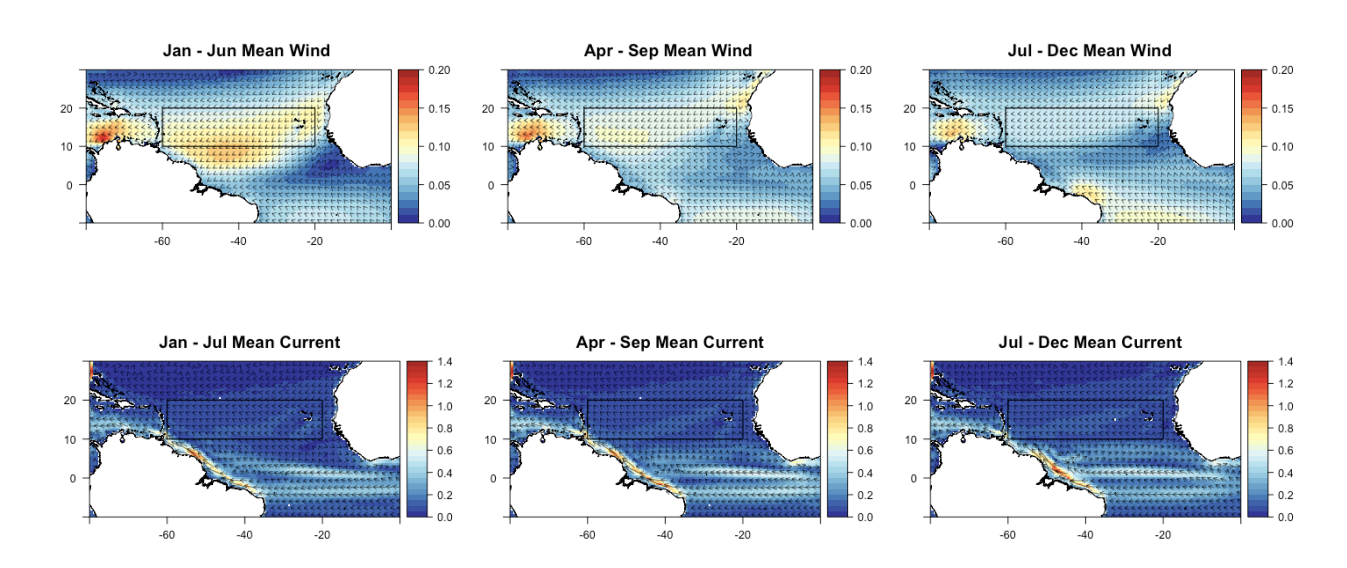


Figure 3.6 ORCA12 1988-2010 averages of 6-month means for wind stress (Nm⁻²) and surface current (ms⁻¹). January-June corresponds to the time of BAC06, April-September to BAC09 and Jul-December to FOR06.

Figure 3.7 depicts warm water pathways into and out of the MDR, as traced with particles, along with the atmospheric and oceanic drivers that contribute to heat content available for hurricane development. Ocean currents transporting water in and out of the MDR are identified as red arrows in this schematic. The Gulf Stream transports heat out of the region. The North Brazil Current bifurcates to partly flow into the MDR. The northern edge of the westward Equatorial Current crosses the southern boundary of the MDR. Variable Easterly trades (blue arrows) drive not only the Atlantic Niño signal, but also vertical mixing (purple arrows) across the 26.5 °C isotherm. A combination of these dynamics and processes generates a larger or smaller pool of

warm water, leading in turn to above or below average hurricane season activity. This warm pool is depicted by the red lines labelled 26.5 °C.

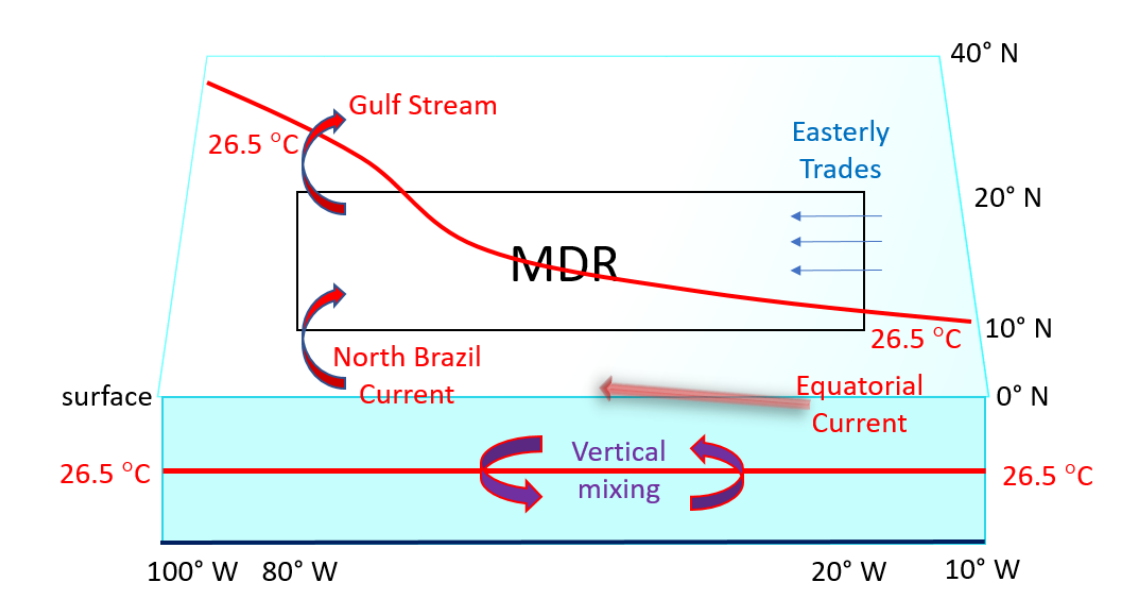


Figure 3.7 Physical mechanisms influencing ocean heat transport divergence in the MDR shown as arrows (see main text above for details).

3.3.3 Interseasonal variability of oceanic pathways into the MDR in relation to hurricane activity

Section 3.1 considered average particle movement across the ORCA12 hindcast, introducing Q_{Lagrangian} as a measure of net surface heat flux into the MDR for potential hurricane development. In this section, we develop Lagrangian diagnostics to compare mechanisms for oceanic heat transfer leading up to the start of the Atlantic hurricane season.

Figure 3.4 indicated that 6 months before the start of the hurricane season, many of the particles terminating in the MDR are already in situ in the MDR. This percentage of particles located within the MDR is plotted for each year, by experiment, in the top row of Figure 3.8. For BAC06, the MDR particle count quickly declines to a mean of 64% by month 2 of the experiment, associated with some of the faster moving pathways, though this varies between 52% and 77% by year. On average for these years in the dataset, 36% of the particles are in the MDR 6 months before the experiment start, varying between 17% and 50%.

Most of the particles from the start of the BAC09 (middle) experiment are in the MDR 2 months before the peak of the hurricane season, with a mean of 91% of the particles in the MDR at that time, and on average 65% of the particles in the MDR in April. Addressing heat loss from the MDR at the start of the hurricane season, in FOR06, on average 71% of particles are still in the

MDR after 2 months from the experiment start time, and 51% by January, at the end of the experiment.

Comparing these experiments by start date, more heat exchange affecting the MDR heat content is via ocean currents from January to June (BAC06). From April to September (BAC09), more heat exchange affecting the MDR heat content is through in situ heat exchange from the atmosphere into the ocean.

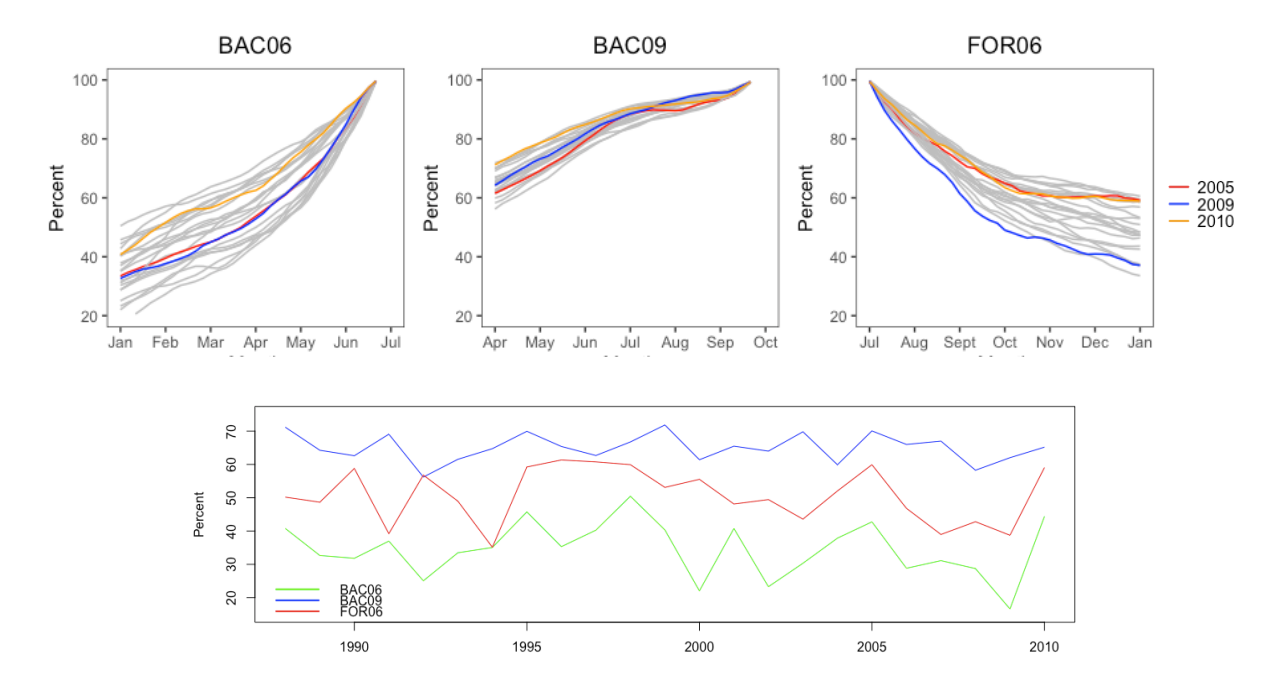


Figure 3.8 Percentage of particles in the MDR at each timestep that were in the MDR and warmer than 26.5 °C at the start of the experiments, for each of the three experiments:

BAC06, BAC09, and FOR06 by year (top panels). Time series of the percentage of these warm particles in the MDR at the end of the 6-month experiments (bottom panel).

The bottom panel in Figure 3.8 is a time series of the percentage of particles in the MDR at 6 months from the start of each experiment, essentially the 'end points' 6 months earlier or later than the start time in the top row. This timeseries shows peak MDR 'residency' for June-backtracked particles in 1995, 1998, 2005 and 2010; these are the years with the warmest MDR in June, and likewise, the most active hurricane seasons. There is a minimum in 2009, conversely a year with one of the lowest number of particles warmer than 26.5 °C, during which only three hurricanes formed in the Atlantic basin. The number of particles in the MDR in January has a Pearson correlation coefficient of 0.78 with the number of particles in the MDR in June, and 0.55 with the annual Atlantic basin hurricane count, significant at the 99% level, suggesting a reasonable level of predictability for MDR heat content in June as well as seasonal basin-scale hurricane activity.

Apart from water resident in the MDR, a clear pathway for water moving into the MDR is the North Brazil Current, which is evident in the climatological analysis in Figure 3.4. To capture particles moving into the MDR via this current, Figure 3.9 shows the percent of particles in each year at each 5-day time timestep, south of 10 °N, between 50 and 60 °W. In BAC06, the greatest percentage of particles in this region is during March through May. Only a small percentage of particles is found in the North Brazil Current throughout BAC09, with variability by year for the 6 months of this experiment.

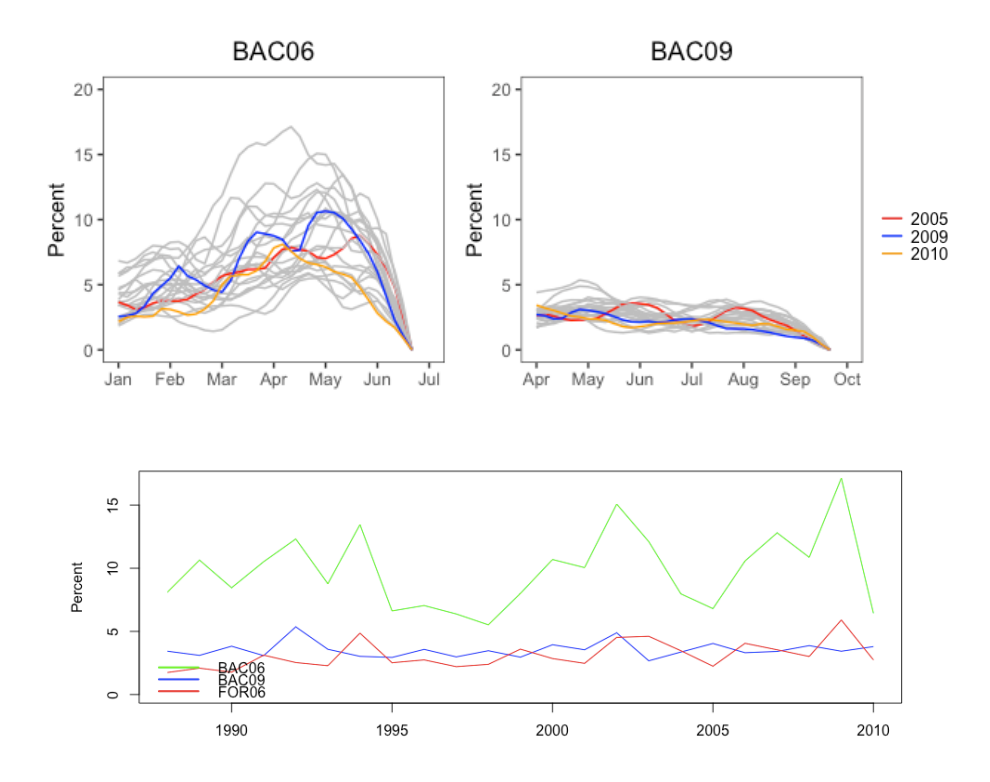


Figure 3.9 Percentage of particles in the North Brazil Current at each timestep that were in the MDR and warmer than 26.5 °C at the start of the experiments, for BAC06 and BAC09, by year (top panels). Time series of the percentage of these warm particles in the North Brazil Current at the end of the 6-month experiments (bottom panel).

The time series in Figure 3.9 (bottom panel) shows the maximum percentage of particles in the North Brazil Current region at any time, rather than at the end of the experiment, recognising that particles may pass through this region throughout the 6-month timespan. The BAC06 experiment maximum percentage of particles in the North Brazil Current timeseries is negatively correlated with the number of particles in the MDR in June, with a maximum in 2009, and minima in the active hurricane seasons. The Pearson correlation coefficient with the initial number of particles is -0.87 and with hurricane count is -0.61, significant at the 99% level.

We have quantified the contributions to warm MDR water coming from water in situ within the MDR six months prior to the start of hurricane season, and flow into the MDR via the North Brazil Current. The remaining water moving into the MDR moves north across the southern boundary

primarily with Ekman drift. MDR warmth in June of warm years is largely in situ already by early/mid spring. This implies that warm years result from the accumulation of heat within the MDR (via surface fluxes), rather than transport of excess heat into the region from more equatorward regions. In cool years, an active North Brazil Current pathway accompanies suppressed MDR heat content. This is consistent with the relatively low heat gain or even heat loss that occurs in the along the main input pathway of the North Brazil Current (see Figure 3.5).

Three sample years were selected to examine oceanic and atmospheric dynamics leading to a smaller or larger than average number of warm particles in the MDR in June: 2005, 2009 and 2010. In 2005, there were a record number of 15 hurricanes, while only 3 hurricanes were recorded in 2009; in 2010, there were 12, well above the climatological average of 7 for 1980-2021 (Figure 3.1). For both 2005 and 2010, there is a relatively large number of warm water particles in the MDR in June. These two years are compared to see if similar antecedent conditions led to a larger warm pool in both years. In 2009, on the other hand, there is a relatively small number of particles in the MDR in June. In summary, around twice as many particles represent water warmer than 26.5 °C in the MDR in 2005 and 2010, than in 2009 (Figure 3.2); comparing 2009 to 2010, we examine how antecedent conditions vary ahead of a cooler year and a warmer year, respectively.

Figure 3.10 shows the number of particles per 0.5 ° grid cell in each of these years from the BAC06 experiments. In 2005 and 2010, we note generally similar locations of particles six months earlier, in January. This suggests similar warm water pathways in the preceding months, with most particles residing in the MDR through this time, a contribution from the North Brazil Current, and the remaining particles drifting northwards across 10 °N into the MDR. In contrast, warm waters in June 2009 originate mainly south of the MDR. These sample years demonstrate how warm years have more limited transport of water via ocean currents into the MDR, and more in situ warming within the MDR.

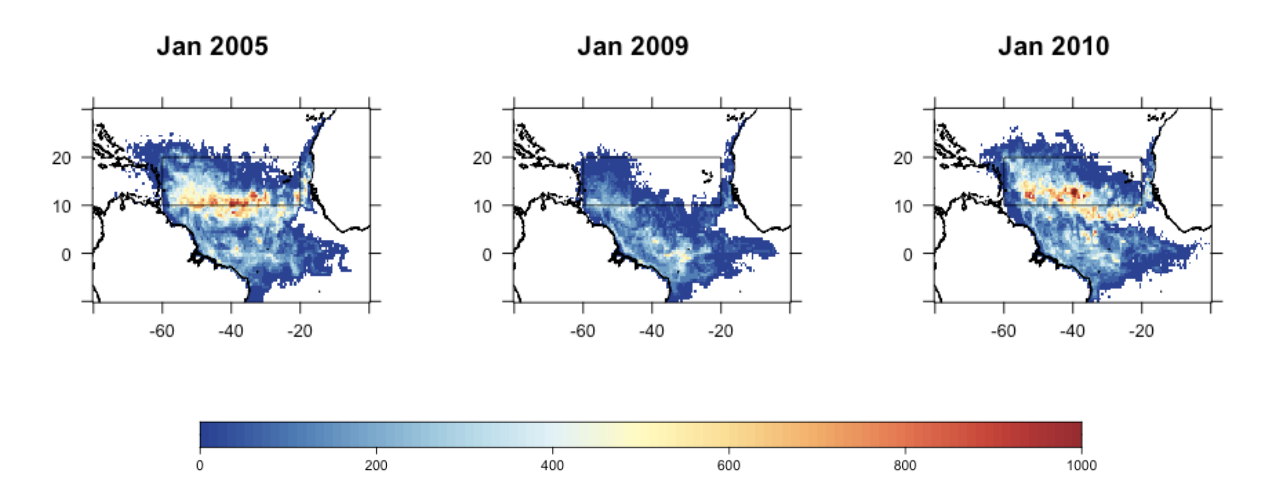


Figure 3.10 Number of particles per 0.5 ° grid cell in January which are in the MDR and warmer than 26.5 °C in June of the same year.

Oceanic and atmospheric conditions preceding June 2005 are compared with those prior to June 2010. We consider how Lagrangian motion and driving oceanic and atmospheric dynamics could potentially differ between these active hurricane seasons with large warm pools. Both years are characterised by negative wind stress anomalies across much of the region in the months preceding June (Figure 3.11a, e), although this is more strongly negative in 2010, particularly north of the MDR. Warm water in the MDR in 2005 therefore is more heavily influenced by Q_{net} , and in 2010 by Ekman dynamics, which other studies have also concluded (Hallam et al., 2019).

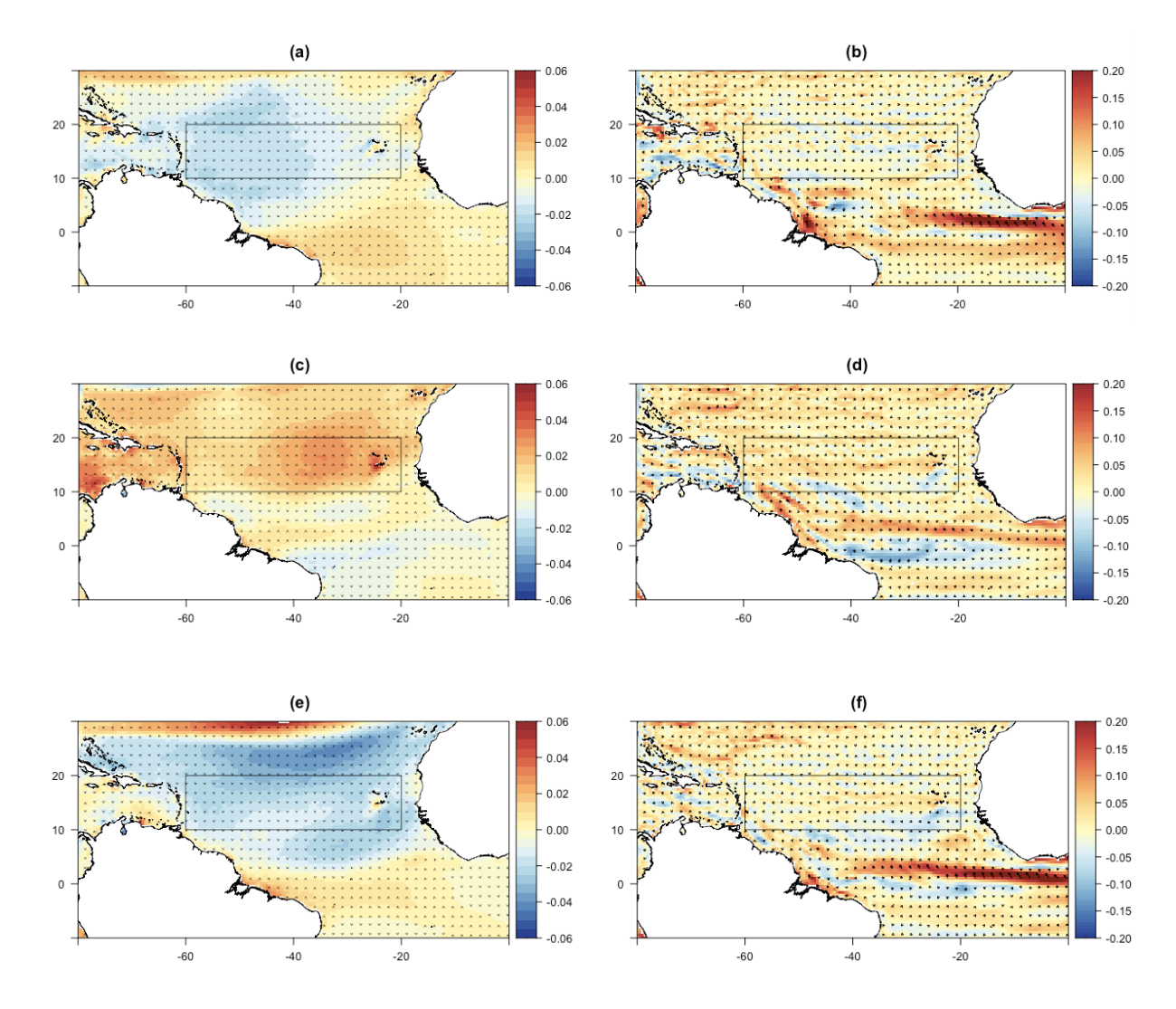


Figure 3.11 Mean January-June 2005 wind stress anomalies (Nm⁻²) (a) and ocean current anomalies (ms⁻¹) (b) vs 2009 (c, d) and 2010 (e, f).

To consider how atmospheric and oceanic forcing may lead to cooler and warmer years in the MDR in June, we now compare the prevailing surface conditions in 2009 and 2010. Lower OHC in June 2009 is coincident with positive wind stress anomalies across the MDR through the

preceding winter and spring (Figure 3.11c). The North Brazil Current and equatorial current are also anomalously positive in this period (Figure 3.11d). Wind stress anomalies, on the other hand, are negative in 2010, both in and around the MDR (Figure 3.11e).

This Lagrangian analysis of interannual variability of transport along pathways into the MDR, in the months preceding a hurricane season, confirms that increased transport from the south via the North Brazil Current and northwards Ekman drift across 10 °N are associated with a smaller warm pool available for hurricane development by the start of the hurricane season; conversely, heat has more time to be exchanged via air-sea fluxes in years with less influential ocean transport.

3.3.4 MDR heat content linked to modes of climate variability

Given the evidence for remote influences on MDR heat content, in particular the equatorial origin of warm water in the BAC06 experiments, and the more local MDR heating in BAC09 experiments, we examine regional patterns and time series of climate variability. Variability in tropical Atlantic temperatures and winds are evident on a range of timescales. Much of the variability can be quantified with two indices, which will be discussed in relation to the Lagrangian analyses and the associated volume of warm water available for hurricane development.

On interannual to decadal timescales, the Atlantic Meridional Mode (AMM) is the dominant statistical mode of tropical Atlantic SST variability (Servain et al, 1999, Chiang and Vimont, 2004). An index for the AMM is based on a leading dipole mode, associated with meridional SST gradient anomalies across the mean latitude of the Intertropical Convergence Zone (ITCZ). When the AMM is in a positive phase, warm SST anomalies are centred at 10 °N, with weak trade winds centred at 5 °N.

A similar SST pattern to the Pacific El Niño had been observed in the tropical Atlantic, with a tongue of SST anomalies centred on the equator off west Africa (Lübbecke et al, 2018). This signal is formed in a similar fashion, as anomalous trade winds result in variations in coastal upwelling. A positive phase occurs when Atlantic trade wind strength is lower than average, allowing more warm water to pool across the eastern equatorial Atlantic. This results in positive feedback with trade winds over the area. The signal peaks in the summer and fall. An Atlantic Niño Index (ANI) is calculated here from ORCA12 output by averaging SST anomalies over 3 °N–3 °S, 0 °–20 °W (following Zebiak, 1993).

The AMM-index is linked with hurricane activity (Vimont and Kossin, 2007) through warmer SST and low wind shear. The AMM-index (blue) in Figure 3.12 exceeds 2.0 in 1997, 2004, 2005, and

2010, with minima in 1994 and 2009. This is significantly correlated with hurricane count, with a Pearson correlation coefficient of 0.54, significant at the 99% level.

The ANI (Figure 3.12, red) is strongest in 1988, and also positive in 1995, 1999, and 2010, although notably fairly neutral in the very active hurricane seasons of 2004 and 2005.

Regardless, the Pearson correlation coefficient with hurricane count for the years in this study is 0.49, significant at the 99% level.

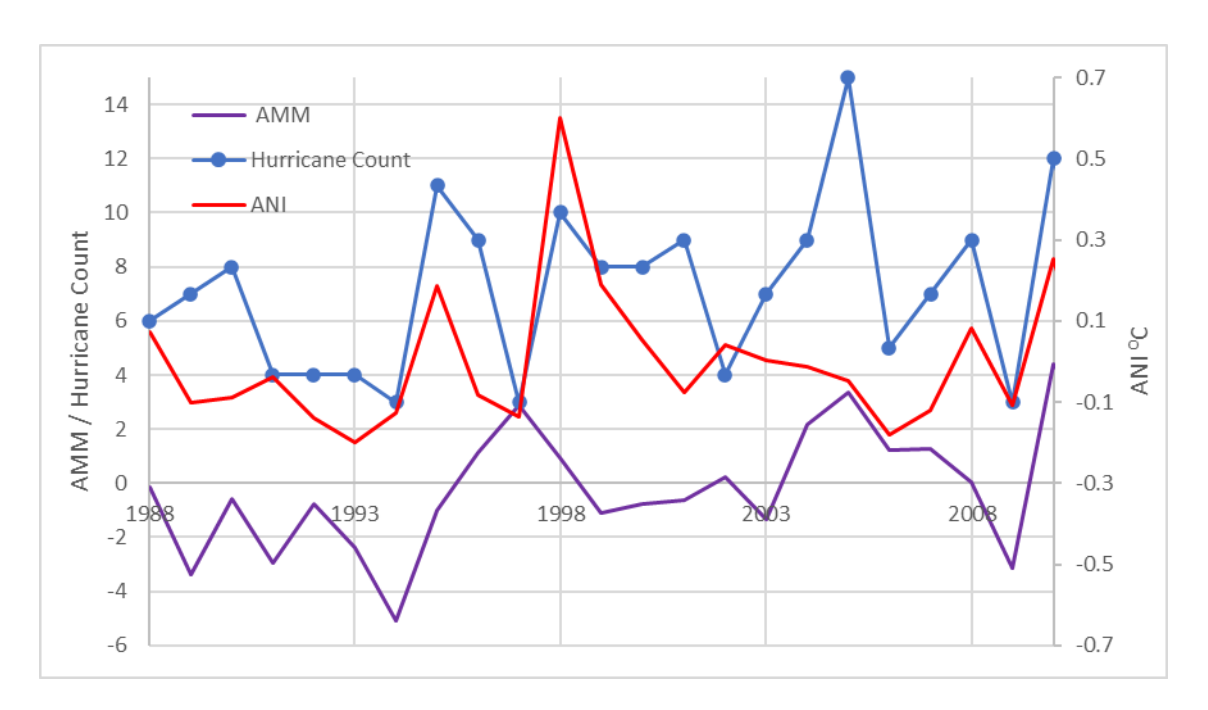


Figure 3.12 Annual mean AMM-index (purple), ANI °C (red), and annual Hurricane count 1988-2010. (Chiang and Vimont (2004).

The North Brazil Current has been discussed in previous sections in relation to inflow of water into the MDR. Transport via this current itself has been observed to exhibit variability on interannual and multidecadal timescales, in connection with AMOC variability (Zhang et al., 2011). However, though much of AMOC variability is buoyancy forced via the formation of North Atlantic Deep Water at higher latitudes, in this region, variability is largely wind-driven (Ruhs et al., 2015).

In summary, the AMM index, AN, and North Brazil Current transport are mainly indicative of trade wind strength which is intimately tied to the development of warm water volume in the northern tropical Atlantic, and the MDR specifically. Changes in tropical circulation associated with larger-scale AMOC variability likely play a secondary role in the MDR heat budget.

3.4 Conclusions

Lagrangian techniques have been used to trace the origin of warm water into the MDR in the Atlantic hurricane season. A climatology is described using high resolution hindcast data spanning 1988-2010. This showed pathways into the MDR via the North Brazil Current, northwards flow across 10 °N, and a component resident in the MDR 6 months earlier, which is more variable in June than September, when most of the near-surface MDR is above the 26.5 °C threshold. On examining heat flux over the 6 months prior to the start of the hurricane season (backtracking experiment BAC06), heat is seen to be lost as water moves along much of these pathways towards the MDR; heat is conversely gained by waters within the MDR, particularly in the spring and summer (BAC09), which is associated with lower easterly wind stress in the region over the backtracking period.

Analysis of warm water source by year showed the variability between seasons, confirming that most of the heat in the MDR by June is resident in the MDR 6 months earlier, and a larger fraction in anomalously warm years with active hurricane seasons. The relative contribution of warm water from the North Brazil Current is hence smaller in these years, pointing to less transport from other potential remote heat sources, leading to anomalously warm and active seasons.

Examination of two warm years, 2005 and 2010, showed different dynamics in these years, with more negative wind stress anomalies in 2010 resulting in less transport into the MDR in connection with Ekman driven slowdown of the AMOC. Smeed et al. (2018) note increased heat transfer into the Atlantic due to this documented phenomenon, including higher sea level along US east coast, which would compound potential storm surge impacts if landfalling hurricanes were to occur in these conditions.

A comparison between a year with a high number of particles warmer than 26.5 °C in the MDR in June (2010) and a year with a low number (2009) highlighted the increased transport in the cooler year across the southern boundary and into the MDR, including the North Brazil Current, driven by anomalously positive wind stress.

Further analysis could use similar methods to trace water north of the MDR backwards from September, to find origins of this larger Atlantic Warm Pool (Wang et al., 2011) in years when the Atlantic is anomalously warm, which is likely more variable than the MDR itself in the late summer.

Selected climate indices are significantly correlated with variability in the interannual contribution of MDR warm water sources. These indices are connected via trade wind strength and offer some insight into seasonal predictability of the climate system in this region.

Predictions for the future also rely on understanding changes in surface heat flux, cloudiness, wind stress, and Ekman transport caused by climate change and variability. Wild (2016) predicts increasing brightness, which would increase atmospheric heat transfer into the ocean. To compound this, Caesar et al. (2021) conclude that the AMOC is weaker than it has been in the last 1000 years, allowing more heat to accumulate in the MDR. These compounded trends are likely to increase MDR heat content further, if persisting into the future.

In summary, we have shown that warm MDR hurricane seasons are characterised by an anomalously large volume of warm water up to 6 months before the start of the hurricane season and relatively low advection of warm water into the MDR. The longer residency of water parcels in the MDR provides more time to be heated by air-sea fluxes, especially in the west of the MDR. Changes in the amount of warm water advected into the MDR are primarily associated with variability of pathways via the North Brazil Current and northwards Ekman drift, both of which are heavily dependent on tropical Atlantic wind stress. We have thus highlighted the relative importance of local and remote drivers of the seasonal warm water volume of the MDR, that in turn drives Atlantic hurricane activity when atmospheric conditions allow.

Acknowledgements

The NEMO-ORCA12 hindcast simulation was carried out by the Marine Systems Modelling group at the National Oceanography Centre (NOC). The version of ARIANE used here was developed by Dr George Nurser of NOC and implemented by Dr Jeffrey Blundell of the University of Southampton. AMM-index data is provided by http://www.aos.wisc.edu/~dvimont/MModes/Data.html.

Chapter 4 Meridional Heat Convergence will Increase Tropical North Atlantic Heat Content Available for Hurricane Intensification

Key Points:

- The volume of warm water increases to the north, east, and in depth, in a high-resolution ocean model with high emissions forcing.
- Convergence of ocean heat transport between 10 °N and 30 °N drives this increase.
- This additional OHC could be available for potential hurricane intensification if atmospheric conditions allow.

Abstract

OHC available for hurricane intensification is expected to increase in a warming world. Mechanisms for growth of the Atlantic Warm Pool to 2050 are examined in a high-resolution coupled ocean and atmosphere model with greenhouse gas forcing. The model warm pool increases in depth as well as northern and eastern extent. While net heat flux from the atmosphere remains stable through the forced model run, heat convergence from reduced heat transport by ocean currents drives growth of the warm pool. While atmospheric heat flux and oceanic heat convergence both contribute to anomalous warm water for hurricane development at present, high resolution ocean modelling suggests that, when atmospheric conditions allow for hurricane formation, increased potential for intensification from a warmer ocean will primarily be due to reduced meridional heat transport.

4.1 Introduction

Recent US landfalling hurricanes have resulted in more than 40 billion USD in damage (NCEI, 2023) in 5 of the last 7 years (2017-2023), bringing to the forefront the need to understand how anthropogenic warming may have contributed to the intensity of these events, and how major hurricanes could develop in a future, warmer climate.

An increasing area of warm tropical Atlantic SST since the 1970s has provided a larger energy source for hurricane intensification (Saunders & Lea, 2008). The Atlantic Warm Pool has maintained feedback loops resulting in lower wind shear and a moist atmosphere (Wang et al., 2007). Annual Atlantic basin major hurricane counts exhibit an increasing trend in the last few

decades (Vecchi, 2021), mainly due to a recovery from anomalously low activity in the 1970s and 80s, compared with subsequent decades (Nyberg et al, 2007, Rousseau-Rizzi & Emanuel, 2022). Recent high major hurricane landfall activity since 2017 (Murakami et al., 2017) marked a return to expected behaviour due to warming Atlantic SSTs, after an unusual gap in the record (Hall & Hereid, 2015). When changes in the observational network are accounted for, there remains significant multidecadal variability, but little upward trend in major hurricane frequency since the 1850s (Vecchi et al., 2021). There is also no upward long-term trend in US landfalling major hurricanes since 1900 (Klotzbach et al., 2018). This record doesn't suffer the same inconsistencies in observational network as the basin count data; few major storms are likely to have been missed, due to fairly continuous population along the US coastline, since the onset of anthropogenic warming.

Observed multi-decadal variability in Atlantic major hurricane activity has been explained by a cool period in the North Atlantic resulting from a combination of sulphate aerosol emissions (Dunstone et al., 2013) and natural variability in ocean circulation (Yan et al., 2017; Zhang et al., 2019). It is difficult to separate the potential impact of climate change on major hurricane frequency from these other atmospheric and oceanic factors which have influenced activity on multidecadal timescales; for example, while Kang and Elsner (2015) found a recent increase in global TC intensity, they do not attribute it to climate change. More generally, while a recent review (Knutson et al., 2019) found mixed evidence to support conjectures that an increase in major hurricane activity has already occurred, continued warming of the tropical ocean due to greenhouse gas forcing could provide the potential for additional hurricane intensification in future decades, provided atmospheric conditions permit tropical cyclone development.

Climate models systematically underestimate the number and strength of tropical cyclones (Walsh et al. 2015). Tropical cyclone activity is simulated in high-resolution climate modelling, HADGEM3-GC3.1-HH, but projected changes for the North Atlantic are inconclusive, particularly as major hurricanes are not produced by even the highest resolution climate models (Roberts et al., 2020a, Davis, 2018). A number of future model projections using downscaling techniques predict a lower frequency of global tropical cyclones, and an increase in the proportion of the most intense storms (Knutson et al., 2020). In general, the reliability of future projections is challenged by the low annual frequency and large variability of TCs (Yoshida et al. 2017). While truly understanding the mechanisms of TC frequency and resolving extreme TCs accurately within climate models remains elusive (Sobel et al., 2021), they can provide insight into the processes which will drive future TC changes.

For example, the AMOC is predicted to decrease in strength due to increased freshwater at high latitudes reducing deep water formation (Madan at al., 2023), as polar ice caps melt. This allows

accumulation of heat in the tropical Atlantic. Variation in inter-model AMOC strength remains a major factor in future climate uncertainty (Bellomo et el., 2021). Liu et al. (2013) consider the historical runs of 19 CMIP5 models, many of which exhibit a cold SST bias in the tropical Atlantic. While this cold bias still exists in CMIP6, higher resolution models more realistically represent ocean processes, so the impacts of continued greenhouse gas warming can be anticipated with greater confidence. Han et al. (2021) examined 33 CMIP6 models and found that model reanalysis skill for tropical cyclone predictor climatology and interannual variability improves with higher horizontal resolution, including tropical SST. This is likely due to the better representation of northwards heat transport via the AMOC (Roberts et al., 2020b), due to increased ocean resolution, as well as improvements in parameterization of the surface mixed layer and interior mixing processes.

Climate models provide projections of the atmospheric variables relevant to hurricane activity, including atmospheric stability, humidity, and vertical wind shear (DeMaria, 2001). Tang and Camargo (2015) propose an index for tropical cyclone activity including vertical wind shear, entropy, and potential intensity, from analysis of CMIP5 models. Tropical Atlantic vertical wind shear, the strength of which is associated with the El Niño Southern Oscillation (ENSO) on interannual timescales, is stronger in climate model projections (Vecchi and Soden, 2007; Emmanuel, 2021), inhibiting hurricane development (Lin et al., 2020). Atlantic vertical wind shear exhibits Interseasonal and intraseasonal variability (Aiyyer and Thorncroft, 2006), leaving windows of opportunity for hurricane development, given existing disturbances and warm SSTs.

Historically, a warmer tropical Atlantic has been linked with increased hurricane activity (Goldenberg et al., 2001, Moharana & Swain, 2023). Warm water is primarily defined here as warmer than 26.5 °C. This has been identified as the threshold temperature for most hurricane development in previous studies (Dare & McBride, 2011; McTaggert-Cowan et al., 2015).

Johnson and Xie (2010) note covariability in tropical SST and convection in satellite precipitation, while Dare and McBride (2011) find that the temperature threshold directly related to tropical cyclogenesis has not been observed to have changed significantly during 1981-2008. However, based on climate model analyses, it has been proposed that the temperature threshold for tropical deep convection could vary with the climate state (Evans and Waters, 2012; Korty et al., 2012; Sugi et al. 2015). Nevertheless, many studies confirm the importance of OHC as a critical ingredient of increased tropical cyclone activity and in model TC simulation (Chan et al., 2021; Hallam et al., 2021; Domingues et al., 2019; Pfleiderer, 2022). The goal here is not to resolve this issue but to diagnose the source of increased ocean heat which will be available for potential TC development when atmospheric conditions allow.

In general, there is low confidence in observed long-term change in major hurricane frequency and uncertainty in their future projections. However, further growth in the amount of warm water available to fuel intense hurricanes would be one factor which could impact Atlantic basin activity in the next few decades. Climate models using high-resolution ocean models can improve projections of hurricane climate predictors, particularly the region of warm water available for hurricane development. In this study, the potential future change in the volume of warm water available for hurricane development is quantified using the HadGEM3-GC3-HH high-resolution climate model with prescribed greenhouse gas forcing following the Shared Socioeconomic Pathway 585 (SSP585) high emissions scenario.

In summary, although climate models suggest that variables other than SST may drive future tropical cyclone frequency, increasing OHC is widely understood to explain recent increases in hurricane activity. Hence the drivers of warm water volume variability in an increasingly warm, forced climate are examined here, including air-sea heat flux into the ocean, and advective heat convergence across the tropical Atlantic. The robustness of the advective heat convergence trend is tested by extending the analysis to three other high-resolution climate models.

4.2 Data and Methods

4.2.1 CMIP6 HighResMIP (High-Resolution Model Intercomparison Project)

High-resolution coupled climate model output is analysed from experiments described by Haarsma et al. (2016). These models start with a short spin-up period of 30 to 50 years and then are run from 1950 through 2050. The control run external forcing is at 1950 levels. Historical forcing is used in years 1950 to 2014. The SSP585 high emissions scenario forcing, where radiative forcing increases to 8.5 Wm⁻² by 2100, is applied during 2015 to 2050.

Our primary focus in this study is analysing the outputs from the high-resolution ocean and atmosphere model HadGEM3-GC31-HH (Roberts et al., 2019), which includes the project's (HighResMIP) highest resolution ocean configuration, at 1/12°. The ocean model is the Nucleus for European Modelling of the Ocean (NEMO) version 3.6 (Madec et al., 2017), with 75 levels. Atmospheric resolution is 50 km.

To sample the diversity of model configuration and resolution, we compare data from three other high-resolution models (Table 1), including HadGEM3-GC31-HM with a lower resolution ocean model, at ¼ ° (HM), EC-Earth3P (ECE), with a similar configuration to HM (Haarsma et al., 2020), and CESM1-3 (CESM), which uses the POP ocean model at 1/10 ° horizontal resolution (Danabasoglu et al., 2012; Small et al., 2014), with 25 km atmospheric resolution.

Table 4.1 HighResMIP Model configurations

			Horizontal Resolution	
Model	Resolution Name	Ocean Model	Ocean	Atmosphere (km)
HadGEM3-GC31	HH	NEMO 3.6	1/12°	50
	HM	NEMO 3.6	1/4°	50
EC-Earth3P	HR	NEMO 3.6	1/4°	50
CESM1-3	HH	POP	1/10°	25

4.2.2 Ocean Data

The observed volume of Atlantic water warmer than specific temperature thresholds, north of 10 °N, was calculated using the UK Met Office Hadley Centre EN4 subsurface ocean temperature analysis, which provides ocean analysis data from 1900 to the present (Good et al., 2013). This dataset contains gridded subsurface temperature at 42 discrete depths, at 1 ° latitude longitude horizontal resolution, from 1900 to the present, from 83 °S to 90 °N. While this dataset offers a longer record than other datasets, direct observations used are increasingly scarce with depth and further back in time.

The mean decadal observed depth of the 26.5 °C isotherm, north of 10 °N, was calculated using the GODAS ocean reanalysis product (Behringer and Xue, 2004). This dataset contains gridded global potential temperature at 40 discrete depths, at 1/3 ° latitude and 1 ° longitude spacing, from 1980.

4.2.3 Atmospheric and Surface Flux Data

ERA5 (Hersbach et al., 2020) is produced by the Copernicus Climate Change Service (C3S) at the European Centre for Medium-Range Weather Forecasts (ECMWF). It is the fifth generation ECMWF atmospheric reanalysis of the global climate covering the period from January 1940 to the present. Hourly 30 km grid data is aggregated to monthly averages. Surface latent heat flux, net solar and longwave radiation, and sensible heat flux are used in this analysis.

4.2.4 Hurricane Data

Annual North Atlantic basin major hurricane counts are collected from the International Best Track Archive for Climate Stewardship (IBTrACS) (Knapp et al., 2010; Knapp et al., 2018) Version 4 dataset for the Atlantic basin. This data consists of storm-centred point data from 1851, which includes maximum 1 minute mean winds at 6-hourly intervals over the ocean, more frequent near land, rounded to the nearest 5 knots. Unique storms reaching greater than 96 knots of maximum wind speed in their lifetime during 1980 to 2022 are identified here, as recorded by the NHC.

4.2.5 Water Mass Transformation

From the original formulation of Walin (1982), the WMT framework (Groeskamp et al. 2019) is applied in temperature space, quantifying volume fluxes across isotherms associated with variations of heat fluxes in that property space. With this diagnostic, we attribute variations in warm water volume to variations in surface heat exchanges. The net surface heat flux, Q_{net} , combines Q_{sw} , Q_{lw} , Q_{sh} , and Q_{lh} . Throughout this study, the convention is that all heat fluxes are positive into the ocean:

$$Q_{\text{net}} = Q_{\text{sw}} + Q_{\text{lw}} + Q_{\text{sh}} + Q_{\text{lh}}$$
 (1)

Across temperature space, the volume of water transformed by Q_{net} is calculated over the North Atlantic, north of 10 °N, where tropical storms are able to form due to sufficient Coriolis acceleration. Firstly, the Diathermal Temperature Flux, $Q_{in}(T)$ (°C m³ s-¹) (2), is found by areaintegrating Q_{net} , where SST is at or above a given value of temperature, T, then dividing by reference density, ρ_0 , and specific heat capacity, c_p :

$$Q_{in}(T) = \frac{1}{\rho_o c_p} \int_{x_w}^{x_e} \int_{y_s}^{y_n} Q_{net}(x, y) \Gamma(SST(x, y), T) dx dy \quad (2)$$

where x, y are distance in west (w) to east (e) and south (s) to north (n) directions, and Γ is a sampling function; $\Gamma = 1$ where SST > T, otherwise $\Gamma = 0$. Q_{net} values at the potential temperature grid points are found using bilinear interpolation.

The thermal water mass transformation rate, $F_T(T)$ (m³ s⁻¹), can then be arrived at by taking differences between $Q_{in}(T)$ across two temperature surfaces:

$$F_T(T - \Delta T/2, T + \Delta T/2) = \frac{Q_{in}(T - \Delta T/2) - Q_{in}(T + \Delta T/2)}{\Delta T}$$
 (3)

The WMT framework is used here to diagnose the contribution of heat flux trends from air-sea interaction to the evolving volume of warm water in the tropical North Atlantic in a warming future climate.

4.2.6 Back-tracking warm water (TRACMASS)

The TRACMASS Lagrangian trajectory code has been designed for use with gridded weather and climate models to track water paths and associated heat and salt fluxes (Aldama-Campino et al., 2020; Döös et al., 2017). One of the unique characteristics of TRACMASS is that it uses differential equations and mass transport fields at the grid cell walls to analytically calculate the trajectory path through grid boxes. The use of mass transport in a grid cell makes TRACMASS a mass-conserving algorithm. From changes in temperature along each path, we obtain

Lagrangian heat divergences, which are ensemble-averaged to obtain heat input to the northward flow across tropical latitudes. Here we track water paths backwards from latitudes currently relevant to hurricane development for water warmer than 26.5 °C. Water parcels are seeded so there is at least one water path start point per HADGEM3-GC3.1-HH grid cell.

4.3 Results

4.3.1 Future Trends in Available Heat Content

In this section, we investigate HADGEM3-GC3.1-HH 1950-2050 predicted changes in the amount of heat potentially available for hurricane intensification. We first evaluate changes in the Atlantic Warm Pool at various temperature thresholds at the peak of hurricane season in the high-resolution model, referencing observational data for model validation. Timeseries of total volume and area of warm water are presented. Maps of the decadal mean depth of the 26.5 °C isotherm are included to highlight the regional extent of warm water through the forced model run.

The total model volume of water in the North Atlantic north of 10 °N and warmer than 26.5 °C, 27.5 °C and 28.5 °C is summed for the month of September, and plotted over time, in Figure 4.1. September is the peak of the hurricane season; 48% of major hurricanes intensified to 96 knots or above in this month during 1900-2023. The forced run is compared with the control run and EN4 observations.

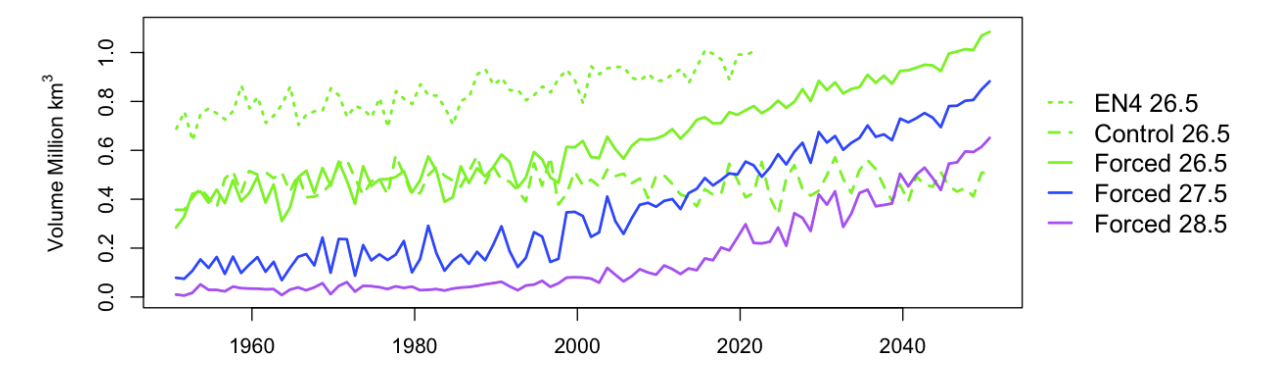


Figure 4.1 September HADGEM3-GC3.1-HH 1950-2050 forced run mean monthly volume (million km³) in the North Atlantic north of 10 °N of water warmer than 26.5 °C (green, solid), 27.5 °C (blue), and 28.5 °C (purple); warmer than 26.5 °C in the control run (green, dashed), and EN4 1950-2022 (green, dotted).

The HADGEM3-GC3.1-HH September volume of warm water (> 26.5 °C) increases gradually from 1950 to around 2000, after which it increases rapidly with additional external forcing in the model high emissions forced years. The 1950-1959 September mean monthly volume warmer

than 26.5 °C is 0.40 million km³. In the final decade of the years with historical forcing, 2005-2014, the mean September volume of warm water has reached 0.64 million km³, an increase of 0.04 million km³ per decade. The rate of change increases with time in the forced run. The model predicts 0.96 million km³ by 2040-2049, an increase of 0.08 million km³ per decade compared with the volume at the end of the period with historical forcing. Hence, the model predicts 56% more warm water by the middle of the 21st century, with high emissions forcing. The trend in observed September volume of water warmer than 26.5 °C is an increase of 0.003 million km³ per year. The model cool bias in the tropical North Atlantic is clear, as the EN4 monthly mean warm water volume (> 26.5 °C) in is nearly twice as large as the warm water volume in the high-resolution model.

HADGEM3-GC3.1-HH mean monthly area and depth of water warmer than 26.5 °C in the North Atlantic north of 10 °N in September is shown in Figure 4.2. As with warm water volume, the area at the surface also increases, with an increase in the rate of change in the forced run. The mean depth of the September 26.5 °C isotherm north of 10 °N also continues to increase in the high emissions years of the forced run. Both the area and depth of the warm water pool increases, so volume changes are not only the result of both increasing area and depth of the 26.5 °C isotherm with atmospheric forcing.

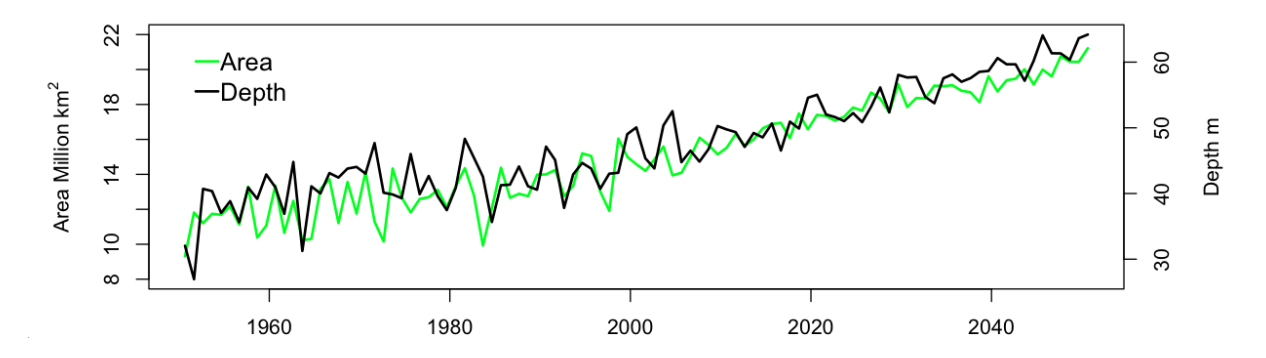


Figure 4.2 September mean monthly area of water (million km²) warmer than 26.5 °C in the North Atlantic north of 10 °: HADGEM3-GC3.1-HH 1950-2050 forced run (green) and depth of the 26.5 °C isotherm (black).

The depth of the HADGEM3-GC3.1-HH forced September 26.5 °C isotherm is plotted by decade, providing spatial insight into the depth and extent of the Atlantic Warm Pool (Figure 4.3, rows 1 and 3). The warm water area expands to the north and east over time and deepens in the Caribbean Sea and western tropical Atlantic. This is compared with GODAS (rows 2 and 4). A larger area of warm water extending vertically to 100 m is evident in the observational data than in the model, due to the HADGEM3-GC3.1-HH cold bias. A thin layer of warm water (light yellow) extends further to the north and east in the HADGEM3-GC3.1-HH maps due to higher resolution of vertical levels near the surface than in the GODAS data. GODAS vertical levels have a 10 m

resolution in the top 100 m. The much higher resolution of HH vertical levels near the surface do not average out very shallow warm temperatures in surface layers.

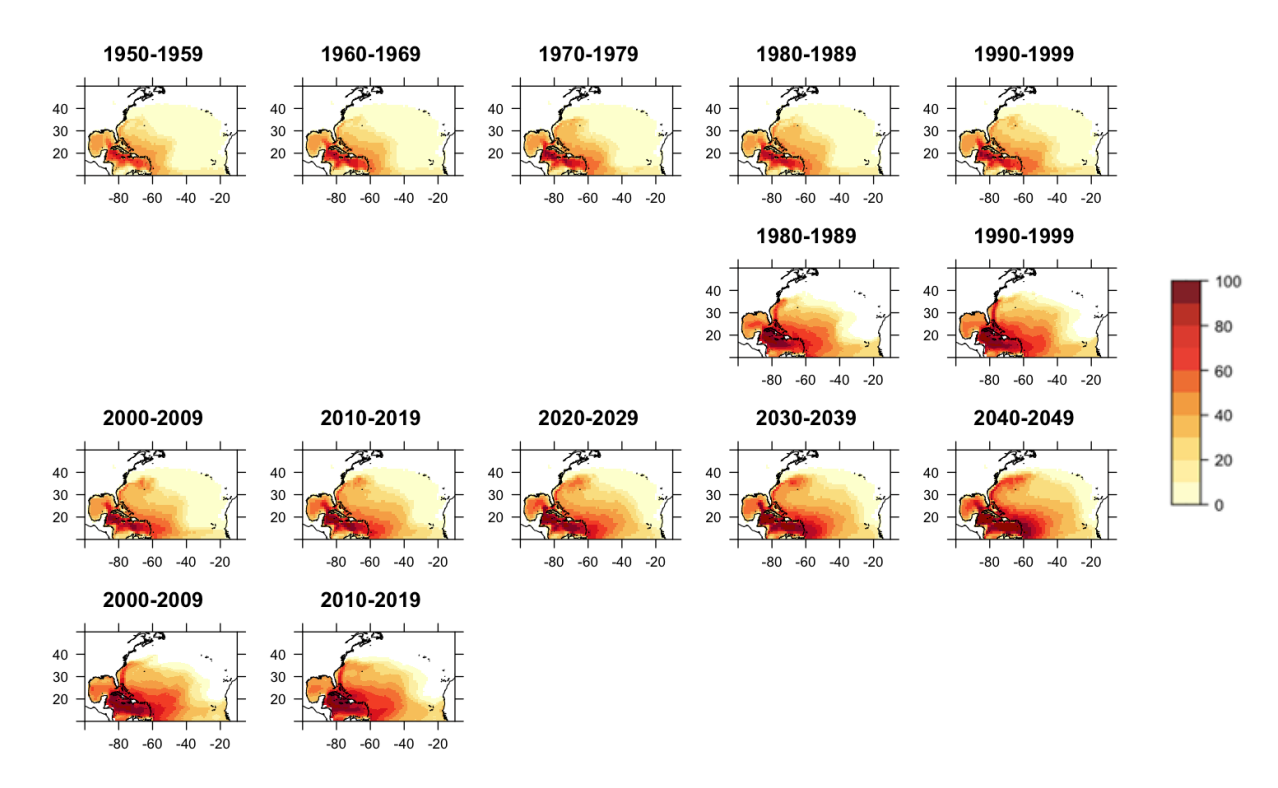


Figure 4.3 Depth of the September 26.5 °C isotherm (m) in the North Atlantic north of 10 °N by decade 1950-2049 HADGEM3-GC3.1-HH forced run (rows 1 and 3) and 1980-2019 GODAS (rows 2 and 4).

The HADGEM3-GC3.1-HH model predicts a high emissions scenario future with a much larger volume of deep warm water extending further north and east than the present day. In the following sections, we analyse changes in the mechanisms of heat transfer into the tropical North Atlantic, to diagnose which processes drive the projected increase in warm water in high resolution forced models, with a focus on HADGEM3-GC3.1-HH.

4.3.2 Changes in Atmospheric Heat Flux

Heat exchange between the atmosphere and ocean is a major driver of interannual variability in the volume of warm water in the tropical North Atlantic, particularly through latent heat flux (Hallam et al., 2019). Similarly, an increasing trend in heat flux into the ocean over surface water which flows through the tropical Atlantic would result in an increase in warm water volume. Additional absorption of heat from the atmosphere could be a result of, for example, higher humidity surface conditions decreasing latent heat flux from the ocean by reducing evaporation, and/or decreased cloudiness, allowing additional short-wave radiation absorption into the ocean.

We inspect the main drivers of heat accumulation in the tropical North Atlantic in HADGEM3-GC3.1-HH, to explain these changes in the warm water pool. HADGEM3-GC3.1-HH heat flux in the North Atlantic between 10 °N and 30 °N is examined. This covers the region of 26.5 °C water, where 90% of hurricanes intensify into major hurricanes (Figure 4.4). We then calculate the volume of water transformed across isotherms, using the WMT framework, to quantify the ocean-atmosphere heat exchange driving Atlantic Warm Pool volume changes.

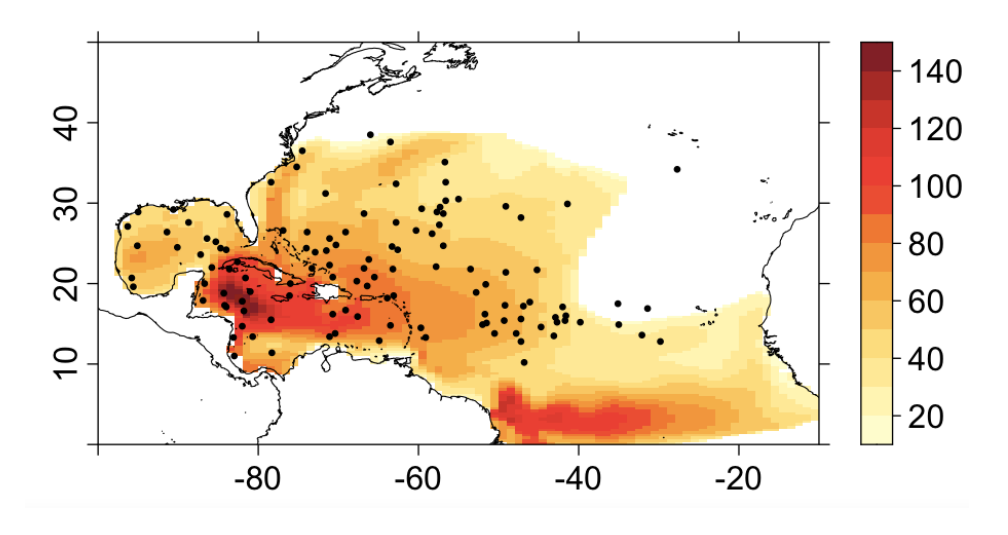


Figure 4.4 1980-2022 Mean depth of GODAS September 26.5 °C isotherm (m) and IBTrACS points 1980-2022 where hurricanes intensified into major hurricanes.

Figure 4.5 shows a small upward trend in Q_{net} into the ocean in HADGEM3-GC3.1-HH over the Atlantic between 10 °N and 30 °N in the forced model run. The mean 2015-2050 Q_{net} is 0.04 Wm⁻² higher than the 1950-2014 mean. This small change in Q_{net} is a consequence of large but compensating changes in the component fluxes (not shown here) in the model. The small change in Q_{net} then suggests that transfer of additional heat from the atmosphere into the ocean at these latitudes is not the driver of increasing Atlantic Warm Pool by 2050 in the high-resolution model.

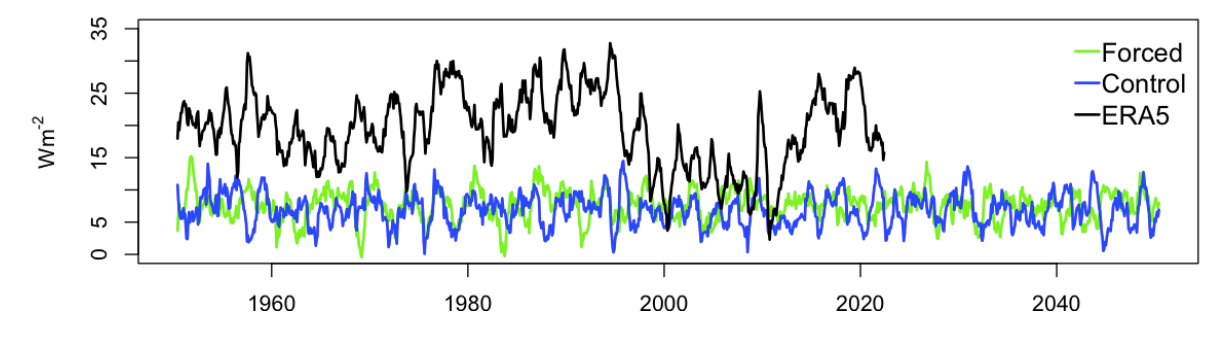


Figure 4.5 Mean monthly Q_{net} into the Atlantic Ocean (Wm⁻²) 10 °N to 30 °N with 12-month centred moving average: HADGEM3-GC3.1-HH 1950-2050 forced run (green) and control (blue), compared with observed ERA5 (black).

Observed (ERA5) Q_{net} is higher into the ocean and exhibits more variability than the model on multidecadal timescales. ERA5 heat input into the ocean has a negative trend in this period of - 0.04 Wm⁻² per year. Mayer et al. (2023) likewise observe a negative trend for a sample location in the tropical North Atlantic, which they suggest is due to global warming.

The volume of water transformed across the isotherms which have historically been relevant to hurricane development in the North Atlantic north of 10 °N can be calculated using the WMT framework (Harris et al., 2022). This metric diagnoses the additional volume of water warmer than these temperature thresholds. The total volume increases due to both deepening of the 26.5 °C isotherm and a larger area of water warmer than 26.5 °C, over which the heat flux into the ocean warms the Atlantic Warm Pool.

Figure 4.6 indicates that the amount of water transformed across the 26.5 °C, 27.5 °C, and 28.5 °C isotherms. For each temperature threshold, the transformed volume is positive from 1950-2050 in the forced run. Using this framework, the rate at which water is transformed by atmospheric heat flux increases around 2000. The transformed volume peaks in the mid-2020s and then begins to decline towards the end of the simulation for water transformed across 26.5 °C, as much of the tropics and subtropics reach this temperature, but continues to increase for higher temperature thresholds.

As the WMT framework calculates the volume transformed by heat flux bounded by the area of water at that temperature, the increase in transformed volume of 26.5 °C water over time must be due to an increasing area of water over which the transformed volume is calculated, rather than an increase in the heat flux into the ocean, as suggested by the absence of a trend in HADGEM3-GC3.1-HH atmospheric heat exchange (Figure 4.5).

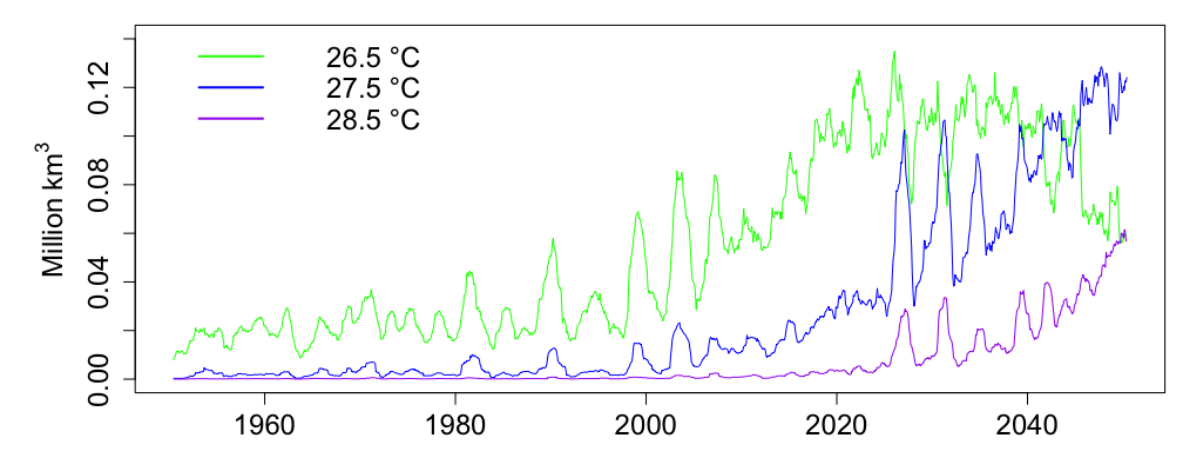


Figure 4.6 Mean monthly volume (million km³) of water transformed across the 26.5 °C (green), 27.5 °C (blue) and 28.5 °C (purple) isotherm, with 12-month centred moving average.

The significant increase in the size of the Atlantic Warm Pool by 2050 in the HADGEM3-GC3.1-HH forced run cannot be attributable to additional absorption of net heat transfer from the atmosphere as greenhouse gases continue to increase (from Figure 4.5). Hence, next, we consider the contribution of advective heat flux by ocean currents.

4.3.3 Climate change and Tropical Atlantic Advective Heat Flux

In this section, the advective component of warm water volume changes in the tropical Atlantic in the HADGEM3-GC3.1-HH forced run are discussed. warm water volume convergence between 10 °N and 30 °N is analysed across a suite of 'HighResMIP' ocean models. These models differ by resolution and ocean model, adding robustness to our results. Employing a complementary technique, we also use TRACMASS Lagrangian analysis applied to HADGEM3-GC3.1-HH forced simulation output to analyse ocean properties and heat convergence along trajectories, and hence, diagnose mechanisms of advective heat transfer into the tropical Atlantic. These trajectories are calculated backwards from 20 °N in the Atlantic for 6 months prior to June 30, near the beginning of the hurricane season.

Figure 4.7 shows the warm water volume convergence between 10 °N and 30 °N. This is calculated by subtracting the volume transport across 30 °N from the volume transport at 10 °N. This has been calculated using meridional mass transport from four high-resolution ocean climate models. All models show an increase in warm water convergence between these latitudes at these temperatures. Convergence of water warmer than 26.5 °C increases after 2000 and begins to decrease after 2030. At this time there is still a larger volume of water warmer than 26.5 °C transported across 10 °N than 30 °N. However, the difference between the transport across the higher and lower latitudes decreases, as the Atlantic Warm Pool extends this far north most of the time by the end of the simulation. At higher temperature thresholds, warm water convergence increases through the model run as the amount of water warmer than these temperatures steadily increases between these latitudes.

HADGEM3-GC3.1-HM behaves in a similar fashion, although the decline in convergence of 26.5 °C and warmer water is less pronounced than in the HADGEM3-GC3.1-HH model. The ECE model convergence of 26.5 °C plateaus in the forced run, rather than declines. The CESM model, on the other hand, shows less increase in convergence at any temperature threshold, which may be due to its near-surface warm bias (Roberts et al., 2020b).

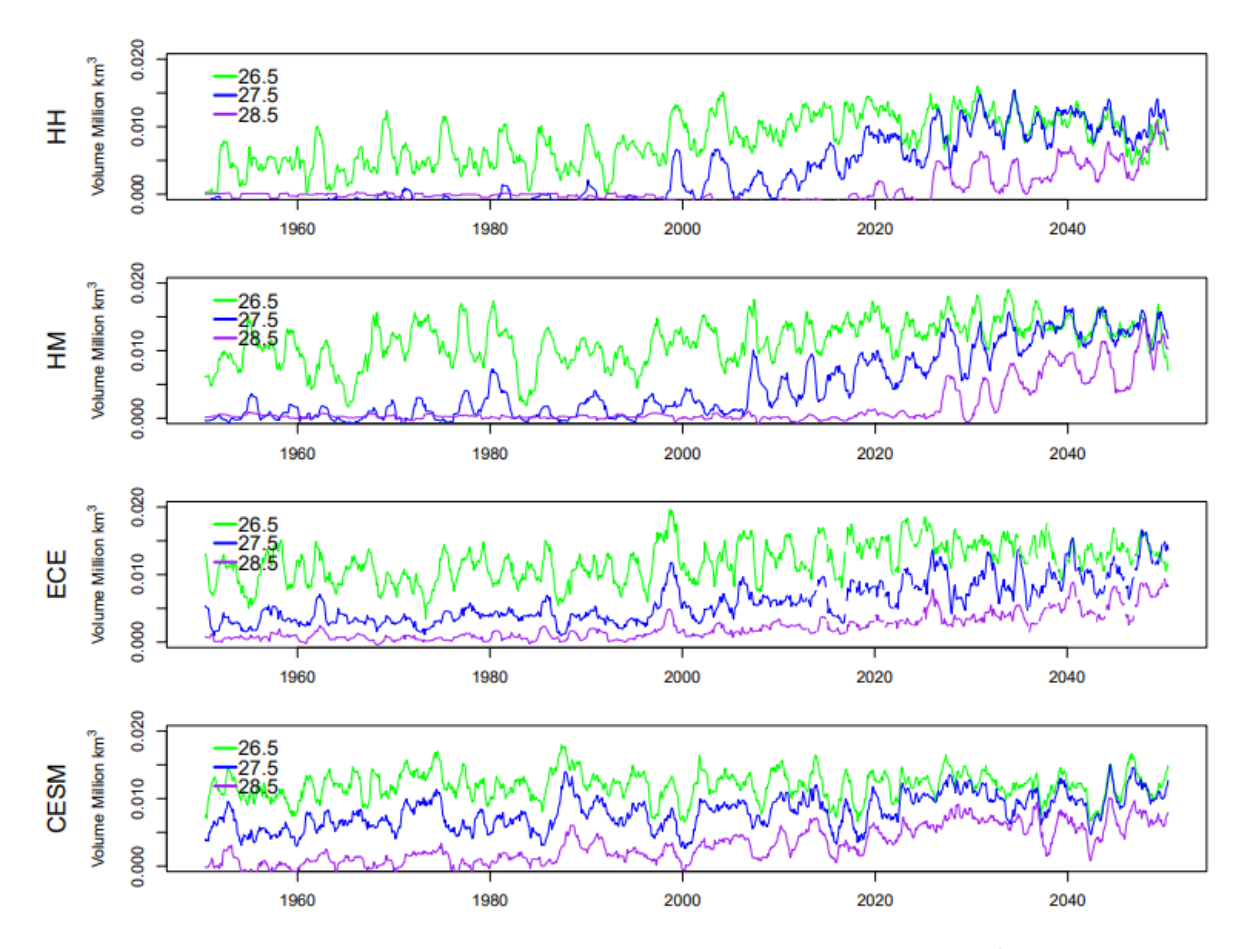


Figure 4.7 Monthly meridional convergence of warm water volume (million km³) convergence between 10 °N and 30 °N with 12-month centred moving average for water warmer than 26.5 °C (green), 27.5 °C (blue), and 28.5 °C (purple) in HADGEM3-GC3.1-HH, HADGEM3-GC3.1-HM, ECE and CESM.

Analysis of output of this suite of high-resolution forced ocean models shows an increase in the volume of water warmer in the region of recent hurricane development. The increase in greenhouse gases in the HADGEM3-GC3.1-HH forced run results in a greater reduction in ocean transport via weakening of the AMOC (Roberts et al., 2020b), when compared to lower resolution ocean models. An oceanic decrease in heat transfer to higher latitudes allows heat to accumulate in the tropical Atlantic, and the Atlantic Warm Pool consequently expands northward and eastward.

To confirm and develop these findings, Lagrangian trajectory analysis of warm water flow into the tropical North Atlantic is undertaken. TRACMASS calculations using output from the HADGEM3-GC3.1-HH forced run are obtained as 6-month backwards trajectories from particles seeded at 20 °N, on June 30 of each of 10 years in 3 decades: 1951-1960, 2001-2010, and 2041-2050. This latitude is in the middle of the region of warm water analysed in previous sections. The choice of start date, near the beginning of the hurricane season, is motivated by the fact that the observed interannual variability at June 30 is higher than in September (Harris et al., 2023), during which time much of water at this latitude is warmer than 26. 5 °C in most historical

Chapter 4

years. The variability is significantly correlated with annual major Atlantic basin hurricane counts over 1980-2022, with Pearson Correlation Coefficient of .44, significant at the 95% level (Figure 4.8).

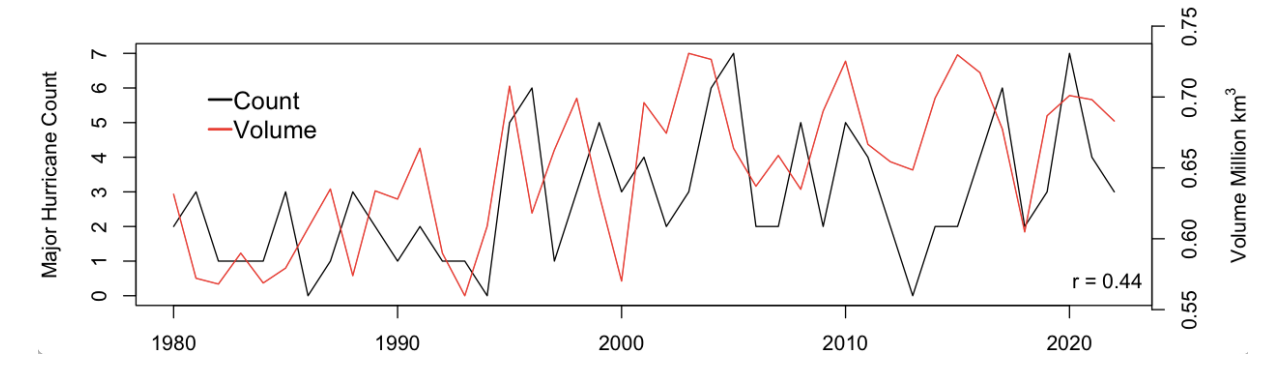


Figure 4.8 GODAS July 1 volume (million km3) of water warmer than 26.5 °C between 10 °N and 30 °N (red) and annual major hurricane count (black) 1980-2022.

The mean January – June temperature of warm water (warmer than 26.5 °C) particle tracks ending at 20 °N at the end of June in the HADGEM3-GC3.1-HH forced run is plotted in Figure 4.9 (right) for the 3 decades representing pre-industrial conditions at the start of the model run, 1951-1960 (top), 2001-2010, near the end of the historical forcing (middle), and the last decade of the high emissions forcing, 2041-2050 (bottom). Particle temperatures at all time stamps through the experiment of particles which are located within 0.5 degree grid boxes are averaged, and then averaged over 10 years to smooth interannual variability. The mean temperature of warm water arriving at 20 °N by July 1 is notably warmer near the coast of central America and in the Amazon outflow region in the 2000s than the 1950s. Warm water sources extend 20 degrees further east of the Caribbean. By the 2040s, warm water sources are 2 °C degrees warmer over most of the Caribbean Sea, and 3 °C warmer near the coast of central America and in the Amazon outflow region. Warm water sources extend as far east as 30 °W in the North Atlantic.

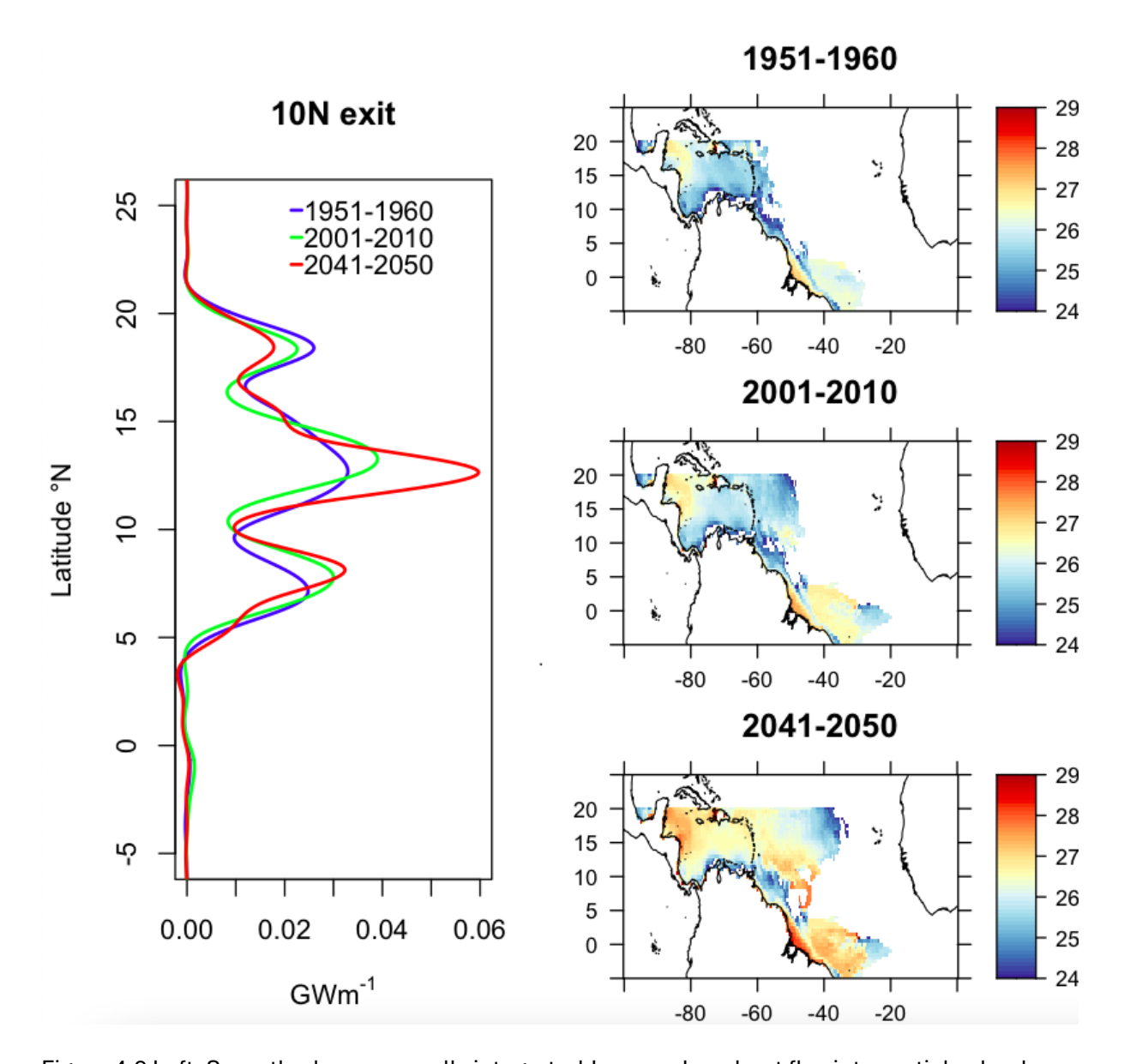


Figure 4.9 Left: Smoothed mean zonally integrated January-June heat flux into particles backtracked from 20 °N, which cross 10 °N (GWm⁻¹ positive for heat gain) by latitude, averaged over 1951-1960 (blue), 2001-2010 (green), and 2041-2050 (red). Right: January-June mean particle temperature (°C) within 0.5 degree grid boxes averaged over a decade; 1951-1960 (top), 2001-2010 (middle), and 2041-2050 (bottom).

The zonally integrated meridional heat flux for particle tracks ending at 20 °N after 6 months, which cross 10 °N, summarises total energy into warm water sources from other regions. This is plotted by latitude in Figure 4.9 (left). Across all latitudes, the total heat flux along these particle tracks changes very little from the first historical decade (1951-1960, 3.8 GW) to the later historical decade (2001-2010, 3.7 GW). By the final future forced decade (2041-2050), the total heat accumulation along particle tracks crossing 10 °N and ending at 20 °N after 6 months, which are warmer than 26.5 °C, is 14% higher than final historical forced decade (4.2 GW).

Heat flux along these tracks peaks between 12 °N and 14 °N. There is 0.01 GWm⁻¹ more zonally-integrated heat convergence at the latitude of smoothed peak heat flux by the present-day decade than the pre-industrial decade, and an additional 0.02 GWm⁻¹ of smoothed peak heat flux by the near-future decade than the present-day. In summary, HADGEM3-GC3.1-HH predicts that more heat will move through the tropical Atlantic from south of 10 °N over the next few decades, with the peak heat flux convergence just north of 10 °N.

This accumulation of heat in the tropical Atlantic is evident in the mean sea temperature map of the 2040s (Figure 4.9, bottom right), where much warmer water, with temperatures greater than 27 °C, reach 20 °N in the previous six months than in the earlier decades, the 1950s and 2000s, where there is less change in the temperature of water parcels approaching 20 °N by July 1.

In summary, two techniques are used here to quantify changes in ocean currents leading to future accumulation of heat in HADGEM3-GC3.1-HH over the region of recent hurricane development. Advective heat convergence between 10 °N and 30 °N is quantified and compared with other high-resolution models. A complementary technique, Lagrangian heat convergence analysis backwards from 20 °N, is used to confirm findings. Both methods highlight the role of reduced meridional ocean transport in the next few decades, allowing more heat accumulation into the tropical Atlantic by the middle of the century, beginning around the present-day.

4.4 Conclusions

We have quantified changes in the volume of warm water related to increasing OHC, which could be available for hurricane intensification in the tropical North Atlantic in the forced run of a high-resolution ocean model. The pool of warm water becomes more widespread to the north and east, as well as deepening. Quantification of changes in tropical North Atlantic mechanisms, leading to heat accumulation in a high-resolution forced ocean model, provide insight into one factor which could impact future hurricane risk, due an increase in deeper, more extensive pool of warm water which would be available for development of major hurricanes when atmospheric conditions are conducive to tropical deep convection.

This warm water volume is positively correlated with annual major Atlantic hurricane counts in the observational record, though climate models suggest lower hurricane frequency in a warmer climate. Looking forward to a warmer future, the HADGEM3-GC3.1-HH volume of water warmer increases steadily towards 2050, at a higher rate than has been observed, albeit from a lower starting point in the model. This indicates that more intense hurricanes are possible in a warmer climate when atmospheric conditions allow.

While net heat flux into the tropical Atlantic does not increase in the HADGEM3-GC3.1-HH forced run, the amount of water transformed across warm isotherms does increase, due to the larger surface area of warm water just below these temperatures. However, this increase in the area is itself not expanding because of heat transfer mechanisms from the atmosphere, but due to oceanic processes.

Heat accumulation in this expanding region of warm water in the North Atlantic stems from slower ocean circulation in HADGEM3-GC3.1-HH. This is quantified by the increasing volume of heat convergence between 10 °N and 30 °N, which is also found in in 3 other high-resolution climate models. Likewise, Lagrangian heat convergence analysis for water arriving at 20 °N by July 1 shows a dramatic increase in warm water parcels by the 2040s, relative to the difference between the changes from the 1950s to the present day. HADGEM3-GC3.1-HH has the highest climate model ocean resolution available and the largest increase in warm water between latitudes currently relevant to major hurricane development, suggesting that, from an ocean heat perspective, there will be more potential for future hurricane intensification not found in previous climate model studies using lower resolution models.

OHC is projected to increase due a larger volume of warm water in the tropical Atlantic, driven by slower ocean circulation, if greenhouse gas emissions continue at the present rate. Future climate model runs at even higher resolutions could better resolve oceanic and atmospheric pathways for heat transfer into the tropical Atlantic, as well as detecting intense hurricanes themselves, and overcoming SST biases, which would increase confidence in future hurricane activity projections.

Acknowledgements

The ORCA12 hindcast was led by Dr Alex Megann of the National Oceanography Centre. The HighResMIP simulations were undertaken by many dedicated colleagues, who have kindly provided the community with access to the model data. Analysis of the ORCA12 hindcast and HighResMIP simulations was undertaken on JASMIN, the UK collaborative data analysis facility. We acknowledge Dr Jeffrey Blundell from the University of Southampton, UK for his unconditional support in setting up TRACMASS on JASMIN.

Chapter 5 Summary

This study has been motivated by striking variations in recent Atlantic hurricane seasonal activity, from the record high activity of 2005, which initiated use of Greek letters to name

storms after the prescribed list was exhausted, to surprisingly low activity in 2013 (Klotzbach et al., 2013). Oceanic drivers of the variability in Atlantic hurricane activity are identified and quantified, with answers developed for open questions in the contribution of these to variable warm water volume on interannual timescales in the recent past and near future, as follows:

- Variability, trends, and drivers of warm water volume relevant to hurricane development are examined using:
 - o Gridded observational ocean data
 - High-resolution climate models
- New techniques are applied which diagnose drivers of anomalous tropical Atlantic warm water volume:
 - o Eulerian approach: WMT framework in temperature space
 - Lagrangian analysis: Ariane and TRACMASS
- Contributions are quantified from both atmospheric and oceanic sources to:
 - o warm water volume historical interannual anomalies
 - warm water volume future trends

This work uses novel methods to more effectively diagnose dynamics of warm water volume accumulation in the tropical Atlantic available for major hurricane development in both the recent past and the near future, when extreme major hurricane activity of the current climate could become the new normal.

5.1 Context and Overview

Hurricane climatology includes distribution of hurricane genesis, seasonality, tracks, and landfall regions (NHC, 2023), all of which are related to temporal and spatial patterns of warm water in the tropics and their influence on atmospheric circulation and stability. While much of this detail is well-documented in studies based on historical data (Bell & Chelliah, 2006; Goldenberg et al., 2001; Zhang & Delworth, 2006), reproducing comparable statistics in climate models has proven to be difficult due not only to low spatial and temporal resolution, but also SST biases (Chan et al., 2021).

Observed hurricane activity varies on a variety of timescales, including sub-seasonal, interannual, and multidecadal, and these variations are related to available tropical OHC on similar timescales. Observed changes in Atlantic SST are associated with both variations in heat exchange with the atmosphere and with variable ocean circulation. More specifically, atmospheric heat flux has been impacted by changes in atmospheric sulphate aerosols (Booth et al., 2012; Dunstone et al, 2013), African dust (Dunion & Velden, 2004), and cloud cover

(Bellomo et al., 2016). AMOC transport variability impacts Atlantic hurricane activity (Yan et al., 2017; Zhang et al., 2019), notably the component driven by Ekman dynamics in the tropics (Duchez et al., 2016). Seasonal forecasting of annual hurricane activity shows little skill at time horizons longer than a few weeks (Lea, 2024), partly due to the chaotic nature of short timescale weather events, so additional insights into more predictable factors like Atlantic SST may be an area where forecasts could be improved.

While investigations strive to explain interannual changes in hurricane activity in the current climate, there is even more concern regarding possible future changes in a warmer climate. Current research on the impacts of anthropogenic climate change on hurricane activity has concluded that, while no signal has been definitively observed in basin or landfall activity to date, hurricane frequency in the Atlantic will decrease in the future, but intensity of the strongest storms will increase (IPCC, 2023). However, much uncertainty remains due to large cold biases in many models, low spatial and temporal resolution, and poor representation of ENSO and the AMOC (Han et al., 2021).

This thesis examines contributions to observed interannual anomalies and future trends in warm water volume attributed to changes in atmospheric heat flux and ocean heat transport.

5.2 Warm water transformation – the Eulerian perspective

Chapter 2 (Harris at el., 2022) quantified the contribution of warm water volume available for hurricane intensification from atmospheric heat exchange with the ocean. This process, in particular latent heat flux, has been highlighted in previous studies as a driver of tropical Atlantic OHC during 2017 (Hallam et al., 2019). The WMT framework in temperature space in the North Atlantic is used to answer this question, which calculates warm water volume produced by heat flux across temperature thresholds related to hurricane development.

The anomalous volume of water warmer than 26.5 °C in the North Atlantic north of 10 °N is compared with annual hurricane counts. Positive anomalies are more common after 1995, as are hurricane counts. This link is fundamental to the subsequent analyses through the thesis. Spatial correlation between the depth of the 26.5 °C in May and annual hurricane counts supports this link, and potential for preseason hurricane activity predictability. The spatial pattern is similar to that of the tripolar AMO, with high positive correlation in a horseshoe shape to the north, east and south of the subtropical gyre. Likewise, locations where storms intensify into hurricanes are spatially coherent with the depth of the 26.5 °C in September.

Positive correlation is found between water transformed across 26.5 °C and observed warm water volume 1980-2019, although these two quantities are out of phase in some years. In 1998,

there was a particularly close match between the observed volume of water in the North Atlantic at this temperature and the calculated volume from atmospheric heat flux. Net heat flux into the ocean had been anomalously positive over most the of the North Atlantic for the months leading up to the peak of the 1998 hurricane season. In 2009/10, on the other hand, observed and transformed warm water volume are not clearly related. This leaves room for oceanic rather than atmospheric contributions to warm water volume, which is supported by the changes in the RAPID heat transport timeseries from the same time period.

Considering individual components of Q_{net} in the transformed volume, the latent heat flux component was found to explain 35% of the total transformed volume. Negative spatial correlations of Q_{th} with surface wind speed and cloud fraction over the warm water volume region provide evidence that low winds and cloud cover diminish heat transfer from the atmosphere into the ocean by latent heat exchange. When less heat is lost through evaporation, in some years this has increased the warm water volume available for hurricane intensification. Thus, the analysis clearly identifies that, though latent heat flux drives warm water volume in some years, additional oceanic processes must explain the warm water volume in the remaining hurricane seasons to close the tropical Atlantic heat budget from an Eulerian perspective.

5.3 Tracing sources of warm water – the Lagrangian perspective

Heat transport via ocean currents naturally accounts for the residual of the previous analysis of heat transfer into hurricane regions from atmospheric heat exchange. However, heat transport into the tropical Atlantic is difficult to quantify due to disparate observational networks. Hence, Chapter 3 (Harris et al. 2023) uses Lagrangian analysis to quantify contributions to warm water volume from oceanic heat transport, revealing oceanic pathways of heat transfer into the MDR.

In this chapter, water particles warmer than 26.5 °C in NEMO-ORAC12 1988-2012 hindcast model output are traced backwards from the MDR in September using the ARIANE package. The number of particles in the MDR in both June and September varies in a similar fashion to the September warm water volume and annual hurricane counts, with peaks in active hurricane seasons. Interannual variability is higher in June, at the beginning of the hurricane season, than September, the peak of the season, when most particles within the MDR are already warmer than 26.5 °C.

In the 6 months prior to the start of the hurricane season, warm water particles flow into the MDR via the North Brazil Current and across 10 °N via Ekman drift, or continuously reside within the MDR. The percentage of particles which are found within the MDR 6 months before the

beginning of the hurricane season has clear peaks corresponding to the most active hurricane seasons during the study period, e.g. 2005 and 2010. Similarly, the percentage of warm particles arriving into the MDR from the North Brazil Current peaks in years with low activity in the MDR, e.g. 2009. In high hurricane activity years, with more warm particles in the MDR in the beginning of the hurricane season and the 6 months prior, wind stress anomalies in the previous 6 months are anomalously low. This demonstrates how low wind stress in the tropical North Atlantic leads to less movement of water into the MDR, allowing water in the MDR to gain heat and drive active hurricane seasons.

This chapter adds clarity to questions around mechanisms of accumulation of warm water volume into the MDR via ocean transport by quantifying interannual differences in particle movement from various sources into the MDR. The MDR itself is materially the main source of warm water available for hurricane development when ocean transport from other sources is lower, resulting in more warm water accumulating in the tropical Atlantic and higher basin hurricane counts.

5.4 Drivers of future changes in Warm Water Volume of likely consequence for hurricane seasons

Chapters 2 and 3 interrogated observational and hindcast datasets to determine methods of warm water volume accumulation in the tropical Atlantic in the current climate. However, it is expected that oceanic conditions will evolve due to increased anthropogenic gas emission. While no trend in basin activity has heretofore been detected to date (Vecchi et al., 2021), studies have identified to the threat of a tipping point in ocean circulation in the near future (van Westen at al., 2024), which would impact hurricane development. High-resolution climate model output is the best tool at our disposal today to assess possible future changes in hurricane activity due to anthropogenic climate change. The final chapter of this thesis quantified modelled extension of warm water volume in the tropical Atlantic and examined evolution of current oceanic drivers of hurricane activity in a warming world.

The two techniques outlined in Chapters 2 and 3 were applied to HadGEM3-GC31-HH high-resolution forced climate model data in Chapter 4 (Harris et al. 2024). This chapter quantified impacts on these dynamics under climate change, in modelling with the most realistic ocean dynamics available. While this coupled model makes major strides over lower resolution climate models in that it does in fact generate hurricane strength cyclones, the fact remains that hurricanes of major hurricane strength, with winds greater than 111 mph, are not resolved (Roberts et al., 2020). These are the most material events to life and property loss, and therefore of most interest to society. Additionally, while the 26.5 °C threshold has been established as a

major factor in observed hurricane genesis, climate model studies have shown larger numbers of hurricanes in a cooler climate (Sugi et al., 2015), and fewer in a future warmer climate (IPCC, 2023). This implies that hurricane activity on longer timescales is affected by additional factors which contribute to future convective potential. Nevertheless, in recent years, MDR SST and hurricane activity have both continued to escalate, with extreme warm SSTs observed in 2023 and 2024, leading to concerns over further heat accumulation in the tropical North Atlantic.

HadGEM3-GC31-HH North Atlantic warm water volume above a variety of temperature thresholds related to observed hurricane activity is shown to increase from 1950-2050, accelerating after 2020 as forcing increases. The Atlantic Warm Pool expands to the north, east, and down the water column, which creates a larger area of the ocean able to support dangerous hurricanes. While the amount of water transformed across relevant temperature thresholds increases after 2000, Q_{net} has little upwards trend, implying that while the amount of energy supplied to the ocean surface remains relatively constant (though individual components vary), the area of water available to be transformed to warmer temperatures increases in area, due to ocean dynamics.

warm water volume convergence increased between 10 °N and 30 °N at 3 temperature thresholds in all 4 HighResMIP models analysed, for the warmest water at these latitudes where major hurricanes develop, providing evidence that slower ocean circulation could lead to accumulation of warm water available for hurricane intensification in a warming climate. Additional support was offered by TRACMASS backwards-in-time Lagrangian calculations, which show much more heat flux into the ocean along water particle trajectories 6 months prior to the beginning of hurricane seasons with additional forcing compared with historical forcing.

Assessment of warm water volume in the highest available resolution climate model, supported by additional HighResMIP models, highlights an increasing trend in Atlantic Warm Pool growth in the high-emissions scenario as greenhouse gases continue to increase. This potentially rapidly-increasing energy source in the near future, which can fuel destructive storm development, should be a source of great concern – adding global pressure to prevent greenhouse gas emissions rising to this level, to prevent such a scenario.

5.5 Concluding Remarks and Outlook

In these analyses, a combination of both Eulerian and Lagrangian diagnostics have provided complementary perspectives on variations of warm water volume that play a key role in the Atlantic hurricane seasons, in current and future climate states. Inputs have been quantified from observational atmospheric and oceanic data into one major driver of hurricane severity

and intensity: the volume of warm water available as an underlying energy source for deep convection. This analysis was extended to high-resolution climate model data for the next couple of decades with high emissions.

Drivers of observed anomalous interannual warm water volume available to fuel dangerous hurricanes were explored: atmospheric heat flux and ocean heat transport. The study determines that combined atmospheric and oceanic dynamics contribute to warm water volume, with contributions from each pathway varying by year. Figure 5.1 Schematics highlighting the relative importance of local and remote forcing of the warm water volume: (a) strong recirculation and heat gain in the MDR leading to enhanced warm water volume (WWV), coincident with weakening imports from the south via the North Brazil Current and Ekman drift; (b) reversed scenario, leading to reduced warm water volume (WWV). Note that the North Brazil Current and Ekman drift are not necessarily strengthened in (b) relative to (a), but are found to contribute proportionately more to the warm water volume in (b), when this volume is backtracked over 6 months. depicts scenario(s) for accumulation of positive (negative) anomalous warm water volume, with increased (decreased) atmospheric heat flux and weaker (stronger) meridional ocean transport.

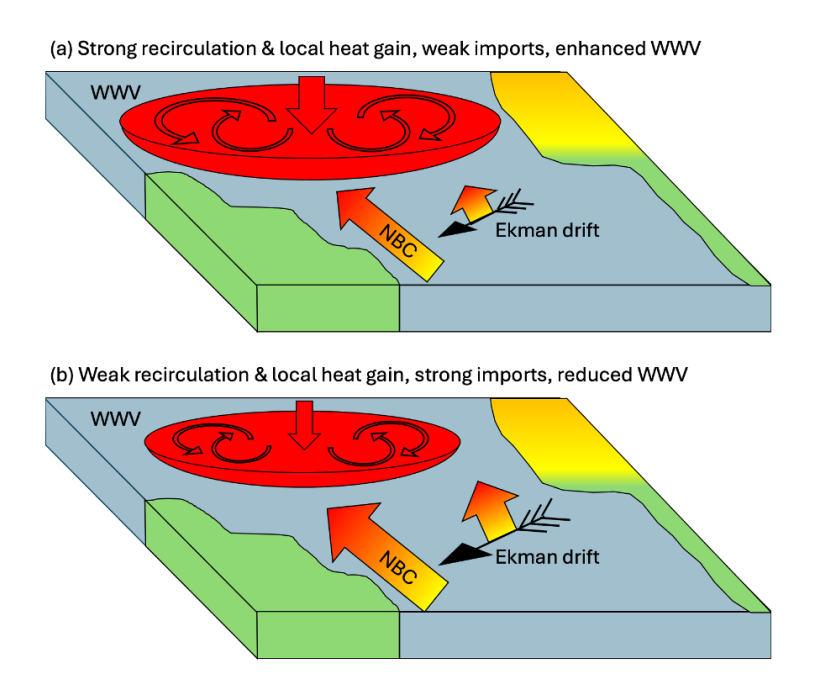


Figure 5.1 Schematics highlighting the relative importance of local and remote forcing of the warm water volume: (a) strong recirculation and heat gain in the MDR leading to enhanced warm water volume (WWV), coincident with weakening imports from the south via the North Brazil Current and Ekman drift; (b) reversed scenario, leading to reduced warm water volume (WWV). Note that the North Brazil Current and Ekman drift are not necessarily strengthened in (b) relative to (a), but are found to

contribute proportionately more to the warm water volume in (b), when this volume is back-tracked over 6 months.

The dual relative importance of both atmospheric and oceanic variables highlights the need for robust monitoring systems to improve seasonal hurricane activity prediction. Real time reporting of remote ocean transport detection (e.g. RAPID programme) would provide necessary information on AMOC transport in advance of the hurricane season, improving predictions for years like the very active 2010 hurricane season, when large, positive OHC anomalies arose as a consequence of weaker meridional transport (Hallam et al., 2019).

Looking forward, high-resolution climate modelling suggests that increasing ocean heat transport into the tropical Atlantic will result in an increasing trend of warm water volume by 2050, if anthropogenic carbon emissions continue to increase. While studies (IPCC, 2023) conclude that hurricane frequency is most likely to decrease in the future, this dramatic rise in warm water volume would allow development of much stronger storms when atmospheric conditions allow for storm intensification. The MDR has been increasingly warm in recent years, with extreme SSTs in 2023 and early 2024, which has generated rapidly intensifying storms, including Category 5 Hurricane Beryl, which was the strongest storm ever to occur in June in the historical record. This is a warning of potential future conditions as the climate continues to warm.

The advances made in this thesis towards the understanding of drivers of major hurricane probability in the current and near future climate will improve societal resilience to upcoming disasters. Current statistical seasonal forecasting techniques based on regression analysis still suffer from unexpected changes in the climate system due to weather noise. Machine learning techniques may allow for more inputs, but miss extreme events not represented by the training data. Climate prediction from combined Al/physics will allow for faster, cheaper climate analyses without the need for supercomputers (Kochkov et al., 2024). As resolution increases, climate models may eventually capture more hurricane activity, but the current low spatial and temporal resolution, as well as SST biases, limit the simulation of the most destructive extreme winds. Continued investigation into understanding hurricane frequency and intensity on interannual and multidecadal timescales due to atmospheric and oceanic factors will improve forecast tools to increase human resilience to these devastating events.

Aiyyer, A. R., & Thorncroft, C. (2006). Climatology of vertical wind shear over the tropical Atlantic. Journal of Climate, 19(12), 2969-2983.

Aldama-Campino, Aitor, Döös, Kristofer, Kjellsson, Joakim, & Jönsson, Bror. (2020). TRACMASS: Formal release of version 7.0 (Version v7.0-beta). Zenodo.

http://doi.org/10.5281/zenodo.4337926

Balaguru, K., Leung, L. R., & Yoon, J. H. (2013). Oceanic control of northeast Pacific hurricane activity at interannual timescales. Environmental Research Letters, 8(4), 044009.

Behringer, D. W., & Xue, Y. (2004, January). Evaluation of the global ocean data assimilation system at NCEP: The Pacific Ocean. In Proc. Eighth Symp. on Integrated Observing and Assimilation Systems for Atmosphere, Oceans, and Land Surface. Seattle, Wash: AMS 84th Annual Meeting, Washington State Convention and Trade Center.

Bell, G. D., & Chelliah, M. (2006). Leading tropical modes associated with interannual and multidecadal fluctuations in North Atlantic hurricane activity. Journal of Climate, 19(4), 590-612.

Bellomo, K., Angeloni, M., Corti, S., & von Hardenberg, J. (2021). Future climate change shaped by inter-model differences in Atlantic meridional overturning circulation response. Nature Communications, 12(1), 3659.

Bellomo, K., Clement, A. C., Murphy, L. N., Polvani, L. M., & Cane, M. A. (2016). New observational evidence for a positive cloud feedback that amplifies the Atlantic Multidecadal Oscillation. Geophysical Research Letters, 43(18), 9852-9859.

Birkel, S. D., Mayewski, P. A., Maasch, K. A., Kurbatov, A. V., & Lyon, B. (2018). Evidence for a volcanic underpinning of the Atlantic multidecadal oscillation. NPJ Climate and Atmospheric Science, 1(1), 1-7.

Blaker, A. T., Hirschi, J. J. M., McCarthy, G., Sinha, B., Taws, S., Marsh, R., et al. (2015). Historical analogues of the recent extreme minima observed in the Atlantic meridional overturning circulation at 26 N. Clim. Dyn. 44, 457–473. Doi: 10.1007/s00382-014-2274-6

Blanke, B. and Raynaud, S. (1997). Kinematics of the Pacific Equatorial Undercurrent: an Eulerian and Lagrangian approach from GCM results. J. Phys. Oceanogr., 27, 1038-1053.

Booth, B. B., Dunstone, N. J., Halloran, P. R., Andrews, T., & Bellouin, N. (2012). Aerosols implicated as a prime driver of twentieth-century North Atlantic climate variability. Nature, 484(7393), 228-232.

Bryden, H. L., Johns, W. E., King, B. A., McCarthy, G., McDonagh, E. L., Moat, B. I., & Smeed, D. A. (2020). Reduction in ocean heat transport at 26 N since 2008 cools the eastern subpolar gyre of the North Atlantic Ocean. Journal of Climate, 33(5), 1677-1689.

Bryden, H. L., King, B. A., McCarthy, G. D., & McDonagh, E. L. (2014). Impact of a 30% reduction in Atlantic meridional overturning during 2009-2010. Ocean Science, 10(4), 683-691.

Buckley, M. W., & Marshall, J. (2016). Observations, inferences, and mechanisms of the Atlantic Meridional Overturning Circulation: A review. Reviews of Geophysics, 54(1), 5-63.

Caesar, L., McCarthy, G. D., Thornalley, D. J. R., Cahill, N., & Rahmstorf, S. (2021). Current Atlantic meridional overturning circulation weakest in last millennium. Nature Geoscience, 14(3), 118-120.

Cai, W., Santoso, A., Collins, M., Dewitte, B., Karamperidou, C., Kug, J. S., ... & Zhong, W. (2021). Changing El Niño–Southern oscillation in a warming climate. Nature Reviews Earth & Environment, 2(9), 628-644.

Cangialosi, J. P., Blake, E., DeMaria, M., Penny, A., Latto, A., Rappaport, E., & Tallapragada, V. (2020). Recent progress in tropical cyclone intensity forecasting at the National Hurricane Center. Weather and Forecasting, 35(5), 1913-1922.

Chan, D., Vecchi, G. A., Yang, W., & Huybers, P. (2021). Improved simulation of 19th-and 20th-century North Atlantic hurricane frequency after correcting historical sea surface temperatures. Science advances, 7(26), eabg6931.

Cheng, L., von Schuckmann, K., Abraham, J. P., Trenberth, K. E., Mann, M. E., Zanna, L., ... & Lin, X. (2022). Past and future ocean warming. Nature Reviews Earth & Environment, 3(11), 776-794.

Cheng, L., von Schuckmann, K., Minière, A., Hakuba, M. Z., Purkey, S., Schmidt, G. A., & Pan, Y. (2024). Ocean heat content in 2023. Nature Reviews Earth & Environment, 1-3.

Chiang, J. C., & Vimont, D. J. (2004). Analogous Pacific and Atlantic meridional modes of tropical atmosphere–ocean variability. Journal of Climate, 17(21), 4143-4158.

Cunningham SA, Kanzow T., Rayner D., Baringer M.O., Johns W.E., et al. (2007), Temporal variability of the Atlantic meridional overturning circulation at 26.5°N. Science, 317:935–938.

Dailey, P.S., Zuba, G., Ljung, G., Dima, I.M., Guin, J. (2009), On the Relationship between North Atlantic Sea Surface Temperatures and U.S. Hurricane Landfall Risk. Journal of Applied Meteorology and Climatology 48, 111-129.

Danabasoglu, G. (2008). On multidecadal variability of the Atlantic meridional overturning circulation in the Community Climate System Model version 3. Journal of Climate, 21(21), 5524-5544.

Danabasoglu, G., Bates, S. C., Briegleb, B. P., Jayne, S. R., Jochum, M., Large, W. G., ... & Yeager, S. G. (2012). The CCSM4 ocean component. Journal of Climate, 25(5), 1361-1389.

Dare, R. A., & McBride, J. L. (2011). The threshold sea surface temperature condition for tropical cyclogenesis. Journal of climate, 24(17), 4570-4576.

Davis, C. A. (2018). Resolving tropical cyclone intensity in models. Geophysical Research Letters, 45, 2082–2087.

DeMaria, M. (1996). The effect of vertical shear on tropical cyclone intensity change. Journal of the atmospheric sciences, 53(14), 2076-2088.

DeMaria, M., Knaff, J. A., & Connell, B. H. (2001). A tropical cyclone genesis parameter for the tropical Atlantic. Weather and Forecasting, 16(2), 219-233.

Dickson, R. R., & Brown, J. (1994). The production of North Atlantic Deep Water: sources, rates, and pathways. Journal of Geophysical Research: Oceans, 99(C6), 12319-12341.

Doi, T., Tozuka, T., and Yamagata, T. (2010). The Atlantic meridional mode and its coupled variability with the Guinea Dome. J. Clim. 23, 455–475. Doi: 10.1175/2009JCLI3198.1

Domingues, R., Kuwano-Yoshida, A., Chardon-Maldonado, P., Todd, R. E., Halliwell, G., Kim, H. S., ... & Goni, G. (2019). Ocean observations in support of studies and forecasts of tropical and extratropical cyclones. Frontiers in Marine Science, 6, 446.

Döös, K., Jönsson, B., & Kjellsson, J. (2017). Evaluation of oceanic and atmospheric trajectory schemes in the TRACMASS trajectory model v6. 0. Geoscientific Model Development, 10(4), 1733-1749.

Duchez, A., Courtois, P., Harris, E., Josey, S. A., Kanzow, T., Marsh, R., ... & Hirschi, J. J. M. (2016). Potential for seasonal prediction of Atlantic sea surface temperatures using the RAPID array at 26 °N. Climate Dynamics, 46, 3351-3370.

Dunion, J. P., & Velden, C. S. (2004). The impact of the Saharan air layer on Atlantic tropical cyclone activity. Bulletin of the American Meteorological Society, 85(3), 353-366.

Dunstone, N. J., Smith, D. M., Booth, B. B. B., Hermanson, L., & Eade, R. (2013). Anthropogenic aerosol forcing of Atlantic tropical storms. Nature Geoscience, 6(7), 534-539.

Elsner, J. B., & Jagger, T. H. (2004). A hierarchical Bayesian approach to seasonal hurricane modeling. Journal of Climate, 17(14), 2813-2827.

Emanuel, K. (2001). Contribution of tropical cyclones to meridional heat transport by the oceans. Journal of Geophysical Research: Atmospheres, 106(D14), 14771-14781.

Emanuel, K. (2021). Response of global tropical cyclone activity to increasing CO 2: Results from downscaling CMIP6 models. Journal of Climate, 34(1), 57-70.

Enfield, D. B., Mestas-Nuñez, A. M., & Trimble, P. J. (2001). The Atlantic multidecadal oscillation and its relation to rainfall and river flows in the continental US. Geophysical research letters, 28(10), 2077-2080.

Evan, A. T., Vimont, D. J., Heidinger, A. K., Kossin, J. P., & Bennartz, R. (2009). The role of aerosols in the evolution of tropical North Atlantic Ocean temperature anomalies. Science, 324(5928), 778-781.

Evans, J. L., & Waters, J. J. (2012). Simulated relationships between sea surface temperatures and tropical convection in climate models and their implications for tropical cyclone activity. Journal of climate, 25(22), 7884-7895.

Ffield, A. (2007). Amazon and Orinoco River plumes and North Brazil Current rings: Bystanders or participants in hurricane events? Journal of Climate, 20(2), 316-333.

Fraza, E., & Elsner, J. B. (2015). A climatological study of the effect of sea-surface temperature on North Atlantic hurricane intensification. Physical Geography, 36(5), 395-407.

Garcia-Soto, C., Cheng, L., Caesar, L., Schmidtko, S., Jewett, E. B., Cheripka, A., ... & Abraham, J. P. (2021). An overview of ocean climate change indicators: Sea surface temperature, ocean heat content, ocean pH, dissolved oxygen concentration, arctic sea ice extent, thickness and volume, sea level and strength of the AMOC (Atlantic Meridional Overturning Circulation). Frontiers in Marine Science, 8, 642372.

George, J. E., & Gray, W. M. (1976). Tropical cyclone motion and surrounding parameter relationships. Journal of Applied Meteorology (1962-1982), 1252-1264.

Goldenberg, S. B., Landsea, C. W., Mestas-Nuñez, A. M., & Gray, W. M. (2001). The recent increase in Atlantic hurricane activity: Causes and implications. Science, 293(5529), 474-479.

Good, S. A., Martin, M. J., & Rayner, N. A. (2013). EN4: Quality controlled ocean temperature and salinity profiles and monthly objective analyses with uncertainty estimates. Journal of Geophysical Research: Oceans, 118(12), 6704-6716.

Gray, W. M. (1975). Tropical cyclone genesis.

Gray, W. M. (1982). Tropical cyclone genesis and intensification. In Intense Atmospheric Vortices: Proceedings of the Joint Symposium (IUTAM/IUGG) held at Reading (United Kingdom) July 14–17, 1981 (pp. 3-20). Berlin, Heidelberg: Springer Berlin Heidelberg.

Gray, W. M., Landsea, C. W., Mielke Jr, P. W., & Berry, K. J. (1992). Predicting Atlantic seasonal hurricane activity 6–11 months in advance. Weather and Forecasting, 7(3), 440-455.

Grist, J. P., S. A. Josey, R. Marsh, Y.-O. Kwon, R. J. Bingham, and A. T. Blaker (2014), The Surface-Forced Overturning of the North Atlantic: Estimates from Modern Era Atmospheric Reanalysis Datasets. J. Climate, 27, 3596-3618. doi: 10.1175/JCLI-D-13-00070.1

Groeskamp, S., & Iudicone, D. (2018). The effect of air-sea flux products, shortwave radiation depth penetration, and albedo on the upper ocean overturning circulation. Geophysical Research Letters, 45(17), 9087-9097.

Groeskamp, S., Griffies, S.M., Iudicone, D., Marsh, R., Nurser, A.G., and J.D. Zika (2019). The water mass transformation framework for ocean physics and biogeochemistry. Ann. Rev. Mar. Sci., 11 (1), 271-305.

Guishard, M. P., Nelson, E. A., Evans, J. L., Hart, R. E., & O'Connell, D. G. (2007). Bermuda subtropical storms. Meteorology and Atmospheric Physics, 97(1), 239-253.

Haarsma, R. J., Roberts, M. J., Vidale, P. L., Senior, C. A., Bellucci, A., Bao, Q., ... & von Storch, J. S. (2016). High resolution model intercomparison project (HighResMIP v1. 0) for CMIP6.

Geoscientific Model Development, 9(11), 4185-4208.

Haarsma, R., Acosta Cobos, M. C., Bakhshi, R., Bretonnière, P. A., Caron, L. P., Castrillo, M., ... & Wyser, K. (2020). HighResMIP versions of EC-Earth: EC-Earth3P and EC-Earth3P-HR–description, model computational performance and basic validation. Geoscientific Model Development, 13(8), 3507-3527.

Hall, T., & Hereid, K. (2015). The frequency and duration of US hurricane droughts. Geophysical Research Letters, 42(9), 3482-3485.

Hallam, S., Guishard, M., Josey, S. A., Hyder, P., & Hirschi, J. (2021). Increasing tropical cyclone intensity and potential intensity in the subtropical Atlantic around Bermuda from an ocean heat content perspective 1955–2019. Environmental Research Letters, 16(3), 034052.

Hallam, S., Marsh, R., Josey, S. A., Hyder, P., Moat, B., & Hirschi, J. J. M. (2019). Ocean precursors to the extreme Atlantic 2017 hurricane season. Nature communications, 10(1), 1-10.

Hallam, S., McCarthy, G. D., Feng, X., Josey, S. A., Harris, E., Düsterhus, A., ... & Hirschi, J. J. (2023). The relationship between sea surface temperature anomalies, wind and translation speed and North Atlantic tropical cyclone rainfall over ocean and land. Environmental Research Communications, 5(2), 025007.

Han, Y., Zhang, M. Z., Xu, Z., & Guo, W. (2021). Assessing the performance of 33 CMIP6 models in simulating the large-scale environmental fields of tropical cyclones. Climate Dynamics, 1-16.

Harris, E., Dey, D., Marsh, R., & Grist, J. (2024). Meridional Heat Convergence Will Increase Tropical North Atlantic Heat Content Available for Hurricane Intensification. In Advances in Hurricane Risk in a Changing Climate (pp. 77-95). Cham: Springer Nature Switzerland.

Harris, E. A., Marsh, R., & Grist, J. P. (2023). Tracing oceanic sources of heat content available for Atlantic hurricanes. Journal of Geophysical Research: Oceans, e2022JC019407.

Harris, E., Marsh, R., Grist, J.P., and G.D. McCarthy (2022). The water mass transformation framework and variability in hurricane activity. Climate Dynamics, 59 (3-4), 961-972.

Hersbach, H., Bell, B., Berrisford, P., Hirahara, S., Horányi, A., Muñoz-Sabater, J., ... & Thépaut, J. N. (2020). The ERA5 global reanalysis. Quarterly Journal of the Royal Meteorological Society, 146(730), 1999-2049.

Hieronymus, M., Nilsson, J., & Nycander, J. (2014). Water mass transformation in salinity–temperature space. Journal of Physical Oceanography, 44(9), 2547-2568.

Holland, G., & Bruyère, C. L. (2014). Recent intense hurricane response to global climate change. Climate Dynamics, 42, 617-627.

Holmes, R. M., Zika, J. D., & England, M. H. (2019). Diathermal heat transport in a global ocean model. Journal of Physical Oceanography, 49(1), 141-161.

Holte, J., Talley, L. D., Gilson, J., & Roemmich, D. (2017). An Argo mixed layer climatology and database. Geophysical Research Letters, 44(11), 5618-5626.

Houze Jr, R. A. (2012). Orographic effects on precipitating clouds. Reviews of Geophysics, 50(1).

IPCC, 2023: Summary for Policymakers. In: Climate Change 2023: Synthesis Report.

Contribution of Working Groups I, II and III to the Sixth Assessment Report of the

Intergovernmental Panel on Climate Change [Core Writing Team, H. Lee and J. Romero (eds.)].

IPCC, Geneva, Switzerland, pp. 1-34, doi: 10.59327/IPCC/AR6-9789291691647.001

Jesús González-Alemán, J., Evans, J. L., Kowaleski, A. M., & Ángel Gaertner, M. (2018, April). Factors affecting the structural evolution and predictability of the tropical transition of Hurricane Alex (2016). In EGU General Assembly Conference Abstracts (p. 475).

Jiang, X., Adames, A., Kim, D., Maloney, E. D., Lin, H., Kim, H., et al. (2020). Fifty years of research on the Madden-Julian oscillation: Recent progress, challenges and perspectives. Journal of Geophysical Research-Atmospheres, 125(17), e2019JD030911.

Johns, W. E., Elipot, S., Smeed, D. A., Moat, B., King, B., Volkov, D. L., & Smith, R. H. (2023). Towards two decades of Atlantic Ocean mass and heat transports at 26.5 N. Philosophical Transactions of the Royal Society A, 381(2262), 20220188.

Johnson, G. C., & Lyman, J. M. (2020). Warming trends increasingly dominate global ocean. Nature Climate Change, 10(8), 757-761.

Johnson, N. C., & Xie, S. P. (2010). Changes in the sea surface temperature threshold for tropical convection. Nature Geoscience, 3(12), 842-845.

Kalnay, E., Kanamitsu, M., Kistler, R., Collins, W., Deaven, D., Gandin, L., ... & Zhu, Y. (1996). The NCEP/NCAR 40-year reanalysis project. Bulletin of the American meteorological Society, 77(3), 437-472.

Kang, N. Y., & Elsner, J. B. (2015). Trade-off between intensity and frequency of global tropical cyclones. Nature Climate Change, 5(7), 661-664.

Kanzow, T., H. L. Johnson, D. P. Marshall, J. J.-M. Hirschi, A. Mujahid, H. L. Bryden, and W. E. Johns (2009). Basin-wide integrated volume transports in an eddy-filled ocean. J. Phys. Knapp, K. R., Kruk, M. C., Levinson, D. H., Diamond, H. J., & Neumann, C. J. (2010). The international best track archive for climate stewardship (IBTrACS) unifying tropical cyclone data. Bulletin of the American Meteorological Society, 91(3), 363-376.

Klotzbach, P. J. (2010). On the Madden–Julian oscillation–Atlantic hurricane relationship. Journal of Climate, 23(2), 282-293.

Klotzbach, P. J. (2011). El Niño-Southern Oscillation's impact on Atlantic basin hurricanes and US landfalls. Journal of Climate, 24(4), 1252-1263.

Klotzbach, P. J., Bowen, S. G., Pielke, R., & Bell, M. (2018). Continental US hurricane landfall frequency and associated damage: Observations and future risks. Bulletin of the American Meteorological Society, 99(7), 1359-1376.

Klotzbach, P., Ventrice, E. B., Saunders, M., Lea, A., & Galarneau, T. (2013). The Surprisingly Quiet 2013 Atlantic Basin Hurricane Season.

Knapp, K. R., Kruk, M. C., Levinson, D. H., Diamond, H. J., & Neumann, C. J. (2010). The international best track archive for climate stewardship (IBTrACS) unifying tropical cyclone data. Bulletin of the American Meteorological Society, 91(3), 363-376.

Knowles, J. T., & Leitner, M. (2007). Visual representations of the spatial relationship between Bermuda High strengths and hurricane tracks. Cartographic Perspectives, (56), 37-51.

Knutson, T., Camargo, S. J., Chan, J. C., Emanuel, K., Ho, C. H., Kossin, J., ... & Wu, L. (2019). Tropical cyclones and climate change assessment: Part I: Detection and attribution. Bulletin of the American Meteorological Society, 100(10), 1987-2007.

Knutson, T., Camargo, S. J., Chan, J. C., Emanuel, K., Ho, C. H., Kossin, J., ... & Wu, L. (2020). Tropical cyclones and climate change assessment: Part II: Projected response to anthropogenic warming. Bulletin of the American Meteorological Society, 101(3), E303-E322.

Kochkov, D., Yuval, J., Langmore, I., Norgaard, P., Smith, J., Mooers, G., ... & Hoyer, S. (2024). Neural general circulation models for weather and climate. Nature, 1-7.

Korty, R. L., Camargo, S. J., & Galewsky, J. (2012). Tropical cyclone genesis factors in simulations of the Last Glacial Maximum. Journal of Climate, 25(12), 4348-4365.

Kossin, J. P. (2018). A global slowdown of tropical-cyclone translation speed. Nature, 558(7708), 104-107.

Kossin, J. P., Camargo, S. J., & Sitkowski, M. (2010). Climate modulation of North Atlantic hurricane tracks. Journal of Climate, 23(11), 3057-3076.

Kossin, J. P., Emanuel, K. A., & Vecchi, G. A. (2014). The poleward migration of the location of tropical cyclone maximum intensity. Nature, 509(7500), 349-352.

Kossin, J. P., Knapp, K. R., Vimont, D. J., Murnane, R. J., & Harper, B. A. (2007). A globally consistent reanalysis of hurricane variability and trends. Geophysical Research Letters, 34(4).

Landsea, C. W. (1993). A climatology of intense (or major) Atlantic hurricanes. Monthly weather review, 121(6), 1703-1713.

Landsea, C. W. and J. L. Franklin, 2013: Atlantic Hurricane Database Uncertainty and Presentation of a New Database Format. Mon. Wea. Rev., 141, 3576-3592.

Landsea, C. W., & Cangialosi, J. P. (2018). Have we reached the limits of predictability for tropical cyclone track forecasting?. Bulletin of the American Meteorological Society, 99(11), 2237-2243.

Lavender, S. L., & McBride, J. L. (2021). Global climatology of rainfall rates and lifetime accumulated rainfall in tropical cyclones: Influence of cyclone basin, cyclone intensity and cyclone size. International Journal of Climatology, 41, E1217-E1235.

Lea, A. (2024) April Forecast Update for North Atlantic Hurricane Activity in 2024. http://ww.tropicalstormrisk.com/

Lin, I. I., Camargo, S. J., Patricola, C. M., Boucharel, J., Chand, S., Klotzbach, P., ... & Jin, F. F. (2020). ENSO and tropical cyclones. El Niño Southern Oscillation in a changing climate, 377-408.

Liu, H., Wang, C., Lee, S. K., & Enfield, D. (2013). Atlantic warm pool variability in the CMIP5 simulations. Journal of climate, 26(15), 5315-5336.

Lübbecke, J. F., Durgadoo, J. V., &Biastoch, A. (2015). Contribution of Increased Agulhas Leakage to Tropical Atlantic Warming, Journal of Climate, 28, 9697–9706.

Lübbecke, J. F., Rodríguez-Fonseca, B., Richter, I., Martín-Rey, M., Losada, T., Polo, I., & Keenlyside, N. S. (2018). Equatorial Atlantic variability—Modes, mechanisms, and global teleconnections. Wiley Interdisciplinary Reviews: Climate Change, 9(4), e527.

Madan, G., Gjermundsen, A., Iversen, S. C., & LaCasce, J. H. (2023). The weakening AMOC under extreme climate change. Climate Dynamics, 1-19.

Madan, Gaurav, Ada Gjermundsen, Silje C. Iversen, and Joseph H. LaCasce. "The weakening AMOC under extreme climate change." Climate Dynamics 62, no. 2 (2024): 1291-1309.

Madec, G. (2008). NEMO reference manual, ocean dynamics component: NEMO-OPA.

Preliminary version. Note du Pole de modélisation, Institut Pierre-Simon Laplace (IPSL), France, 27, 1288-161.

Madec, G., Bourdallé-Badie, R., Bouttier, P. A., Bricaud, C., Bruciaferri, D., Calvert, D., & Vancoppenolle, M. (2017). NEMO ocean engine (Version v3. 6), Notes du Pôle de modélisation de l'Institut Pierre-simon Laplace (IPSL), 27, Zenodo

Mainelli, M., DeMaria, M., Shay, L. K., & Goni, G. (2008). Application of oceanic heat content estimation to operational forecasting of recent Atlantic category 5 hurricanes. Weather and Forecasting, 23(1), 3-16.

Mann, M. E., Steinman, B. A., Brouillette, D. J., & Miller, S. K. (2021). Multidecadal climate oscillations during the past millennium driven by volcanic forcing. Science, 371(6533), 1014-1019.

Marsh, R., Addo, K. A., Jayson-Quashigah, P. N., Oxenford, H. A., Maxam, A., Skliris, N., Anderson, R., Dash, J., Tompkins, E. L. (2021). Seasonal predictions of holopelagic sargassum across the tropical Atlantic accounting for uncertainty in drivers and processes: the SARTRAC ensemble forecast system.

Marsh, R., S. A. Josey, B. A. de Cuevas, L. J. Redbourn, and G. D. Quartly (2008). Mechanisms for recent warming of the North Atlantic: Insights gained with an eddy-permitting model, J. Geophys. Res., 113, C04031, doi:10.1029/2007JC004096.

Marsh. R., de Cuevas, B. A., Coward, A. C., Nurser, A. J. G., and S. A. Josey (2005). Water mass transformation in the North Atlantic over 1985-2002 simulated in an eddy-permitting model.

Ocean Science, 1, 127-144.

Mayer, J., Haimberger, L., & Mayer, M. (2023). A quantitative assessment of air-sea heat flux trends from ERA5 since 1950 in the North Atlantic basin. Earth System Dynamics Discussions, 2023, 1-36.

Mazza, E., & Chen, S. S. (2023). Modulation of tropical cyclone tracks and rainfall by the North Atlantic Oscillation. Journal of Geophysical Research: Atmospheres, 128(13), e2022JD038107.

McCloskey, T. A., Bianchette, T. A., & Liu, K. B. (2013). Track patterns of landfalling and coastal tropical cyclones in the Atlantic basin, their relationship with the North Atlantic Oscillation (NAO), and the potential effect of global warming.

McTaggart-Cowan, R., Davies, E. L., Fairman, J. G., Galarneau, T. J., & Schultz, D. M. (2015). Revisiting the 26.5 ° C sea surface temperature threshold for tropical cyclone development. Bulletin of the American Meteorological Society, 96(11), 1929-1943.

Moharana, S. S., & Swain, D. (2023). On the recent increase in Atlantic Ocean hurricane activity and influencing factors. Natural Hazards, 1-13.

Mueller, T. J., Patricola, C. M., & Bercos-Hickey, E. (2024). The influence of ENSO diversity on future Atlantic tropical cyclone activity. Journal of Climate.

Murakami, H., Levin, E., Delworth, T. L., Gudgel, R., & Hsu, P. C. (2018). Dominant effect of relative tropical Atlantic warming on major hurricane occurrence. Science, 362(6416), 794-799.

National Hurricane Center (2023). Tropical Cyclone Climatology. https://www.nhc.noaa.gov/climo/

NOAA National Centers for Environmental Information (NCEI) U.S. Billion-Dollar Weather and Climate Disasters (2020). https://www.ncdc.noaa.gov/billions/, DOI: 10.25921/stkw-7w73

NOAA National Centers for Environmental Information (NCEI) U.S. Billion-Dollar Weather and Climate Disasters (2022). https://www.ncei.noaa.gov/access/billions/, DOI: 10.25921/stkw-7w73

NOAA National Centers for Environmental Information (NCEI) (2023). US billion-dollar weather and climate disasters. https://www.doi.org/10.25921/stkw-7w73

Nyberg, J., Malmgren, B. A., Winter, A., Jury, M. R., Kilbourne, K. H., & Quinn, T. M. (2007). Low Atlantic hurricane activity in the 1970s and 1980s compared to the past 270 years. Nature, 447(7145), 698-701.

Pasch, R. J., Avila, L. A., and J. L. Guiney (2001). Atlantic Hurricane Season of 1998. Mon. Wea. Rev., 129, 3085-3123.

Patricola, C. M., Cassidy, D. J., & Klotzbach, P. J. (2022). Tropical oceanic influences on observed global tropical cyclone frequency. Geophysical Research Letters, 49(13), e2022GL099354.

Patricola, C. M., Hansen, G. E., & Sena, A. C. (2024). The Influence of Climate Variability and Future Climate Change on Atlantic Hurricane Season Length. Geophysical Research Letters, 51(8), e2023GL107881.

Pfleiderer, P., Nath, S., & Schleussner, C. F. (2022). Extreme Atlantic hurricane seasons made twice as likely by ocean warming. Weather and Climate Dynamics, 3(2), 471-482.

Philander, S. G. (2001). Atlantic Ocean equatorial currents (pp. 188-191). Elsevier: London, UK.

Roberts, C. D., Waters, J., Peterson, K. A., Palmer, M. D., McCarthy, G. D., Frajka-Williams, E., ... & Zuo, H. (2013). Atmosphere drives recent interannual variability of the Atlantic meridional overturning circulation at 26.5 N. Geophysical Research Letters, 40(19), 5164-5170.

Roberts, M. J., Baker, A., Blockley, E. W., Calvert, D., Coward, A., Hewitt, H. T., ... & Vidale, P. L. (2019). Description of the resolution hierarchy of the global coupled HadGEM3-GC3. 1 model as used in CMIP6 HighResMIP experiments. Geoscientific Model Development, 12(12), 4999-5028.

Roberts, M. J., Camp, J., Seddon, J., Vidale, P. L., Hodges, K., Vannière, B., ... & Wu, L. (2020). Projected future changes in tropical cyclones using the CMIP6 HighResMIP multimodel ensemble. Geophysical research letters, 47(14), e2020GL088662.

Roberts, M. J., Jackson, L. C., Roberts, C. D., Meccia, V., Docquier, D., Koenigk, T., ... & Wu, L. (2020b). Sensitivity of the Atlantic meridional overturning circulation to model resolution in CMIP6 HighResMIP simulations and implications for future changes. Journal of Advances in Modeling Earth Systems, 12(8), e2019MS002014.

Rousseau-Rizzi, R., & Emanuel, K. (2022). Natural and anthropogenic contributions to the hurricane drought of the 1970s–1980s. Nature Communications, 13(1), 5074.

Rühs, S., Getzlaff, K., Durgadoo, J. V., Biastoch, A., & Böning, C. W. (2015). On the suitability of North Brazil Current transport estimates for monitoring basin-scale AMOC changes. Geophysical Research Letters, 42(19), 8072-8080.

Saunders, M. A., & Lea, A. S. (2008). Large contribution of sea surface warming to recent increase in Atlantic hurricane activity. Nature, 451(7178), 557-560.

Servain, J., I. Wainer, J. P. McCreary, and A. Dessier (1999), Relationship between the equatorial and meridional modes of climatic variability in the tropical Atlantic, Geophys. Res. Lett., 26, 485–488

Shapiro, L. J., & Goldenberg, S. B. (1998). Atlantic sea surface temperatures and tropical cyclone formation. Journal of Climate, 11(4), 578-590.

Small, R. J., Bacmeister, J., Bailey, D., Baker, A., Bishop, S., Bryan, F., ... & Vertenstein, M. (2014). A new synoptic scale resolving global climate simulation using the Community Earth System Model. Journal of Advances in Modeling Earth Systems, 6(4), 1065-1094.

Smeed, D. A., Josey, S. A., Beaulieu, C., Johns, W. E., Moat, B. I., Frajka-Williams, E., ... & McCarthy, G. D. (2018). The North Atlantic Ocean is in a state of reduced overturning. Geophysical Research Letters, 45(3), 1527-1533.

Sobel, A. H., Wing, A. A., Camargo, S. J., Patricola, C. M., Vecchi, G. A., Lee, C. Y., & Tippett, M. K. (2021). Tropical cyclone frequency. Earth's Future, 9(12), e2021EF002275.

Sousounis, P. (2021). The Atlantic Multidecadal Oscillation—Has the Truth Erupted? https://www.air-worldwide.com/blog/posts/2021/4/the-atlantic-multidecadal-oscillation-has-the-truth-erupted/

Sugi, M., K. Yoshida, and H. Murakami, 2015: More tropical cyclones in a cooler climate. Geophys. Res. Lett., 42(16), 6780-6784.

Tang, B., & Camargo, S. J. (2014). Environmental control of tropical cyclones in CMIP5: A ventilation perspective. Journal of Advances in Modeling Earth Systems, 6(1), 115-128.

Titley, H. A., Cloke, H. L., Harrigan, S., Pappenberger, F., Prudhomme, C., Robbins, J. C., ... & Zsótér, E. (2021). Key factors influencing the severity of fluvial flood hazard from tropical cyclones. Journal of Hydrometeorology, 22(7), 1801-1817.

Touma, D., Stevenson, S., Camargo, S. J., Horton, D. E., & Diffenbaugh, N. S. (2019). Variations in the intensity and spatial extent of tropical cyclone precipitation. Geophysical Research Letters, 46(23), 13992-14002.

Truchelut, R. E., Klotzbach, P. J., Staehling, E. M., Wood, K. M., Halperin, D. J., Schreck III, C. J., & Blake, E. S. (2022). Earlier onset of North Atlantic hurricane season with warming oceans.

Nature communications, 13(1), 4646.

Uppala, S. M., Kållberg, P. W., Simmons, A. J., Andrae, U., Da Costa Bechtold, V., Fiorino, M., et al. (2005). The ERA-40 Reanalysis. Q. J. R. Meteorol. Soc. 131, 2961–3012. Doi: 10.1256/qj.04.176

van Westen, R. M., Kliphuis, M., & Dijkstra, H. A. (2024). Physics-based early warning signal shows that AMOC is on tipping course. Science advances, 10(6), eadk1189.

Vecchi, G. A., & Soden, B. J. (2007). Increased tropical Atlantic wind shear in model projections of global warming. Geophysical Research Letters, 34(8).

Vecchi, G. A., Landsea, C., Zhang, W., Villarini, G., & Knutson, T. (2021). Changes in Atlantic major hurricane frequency since the late-19th century. Nature communications, 12(1), 4054.

Vimont, D. J., & Kossin, J. P. (2007). The Atlantic meridional mode and hurricane activity. Geophysical Research Letters, 34(7).

Walin, G. (1982). On the relation between sea-surface heat flow and thermal circulation in the ocean. Tellus, 34(2), 187-195.

Walsh, K. J., McBride, J. L., Klotzbach, P. J., Balachandran, S., Camargo, S. J., Holland, G., ... & Sugi, M. (2016). Tropical cyclones and climate change. Wiley Interdisciplinary Reviews: Climate Change, 7(1), 65-89.

Wang, C., & Lee, S. K. (2007). Atlantic warm pool, Caribbean low-level jet, and their potential impact on Atlantic hurricanes. Geophysical research letters, 34(2).

Wang, C., & Picaut, J. (2004). Understanding ENSO physics—A review. Earth's Climate: The Ocean–Atmosphere Interaction, Geophys. Monogr, 147, 21-48.

Wang, C., Dong, S., Evan, A. T., Foltz, G. R., & Lee, S. K. (2012). Multidecadal covariability of North Atlantic sea surface temperature, African dust, Sahel rainfall, and Atlantic hurricanes. Journal of Climate, 25(15), 5404-5415. Walin, G. (1982). On the relation between sea-surface heat flow and thermal circulation in the ocean. Tellus, 34(2), 187-195.

Wang, C., Liu, H., Lee, S. K., & Atlas, R. (2011). Impact of the Atlantic warm pool on United States landfalling hurricanes. Geophysical Research Letters, 38(19).

Watanabe, M., & Tatebe, H. (2019). Reconciling roles of sulphate aerosol forcing and internal variability in Atlantic multidecadal climate changes. Climate Dynamics, 53(7), 4651-4665.

Weaver, M. M., & Garner, A. J. (2023). Varying genesis and landfall locations for North Atlantic tropical cyclones in a warmer climate. Scientific Reports, 13(1), 5482.

Wild, M. (2016), Decadal changes in radiative fluxes at land and ocean surfaces and their relevance for global warming. WIREs Clim Change, 7: 91-107. https://doi.org/10.1002/wcc.372

Xie, S.-P., and Carton, J. A. (2004). "Tropical Atlantic variability: patterns, mechanisms, and Impacts," in Earth's Climate, eds C. Wang, S.-P. Xie, and J. A. Carton (Washington, DC: American Geophysical Union).

Yan, X., Zhang, R., & Knutson, T. R. (2017). The role of Atlantic overturning circulation in the recent decline of Atlantic major hurricane frequency. Nature Communications, 8(1), 1695.

Yan, X., Zhang, R., & Knutson, T. R. (2019). A multivariate AMV index and associated discrepancies between observed and CMIP5 externally forced AMV. Geophysical Research Letters, 46(8), 4421-4431.

Yang, J. (2015). Local and remote wind stress forcing of the seasonal variability of the Atlantic Meridional Overturning Circulation (AMOC) transport at 26.5 °N, J. Geophys. Res. Oceans, 120, 2488–2503, doi:10.1002/2014JC010317.

Yeager, G., & Robson, J. I. (2017). Recent progress in understanding and predicting Atlantic decadal climate variability. Current Climate Change Reports, 3, 112-127.

Yoshida, K., Sugi, M., Mizuta, R., Murakami, H., & Ishii, M. (2017). Future changes in tropical cyclone activity in high-resolution large-ensemble simulations. Geophysical Research Letters, 44(19), 9910-9917.

Zebiak, S. E. (1993). Air–sea interaction in the equatorial Atlantic region. J. Clim. 6, 1567–1586.

Zhang, D., Msadek, R., McPhaden, M. J., & Delworth, T. (2011). Multidecadal variability of the North Brazil Current and its connection to the Atlantic meridional overturning circulation. Journal of Geophysical Research: Oceans, 116(C4).

Zhang, R., & Delworth, T. L. (2006). Impact of Atlantic multidecadal oscillations on India/Sahel rainfall and Atlantic hurricanes. Geophysical Research Letters, 33(17).

Zhang, R., Sutton, R., Danabasoglu, G., Kwon, Y. O., Marsh, R., Yeager, S. G., ... & Little, C. M. (2019). A review of the role of the Atlantic meridional overturning circulation in Atlantic multidecadal variability and associated climate impacts. Reviews of Geophysics, 57(2), 316-375.